NASA CR-54256

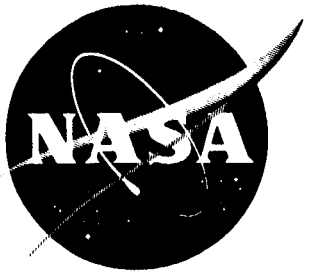

THE ALPHA-CELL DIRECT-CONVERSION GENERATOR

by

A. M. Plummer, W. J. Gallagher, R. G. Matthews,

and J. N. Anno

prepared for

NATIONAL AERONAUTICS AND SPACE ADMINISTRATION

Contract NAS 3-2797

BATTELLE

MEMORIAL INSTITUTE

Requests for copies of this report should be referred to

National Aeronautics and Space Administration
Office of Scientific and Technical Information
Attention: AFSS-A
Washington, D.C. 20546

FINAL REPORT

THE ALPHA-CELL DIRECT-CONVERSION GENERATOR

by

A. M. Plummer, W. J. Gallagher,
R. G. Matthews, and J. N. Anno

prepared for

NATIONAL AERONAUTICS AND SPACE ADMINISTRATION

November 30, 1964

CONTRACT NAS 3-2797

Technical Management
NASA Lewis Research Center
Cleveland, Ohio
Space Power Systems Division
Solar and Chemical Power Branch
Ernest A. Koutnik

BATTELLE MEMORIAL INSTITUTE
505 King Avenue
Columbus, Ohio 43201

TABLE OF CONTENTS

TABLE OF CONTENTS
(Continued)

TABLE OF CONTENTS
(Continued)

LIST OF TABLES

LIST OF FIGURES

LIST OF FIGURES
(Continued)

LIST OF FIGURES
(Continued)

THE ALPHA-CELL DIRECT-CONVERSION GENERATOR

by

A. M. Plummer, W. J. Gallagher,
R. G. Matthews, and J. N. Anno

ABSTRACT

Experiments performed on a generator in which alpha-particle kinetic energy is converted directly to electrical energy resulted in voltage buildup in the 50- to 100-kilovolt range. Microdischarging in the experimental cell was determined to be the factor preventing higher voltage buildup. The experiments also provided information on generator design, especially on the factors influencing control of secondary electrons by an electrical grid.

Methods of converting the high-voltage (megavolt range) expected from improved experimental cells to lower voltage were also investigated. A converter incorporating a piezoelectric transformer was conceived and designed.

INTRODUCTION

Under contract with the Lewis Research Center of the National Aeronautics and Space Administration, Battelle has studied a generator which converts alpha-particle energy directly into electricity by causing the high-energy alpha particles to do work against an electric field. This concept is referred to as the "alpha electric cell", or simply the "alpha cell". A source material such as polonium-210, or other high-energy alpha emitter, is distributed in a thin layer over a surface which will be called the cathode. The emitting surface is capable of charging a collecting electrode, which will be called the anode. In time, a retarding electric field is established, and the positively charged alpha particles do work against this field, i.e., their kinetic energy is transformed to available electrical energy. The alpha cell is basically a high-voltage (megavolt range), low-current device.

The power range for a generator based on this direct-conversion concept is not yet firmly established. However, it appears at present that generators with useful outputs of 10 to 100 watts may be achieved. The applications for such a generator are likewise unspecified at this early stage in development. Applications as primary or auxiliary space power for satellites are visualized, but other applications might prove to be of greater interest. For example, the alpha cell could serve as the high-voltage source for an electrostatic propulsion unit using heavy particles; it could also serve as the high-voltage source for antennae for satellite communications. As the operating characteristics and practicality of the concept become better known, the applications should become more evident.

Battelle-sponsored experiments performed in late 1962 showed that the principles of operation of the device were sound in the relatively low-voltage range obtained at that time (approximately 50,000 volts).* However, for efficient operation the device must operate in the range near 1 megavolt. The objective of the NASA-sponsored program was to extend the voltage capability of the alpha cell to this higher range and to determine the characteristics of the cell under this condition. Because of microdischarging in the cell, significantly higher voltage was not achieved. However, the experiments provided additional useful information on cell performance and design parameters.

This report summarizes the results of the 8-month study on the alpha-particle generator. Prior to a presentation of the experimental results, the principles of operation are reviewed and the results of previous studies at Battelle are summarized.** This information embodies essentially everything Battelle knows to date about the alpha cell.

As with any concept, the alpha cell presents problems. The most pressing problem, shown by the experimental results, is microdischarging in the cell, which limits voltage buildup to 50,000 to 100,000 volts. Probably the next most important problem is converting the high-voltage electricity to lower voltage. Whether or not these problems will be insurmountable must await results of further studies. A concept for converting the high voltage electricity produced in the cell to a more useful form is presented near the end of the report. However, intense pursuit of the conversion scheme would appear pointless until it has been demonstrated that voltages of the order of a megavolt can be achieved in an experimental cell.

The Battelle team participating in this study is listed as the authors of this report. The contract for this work was administered at Lewis Research Center by Mr. John E. Dilley, Contracting Officer, with Mr. Ernest Koutnik, Solar and Chemical Power Branch, as Project Manager. The technical advisors for this project were Mr. William R. Mickelsen and Mr. Charles A. Low, Jr. Mr. Low is a member of the staff of the Electromagnetic Propulsion Division at NASA, Lewis Research Center.

Comments from interested persons on this concept and on the results presented in this report are encouraged.

SUMMARY

The results of the study indicated that microdischarging in the experimental alpha cell was preventing high-voltage buildup. Although approximately 100 kilovolts was achieved initially, typically the cell voltage buildup terminated at about 50 kilovolts, the microdischarging threshold voltage. The results of the study further showed that the electrical grid in the cell, which is necessary to suppress secondary-electron emission from the surface of the alpha-emitting material, functioned successfully and as predicted by application of electron-tube technology to the system design. In addition to substantiating results of the preliminary Battelle-supported study, the experiments uncovered several new features of the cell physics, primarily in the area of secondary-electron emission and control.

*Publications summarizing the results of the Battelle-sponsored experiments are listed as "Bibliography" at the end of this report.

**Most of this information was presented in the program midpoint report, Lewis Research Center Report Number CR-54162, but is repeated for the sake of completeness.

As a result of the investigation of methods of voltage conversion, a piezoelectric transformer was selected for further study and a converter was conceived and designed. Preliminary analyses indicate that the piezoelectric system may be uniquely adaptable to the alpha cell, with possibilities for reasonable conversion efficiencies. Sample calculations of converter operation in the nonresonant mode showed efficiencies of about 10 per cent. It is anticipated that proper selection of system parameters will result in higher efficiency; operation in the resonant mode may also improve efficiency.

The principal conclusion from the program is that microdischarging presents a more fundamental problem to alpha-cell experiments than initially anticipated. Analysis of the accumulated data on cell performance, coupled with the literature on the microdischarging phenomenon, suggests several approaches to relieving or circumventing the problem for continued cell studies.

THEORY OF ALPHA-CELL OPERATION

This section of the report presents the theory of alpha-cell operation in its present state of development. In this discussion, the currents, efficiencies, etc., relate to a single isolated cell. Further, the change in efficiency due to the high-voltage conversion technique is not considered here since this area is undergoing preliminary study.

FUNDAMENTAL PRINCIPLES OF OPERATION OF THE ALPHA CELL

The alpha particle, with mass of 4.003 amu, is essentially a helium atom with the two electrons removed. Certain radioisotopes decay by emission of an alpha particle, the half-life of the decay varying widely with the isotope. The half-life ranges from 3×10^{-7} sec for polonium-212 (ThC') to 1.4×10^{10} years for thorium-232. The alpha particles thus emitted are monoenergetic, with energies for isotopes of interest typically in the range of 5 to 6 Mev. At birth each alpha particle has a charge of +2. A brief reflection on this fact points out the underlying principle of the alpha cell process: in the phenomenon of alpha decay we have electricity in its most elementary form – charged particles in motion.

The more conventional methods of using radiosotope energy do not make use of the alpha-particle kinetic energy and positive charge in a direct manner. Rather, the alpha particles dissipate their energy and charge in a thick fuel material, producing heat. The heat generated in the fuel is typically used to raise the temperature of a thermionic or thermoelectric material which, in turn, produces electricity.

However, if the isotope is distributed in a sufficiently thin layer rather than in a thick fuel region, so that an appreciable fraction of all the alpha particles produced in the layer can escape from the surface with much of their initial energy and charge intact, these particles can be collected on an insulated electrode. The first few alphas reaching the electrode will deposit their charge and dissipate their kinetic energy as heat. However, after a number of alphas have been collected, the insulated electrode, by virtue of its surplus of positive charge, will attain a high voltage with respect to the emitter layer. Subsequent alpha particles will "do work" against this electric field: they will arrive at the electrode with their initial kinetic energy exhausted but will deposit their charge. The space between the electrodes is evacuated to prevent energy loss by ionization of intervening gas and to permit high voltage buildup by serving as an electrical insulator. The voltage characteristic of this process is (E_o/Z_o), the ratio of the initial kinetic energy of the alpha particle in electron volts divided by its charge magnitude. This follows from the definition of the electron volt as the work done per unit charge when the unit charge is moved through a potential difference of one volt. Since E_o is typically of the order of 5-million electron volts and Z_o is +2, the characteristic voltage of the process is several megavolts.

In effect, the arrangement discussed above is analogous to a capacitor, as shown in Figure 1, with the alpha particles doing the charging. The charge separation caused by the energetic alpha particles driving their way to the insulated electrode, the

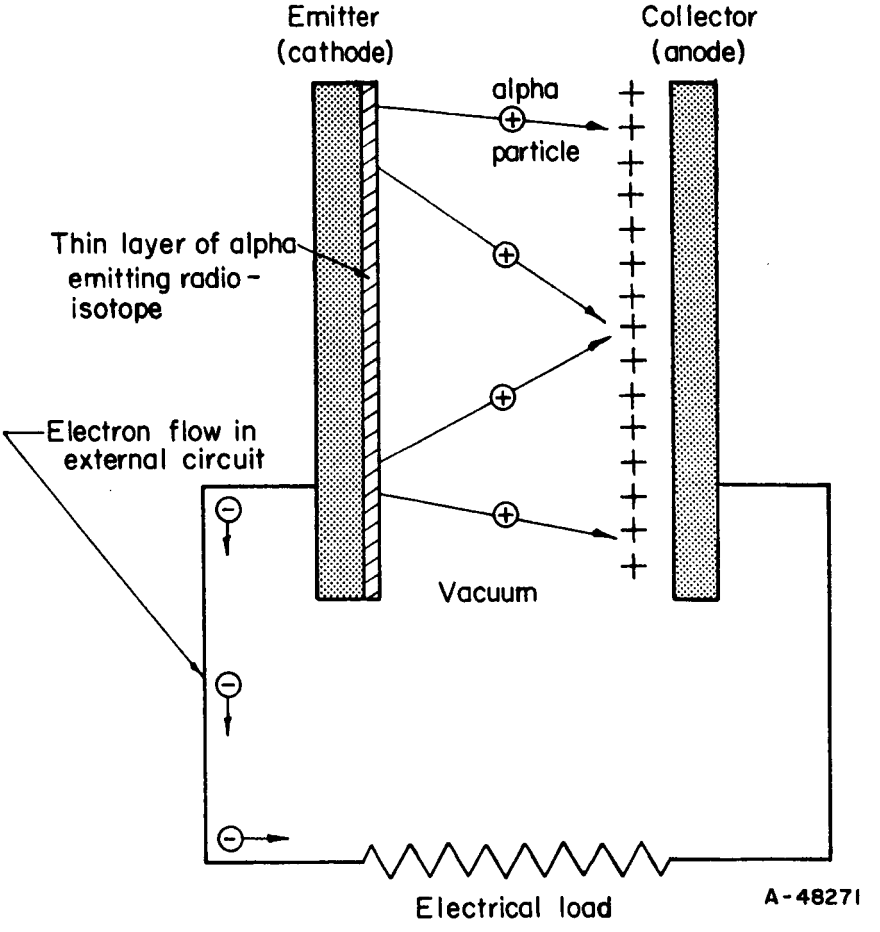

FIGURE 1. THE PRINCIPLE OF THE ALPHA CELL'S OPERATION

collector, is neutralized by a flow of the electrons which were left behind through an external circuit. This electron flow through an external circuit is a source of direct electricity produced without the use of a heat cycle. The high-voltage d-c electricity thus produced can be used directly, reduced to a lower voltage or inverted to a-c electricity. The direct conversion occurs in the use of the alpha-particle kinetic energy to effect a charge separation across a high potential difference.

The discovery that charged-particle emission can build up a voltage on a properly insulated electrode may be traced to work by Mosely in 1913.[1]* The direct application of this idea for a high-voltage generator has been considered by others during the past several decades, for example, the work of Linder and Christian at RCA.[2] However, a critical problem exists in reducing the concept to practice. Along with the positively charged alpha particles come secondary electrons which have an opposing charge. Measurements indicate that approximately 10 secondary electrons are released from the surface with each alpha particle.[3] Although these secondary electrons have very low energy (approximately 97 per cent have energy less than 100 ev), they are produced in such abundance that their total negative charge more than offsets the positive-charge buildup. Thus, a low-energy net negative charge, rather than the desired positive high-energy charge, is emitted from the cathode.

A properly designed control grid placed close to the cathode can be used to overcome this difficulty. A negative potential applied to the grid will repel the secondary electrons to the cathode. A simple configuration which illustrates the concept is shown in Figure 2. A cylindrical electrode, the emitter or cathode, can be a tube or rod coated with a layer of alpha emitter several microns thick. This thickness is required since the range of alpha particles in metals is of the order of 10 microns. Surrounding the cathode in this example is a "squirrel-cage" grid at negative voltage with respect to the cathode. The grid is composed of small-diameter wires and is sufficiently open to permit the alpha particles to reach the collector, or anode, while at the same time preventing the secondary electrons from escaping. Because the electrons have very low energy, only a few hundred volts' bias on the grid will suppress them. To hold back the electrons when the anode is at several million volts requires an increase in voltage to the kilovolt range. The grid can be designed to be almost completely open; typically 90 per cent or more of the total grid area is not blocked by grid wires.

From the previous discussion it is apparent that the grid is the key to the successful operation of the alpha cell. As will be discussed in a later section of the report, its design has a considerable bearing on the efficiency of the operation and may acquire added significance in the conversion of the high voltage d-c electricity to lower voltage a-c electricity. One can also conceive of suppressing the secondary electrons with a magnetic field, but for reasons which will be discussed later, under existing technology the use of a grid appears to have a significant advantage.

CONVERSION EFFICIENCY OF IDEAL CELLS

The efficiency of conversion of alpha-particle kinetic energy into electrical energy is dictated principally by the geometry of the alpha cell. In this section, the conversion will be derived for ideal cells, those which contain a transparent yet completely

*References are listed on page 103.

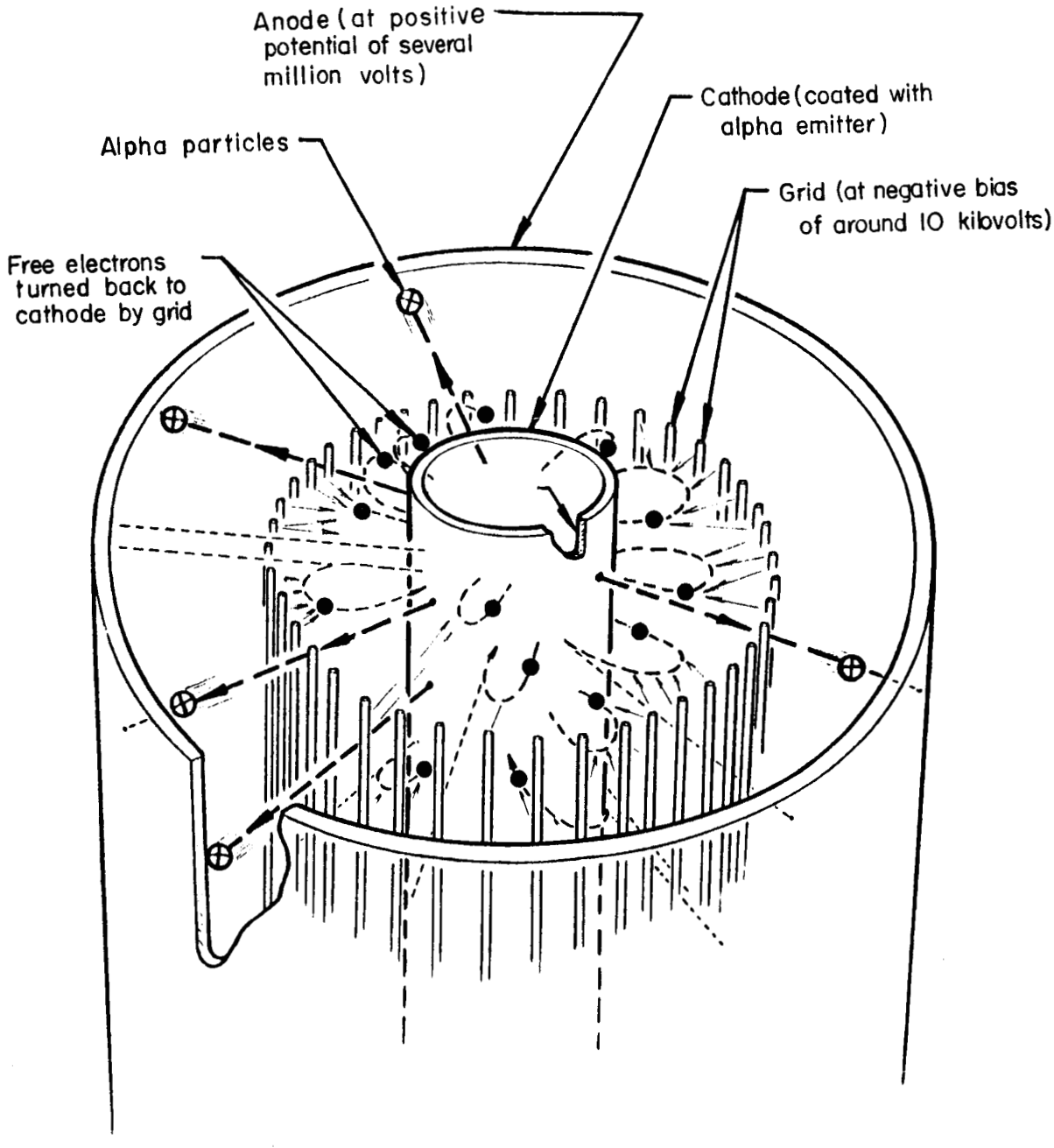

FIGURE 2. USE OF A GRID TO REPEL SECONDARY ELECTRONS (COAXIAL-CYLINDER GEOMETRY)

effective grid. The effects of geometry on conversion efficiency can best be illustrated by discussing the more common geometries: parallel planes, coaxial cylinders, and concentric spheres.

Efficiency for Common Geometries

For the initial calculation of efficiencies, it will be assumed that the total cell efficiency is purely a geometrical one. The thickness of isotope of the emitter will be assumed sufficiently thin that no energy losses are incurred in the alphas escaping from the fuel. By the same token, the alpha particles will be assumed to be mono-energetic. (It will later be shown that one of the effects of a finite fuel layer is to spread the energy distribution of the alpha particles.)

Concentric Spheres

The most efficient but perhaps least practical geometry for the alpha cell is that of a concentric, spherical emitter and collector. In the limit of large collector diameter compared with emitter diameter, this case is that of a point source emitter surrounded by a spherical collector. All alpha particles are emitted radially and hence normal to the collector surface. As can easily be seen, the conversion efficiency P in this case is

$$P = \frac{1}{2}\frac{VZ_o}{E_o} = \beta/2 \quad , \tag{1}$$

where $\beta = \frac{VZ_o}{E_o}$ is a dimensionless voltage parameter ranging from 0 to 1. The factor of 1/2 in this relation arises from the fact that for a thick fuel substrate only 1/2 of the alpha particles are directed radially outward; the other half embed in the cathode structure. Thus, for concentric spheres the efficiency increases linearly with anode voltage, reaching 50 per cent for the maximum possible voltage of (E_o/Z_o).

Coaxial Cylinders

In a coaxial-cylinder geometry with the cathode diameter small compared with the anode diameter (in the limit, a line source cathode coaxial with a cylindrical anode), the efficiency can be calculated as follows. If n_o represents the total number of alpha particles produced per unit time, then half of the particles, $n_{o/2}$ will be emitted with an outward radial component. With the anode at some voltage V with respect to the cathode, some of these particles will have insufficient velocity component perpendicular to the anode to reach it. The initial particle velocity is $v_o = \sqrt{\frac{2E_o}{m}}$ where m is the alpha-particle mass. The radial component of the initial velocity is $v_o \cos\theta$, where θ is the angle which the path of the particle makes with the normal to the emitting surface. For the alpha particle to overcome the electric field to arrive at the anode, it is necessary that

$$\frac{m(v_o \cos\theta)^2}{2} \geq VZ_o \quad ,$$

or, hence, that

$$E_o \cos^2\theta \geq VZ_o \quad . \tag{2}$$

The maximum angle, θ_{max}, at which an emitted particle will just reach the anode is seen from Equation (2) to be given from the relation

$$\cos \theta_{max} = \sqrt{\frac{VZ_o}{E_o}} = \sqrt{\beta} \ . \tag{3}$$

Particles emitted at angles less than θ_{max} will reach the anode; those emitted at angles greater than θ_{max} will not.

In the coaxial-cylinder configuration, the number which reach the anode for isotropic emission is*

$$n = \frac{n_o}{2} \sin \theta_{max} = \frac{n_o}{2} \sqrt{1 - \frac{VZ_o}{E_o}} \ , \tag{4}$$

and the conversion efficiency is

$$P = \frac{n}{n_o} \frac{VZ_o}{E_o} = \frac{1}{2} \frac{VZ_o}{E_o} \sqrt{1 - \frac{VZ_o}{E_o}} = \frac{\beta}{2} \sqrt{1-\beta} \ . \tag{5}$$

This equation shows a maximum efficiency of about 19 per cent for $\beta = 2/3$. (See Figure 3). Using as characteristic values $Z_o = 2$ charges and $E_o = 5$ Mev, the voltage at maximum efficiency is 1.7 megavolts.

Parallel Planes

For the case of parallel planes infinite in extent, integration over the particles emitted within the angular range $0 \leq \theta \leq \theta_{max}$ gives directly

$$n = \frac{n_o}{2} (1 - \cos \theta_{max}) = \frac{n_o}{2} \left(1 - \sqrt{\frac{VZ_o}{E_o}} \right) , \tag{6}$$

and the conversion efficiency is

$$P = \frac{n}{n_o} \frac{VZ_o}{E_o} = \frac{\beta}{2} \left(1 - \sqrt{\beta} \right) \ . \tag{7}$$

For this configuration, maximum conversion efficiency is 7.4 per cent for $\beta = 4/9$ (1.1 megavolts when using the values of $Z_o = 2$ and $E_o = 5$ Mev as in the previous example).

Figure 3 is a graphical representation of the efficiencies for the three common geometries considered above. This comparison illustrates the gain in efficiency to be made in progression from parallel-plane to spherical geometry. It also shows that, for the cases of coaxial cylinders or parallel planes, the efficiency curve has a rather broad maximum. This means that in these geometries, precise control of anode voltage is not necessary to maintain efficiency near the optimum value.

Table 1 summarizes the maximum conversion efficiencies attainable with three common geometries. In the simplest cases previously calculated, the fuel would be deposited in a thin layer on a thick substrate so that only half of the alpha particles could escape from the surface. In more advanced designs, it is possible to visualize two-sided emission geometries (fuel deposited on a screen-like substrate, fuel in the form of thin wires or gauze, etc.).

*The required integration is most readily performed by first considering the number of particles missing the anode, i.e., integrating from θ_{max} to $\pi/2$.

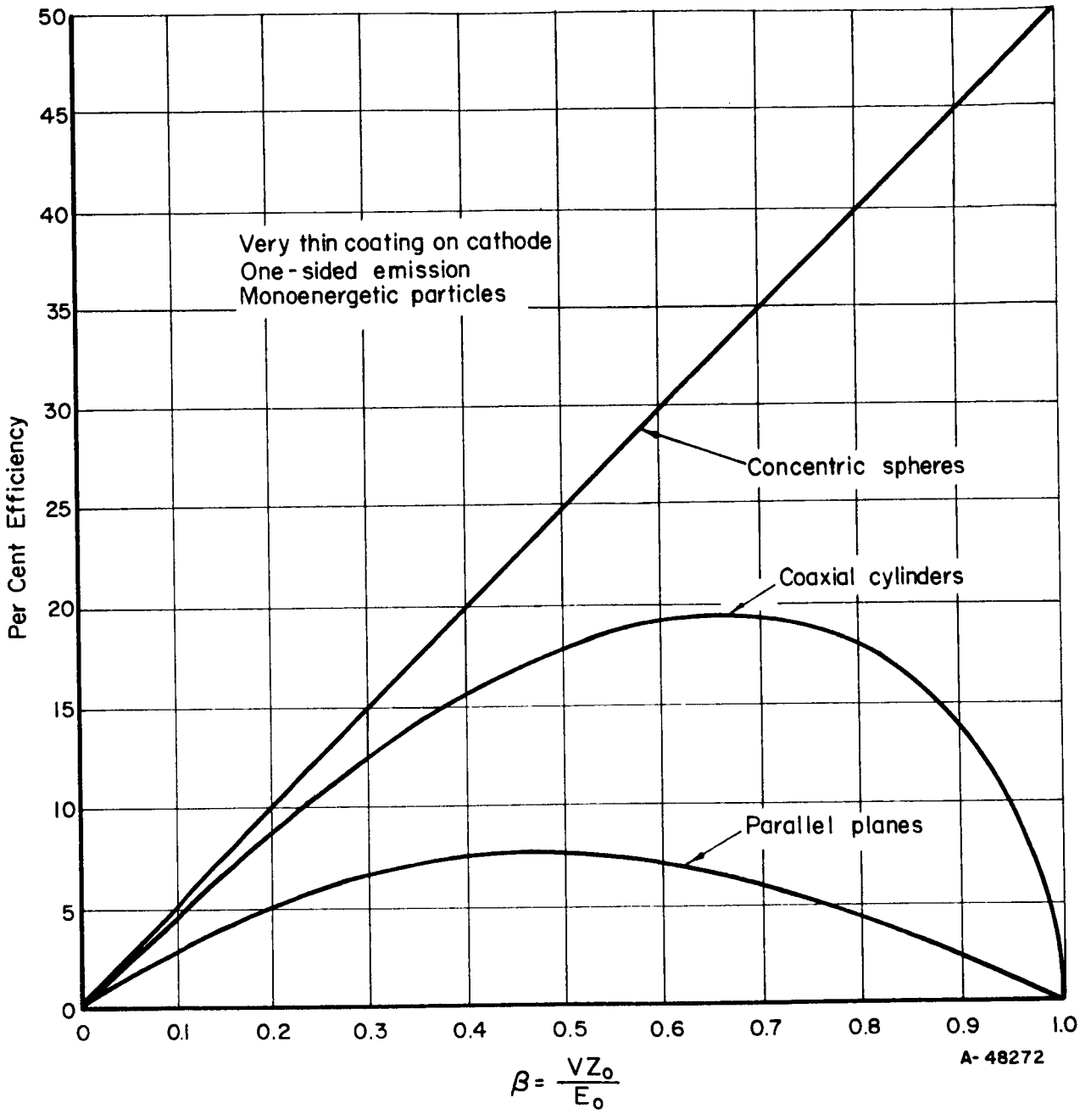

FIGURE 3. EFFICIENCY VERSUS VOLTAGE FOR THREE COMMON GEOMETRIES

TABLE 1. MAXIMUM CONVERSION EFFICIENCIES FOR THREE COMMON GEOMETRIES

Geometry	Maximum Theoretical Efficiency	
	One-Sided Emission	Two-Sided Emission
Parallel planes	7.4	14.8
Coaxial cylinders	19.2	38.4
Concentric spheres	50.0	100.0

Similar efficiency calculations can be made for these geometries in which the cathode diameter is a significant fraction of anode diameter. As would be expected, these cases are intermediate between the ones presented here. A fact which is perhaps not obvious is that by selective choice of an "uncommon" finite geometry, efficiencies greater than that of the infinite coaxial-cylinder geometry can possibly be obtained in quasicylindrical geometry. The choice of geometry is not simply one between cylindrical or spherical, but of any compromise of the two.

CELL CURRENTS IN GRIDDED DEVICES

The presence of a grid modifies the charging current to the collector due to several effects. Cell currents in a gridded device are discussed below under various conditions.

Currents With Anode at Zero Voltage

The expressions for the currents in a gridded device can be derived from the following definitions.

I_o = current carried from cathode by positively charged alpha particles

f = fraction of alpha particles emerging from the cathode which strike the grid wires

x = fraction of secondary electrons produced at the grid which escape the grid-cathode assembly,

η_g = charge ratio, the magnitude of the ratio of the secondary electrons produced at the grid to the charge of alpha particles striking the grid.

It is assumed that the grid is at large negative bias, the condition required for cell operation. Considering first the grid current, the fraction f of the alpha particles striking the grid carry current of positive charges of ($f I_o$) to the grid. These alpha particles striking the grid produce secondary electrons, so that a secondary-electron current of ($f \eta_g I_o$) is produced at the grid. Since the grid is at a large negative bias, all of these secondaries escape from the grid. The total current from the grid is the sum of the two components:

$$I_g = I_{grid} = -(f\, I_o) - (f\, \eta_g I_o) = -\, f\, (1 + \eta_g)\, I_o \qquad (8)$$

This current is supplied by the grid power supply, but since it is supplied at a voltage much less than the anode voltage, the power expenditure is negligible. The minus sign is assigned to this current according to the convention that a flow of positive charges from the cathode is a positive current. The cathode current also consists of two components. A current I_o of alpha particles leaves the cathode, but a fraction $(1 - x)$ of the secondary electrons produced by the few alphas which strike the grid returns to the cathode. The cathode current is then

$$I_{co} = I_{cathode} = I_o + (1 - x)\, (f\, \eta_g\, I_o) = [1 + (1 - x)\, f\, \eta_g] I_o \qquad (9)$$

The net current from the grid-cathode assembly is the algebraic sum of the grid and cathode currents and represents the current available to charge the anode.

$$I_c = I_{net} = [(1 - f) - x\, f\, \eta_g]\, I_o = [1 - f\, (1 + x\, \eta_g)]\, I_o \qquad (10)$$

It will be noted that this charging current is diminished from the original alpha-particle current I_o by two factors. First, due to the physical interception of some alpha particles by the grid, only $(1 - f)$ of the alpha particles escapes from the grid-cathode assembly. Second, a fraction x of the secondary electrons formed at the grid escapes to the anode and reduces the net flow of positive charge. Note that the loss in charging current is proportional to $f\, (1 + x\, \eta_g)$. It is apparent that the interception fraction at the grid, the f-factor, must be as small as possible to minimize losses in the charging current. How this bears on grid design will be discussed later.

Figure 4 shows how these currents would be expected to behave as a function of grid bias. Below about 100 volts on the grid, the energy distribution of the secondary electrons will affect the currents. At high negative grid bias, these currents should be independent of grid bias. From the previous analyses, as shown in Figure 4, the cathode current would be expected to be larger than the alpha-particle current by an amount $(1 - x)\, f\, \eta_g\, I_o$, which represents a flow of secondary electrons formed at the grid back to the cathode. Of course, it would be hoped that the grid current is small enough that a positive net current is obtained from the device, i.e., $I_{co} + I_g > 0$. It should be mentioned that these current relations are simplified to the extent that second-order effects have been neglected, such as the formation of secondary electrons by gamma radiation accompanying the alpha decays. However, for an alpha emitter such as polonium-210, these relations should be a good approximation to the actual currents.

Currents at Large Anode Voltage (Common Geometries)

As seen from the calculations of efficiency for the common geometries, the current to the collector generally decreases with increasing anode voltage (except for the concentric spherical case with point source anode) due to the repulsion of the alpha particles by the electric field. For an ideal grid (f-factor of zero), the behavior of the charging current with anode voltage in the three cases derived previously is

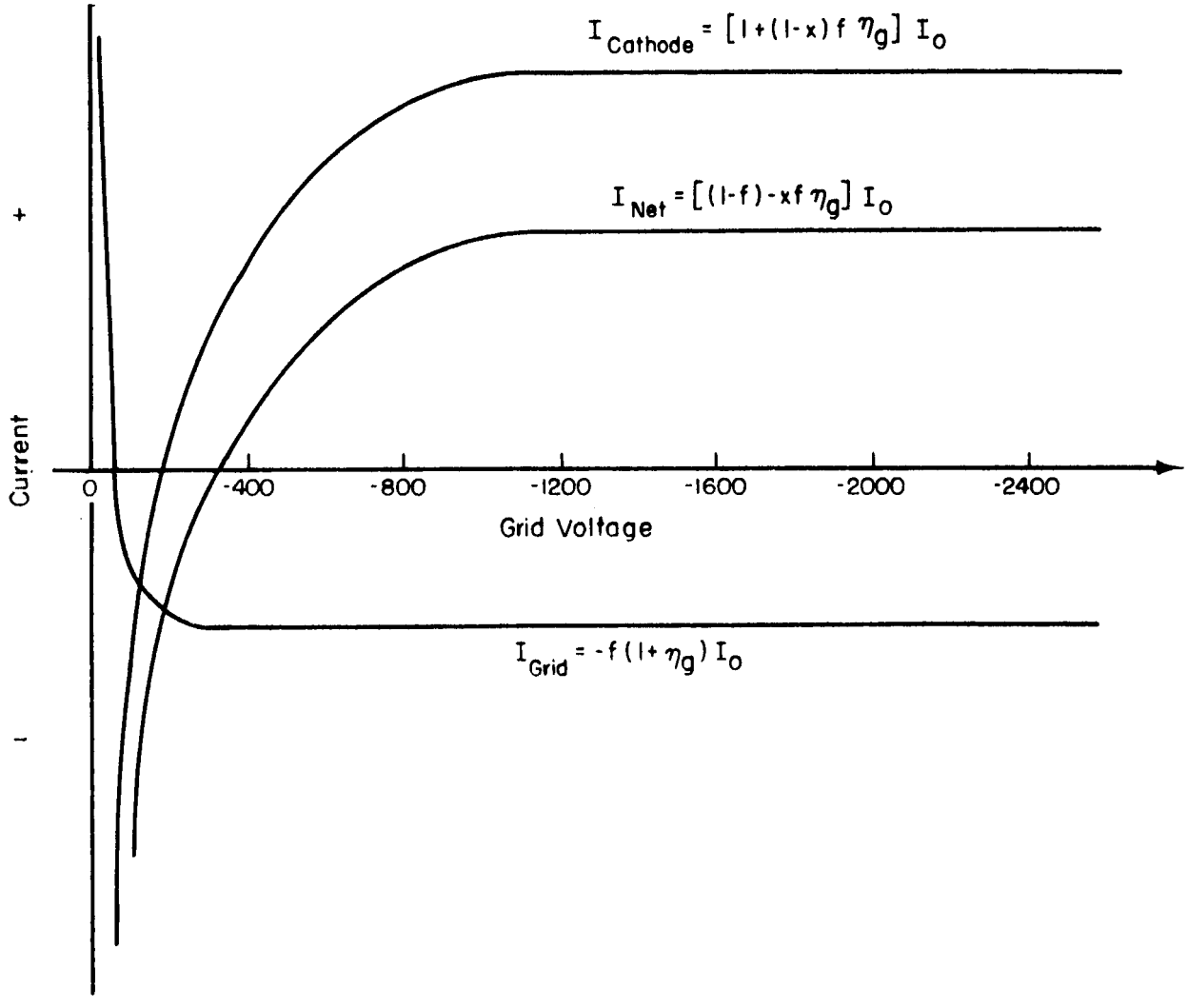

FIGURE 4. BEHAVIOR OF CURRENTS WITH GRID VOLTAGE FOR AN IDEAL ALPHA CELL (ZERO ANODE VOLTAGE)

$$I_c = I_o \qquad \text{(concentric spheres)} \qquad (11)$$

$$I_c = I_o \sqrt{1 - \frac{VZ_o}{E_o}} \qquad \text{(coaxial cylinders)} \qquad (12)$$

$$I_c = I_o \left(1 - \sqrt{\frac{VZ_o}{E_o}}\right) \text{(parallel planes)} \qquad (13)$$

The previous discussion considered the modification to the charging current at zero anode voltage due to a grid with finite f-factor, and the grid, cathode, and net currents were derived under these conditions. At large anode voltage another effect, apart from repulsion of the alphas by the field, also appears due to the grid. This effect is the striking of the grid by the "fall-back" particles, i.e., by those alpha particles which initially escape the grid-cathode assembly but do not have sufficient energy to reach the collector. The derivation and consequences of this effect will be briefly discussed. As might be expected, the analysis again emphasizes the importance of grid design, viz., of a low f-factor grid, and the importance of the geometry of the cell.

To illustrate the derivation of the expressions for the cell currents, coaxial-cylinder geometry will be used in the analysis. The extension to other geometries follows immediately. It is convenient to define the following terms, which are similar in definition to their counterparts used in the analysis of the cell currents at zero anode voltage. Let

f' = fraction of fall-back alpha particles which strike the grid on return toward the cathode.

η_g' = magnitude of the charge ratio of secondary electrons to fall-back particles which strike the grid. (This may differ from η_g due to angular variations in the striking particles.)

x' = fraction of the secondaries formed at the grid by the fall-back particles which escapes to the anode; $(1 - x')$ escapes to the cathode.

Then the grid current at large anode voltage is

$$I_g = \underbrace{-f(1 + \eta_g)I_o}_{\text{low-voltage current}} \underbrace{- f'(1 - f)\left[1 - \sqrt{1 - \frac{VZ_o}{E_o}}\right] I_o}_{\text{current to grid from fall-back particles which strike the grid on return to the cathode}}$$

$$\underbrace{- f'\eta_g'(1 - f)\left[1 - \sqrt{1 - \frac{VZ_o}{E_o}}\right] I_o}_{\text{secondary-electron current produced by the fall-back particles at the grid}}$$

$$= - f(1 + \eta_g) I_o - f' (1 + \eta_g') (1 - f) \left[1 - \sqrt{1 - \frac{VZ_o}{E_o}} \right] I_o$$

$$= (I_g)_o \left\{ 1 + \frac{f'(1-f)}{f} \frac{(1 + \eta_g')}{(1 + \eta_g)} \left[1 - \sqrt{1 - \frac{VZ_o}{E_o}} \right] \right\} . \qquad (14)$$

where $(I_g)_o$ is the grid current at zero anode voltage. Next, examining the cathode current,

$$I_{co} = \underbrace{[1 + (1-x) f\eta_g] I_o}_{\text{low-voltage current}} - \underbrace{(1-f') (1-f) \left[1 - \sqrt{1 - \frac{VZ_o}{E_o}} \right] I_o}_{\text{charged-particle current returning to the cathode due to the fall-back particles which get past the grid}}$$

$$\underbrace{+ (1-x') f' \eta_g' (1-f) \left[1 - \sqrt{1 - \frac{VZ_o}{E_o}} \right] I_o}_{\text{secondary-electron current flowing to cathode due to fall-back particles which strike the grid}}$$

$$= [1 + (1-x) f\eta_g] I_o - [(1-f') - (1 - x') f' \eta_g'] (1 - f) \left[1 - \sqrt{1 - \frac{VZ_o}{E_o}} \right] I_o$$

$$= (I_{co})_o \left\{ 1 - \frac{[(1 - f') - (1 - x')f'\eta_g'] (1 - f) \left[1 - \sqrt{1 - \frac{VZ_o}{E_o}} \right]}{[1 + (1-x)f\eta_g]} \right\} , \qquad (15)$$

where $(I_{co})_o$ is the cathode current at zero anode voltage.

The net current, which is the charging current available to charge the anode, is the algebraic sum of the grid and cathode currents and can be written as

$$I_c = I_{co} + I_g$$

$$= [1 - f (1 - x\eta_g) I_o - [1 - f'(1 - x'\eta_g')] (1 - f) \left[1 - \sqrt{1 - \frac{VZ_o}{E_o}} \right] I_o$$

$$= (I_c)_o \left\{ 1 - \frac{[1 - f'(1 - x'\eta_g')] (1 - f) \left[1 - \sqrt{1 - \frac{VZ_o}{E_o}} \right]}{[1 - f(1 + x\eta_g)]} \right\} , \qquad (16)$$

where $(I_c)_o$ is the net current at zero anode voltage. This relation can be written in more compact form as

$$I_c = (I_c)_o \left\{ 1 - k \left[1 - \sqrt{1 - \frac{VZ_o}{E_o}} \right] \right\} , \tag{17}$$

where

$$k = \frac{[1 - f'(1 - x'\eta_g')]\,(1 - f)}{[1 - f(1 + x\eta_g)]} , \tag{18}$$

and $k \geq 1$ always. Note that for a perfectly transparent grid ($f' = f = 0$), we have

$$I_c = (I_c)_o \sqrt{1 - \frac{VZ_o}{E_o}} , \tag{19}$$

which is equivalent to Equation (12). It is seen from Equation (17) that the effect of the "fall-back" particles is to reduce the charging current to the anode. The smaller the value of k, the less the reduction.

Similar considerations to those above for the coaxial-cylinder geometry lead to a charging current for the parallel-plane case at large anode voltage of

$$I_c = (I_c)_o \,(1 - k\sqrt{\beta}) . \tag{20}$$

Note that in the ideal case of concentric spheres, where the cathode is small enough to appear as a point source to the collector, there are no fall-back particles, which further emphasizes the desirability of spherical geometry. Of course, when the emitted particles are not monoenergetic, a fall-back problem arises even in the spherical case.

The factors appearing in the expressions for the cell currents at large anode voltage should be independent of anode voltage, except perhaps the x and x′ factors. The fraction of secondary electrons formed at the grid which escape to the anode is sensitive to the configuration of the electric field in the vicinity of the grid wires.

CONVERSION EFFICIENCY OF GRIDDED DEVICES

The conversion efficiency of ideal alpha cells (completely transparent but completely effective grid) was discussed earlier. This section of the report analyzes briefly the effect of a grid with finite f-factor on conversion efficiency. As before, the discussion is presented in terms of the three common geometries with only a brief look at uncommon ones.

Common Geometries

Concentric Spheres

As shown previously, the concentric spherical geometry, with emitter diameter much smaller than collector diameter, is unique in that there is ideally no problem

with fall-back alpha particles. In this case, the only effects of the grid are the blockage of a small fraction of the alpha particles and a current loss due to secondary-electron production at the grid. The efficiency in this geometry for a gridded device is thus

$$P = C\beta \tag{21}$$

where $C = \frac{(I_c)_o}{2I_o}$ and $(I_c)_o$ is defined from Equation (10). As the grid approaches transparency, C approaches 1/2 and Equation (21) becomes identical with the efficiency expression developed for an ideal grid.

Coaxial Cylinders

In the coaxial-cylinder geometry with emitter diameter << collector diameter, the expression for efficiency in a gridded device becomes

$$P = C\beta\left[(1 - k) + k\sqrt{1 - \beta}\right] \tag{22}$$

compared with $P = 1/2\ \beta\sqrt{1 - \beta}$ for the ideal case. Expressed in this fashion, $C = \frac{(I_c)_o}{2I_o}$ accounts for the effects of grid blockage and k for the effects of the fall-back alphas. By differentiation of this expression, it can be seen that peak efficiency occurs at a voltage given by

$$\beta = \frac{2}{9}\left[(3 - q) - \sqrt{q(q + 3)}\right] \tag{23}$$

where $q = \left(\frac{k-1}{k}\right)^2$. Note that when k = 1 (transparent grid), $\beta = 2/3$ for peak efficiency, but as k increases from unity, the voltage at which maximum efficiency occurs decreases.

Parallel Planes

Similar analysis shows that for a parallel-plane geometry infinite in extent, for a gridded device

$$P = C\beta(1 - k\sqrt{\beta}) \ , \tag{24}$$

compared with the ideal efficiency of $P = 1/2\ \beta\ (1 - \sqrt{\beta})$. The effects of the grid are similar to those in the coaxial cylinder case.

The analyses clearly show that, except for the ideal concentric spherical geometry, it is extremely important to minimize the factor k in a device constructed in a geometry approximately one of the common geometries. The effect of a grid on efficiency is illustrated in Figure 5 for several values of k and for a coaxial-cylinder geometry. The values of k selected for this illustration correspond approximately to the following parameters:

k = 1: a transparent grid, $f' = f = 0$

k = 1.5: a "reasonable" grid, $f' = f = 0.1$

k = 5: a worst case, $f' = 1.0$, $f = 0.1$,

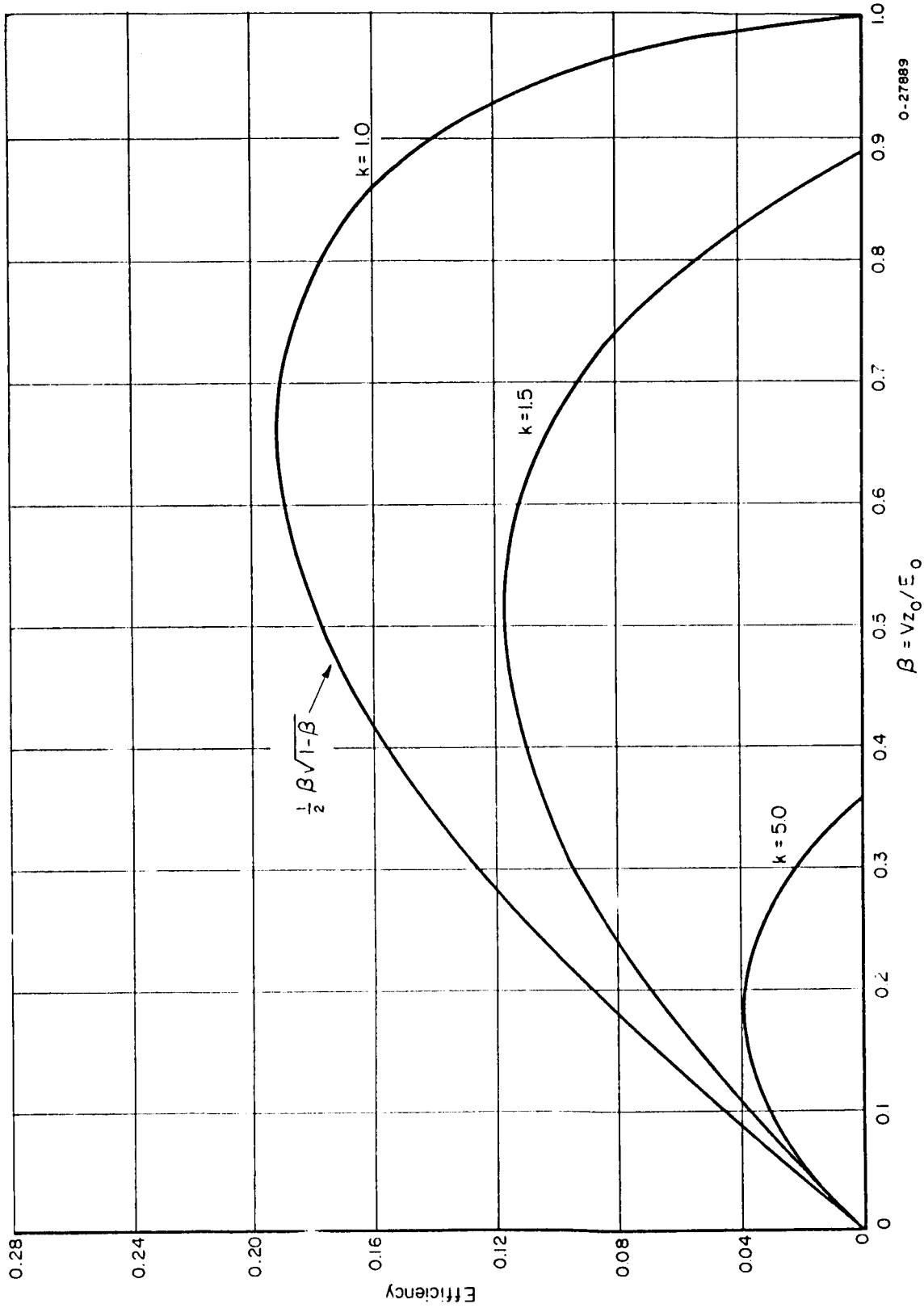

FIGURE 5. EFFICIENCY FOR COAXIAL CYLINDRICAL GEOMETRY WITH GRID

Thin-film coating; one-sided emission

where, for the sake of example, values of the other parameters have been selected as $x = 0.1$, $x' = 1.0$, $\eta_g = \eta_g' = 5$. It is seen from this graph that for a k value of only 1.5, the peak efficiency is reduced from 19 per cent in the ideal case to approximately 12 per cent. A large k reduces efficiency even more drastically.

Uncommon Geometries

Although each geometry must be considered separately, several general facts can be pointed out concerning the efficiency of gridded devices in the uncommon geometries. If complete electrostatic focusing of the alpha particles away from the grid is accomplished in a certain geometry, the fall-back problem with the alpha particles is completely removed. In this case the only effects of the grid are blockage of alpha particles and production of secondary electrons; i.e., $k = 1$ and the change in efficiency from an ideal device is contained in the factor $C = \frac{(I_c)_o}{2I_o}$. This savings provides further incentive to seek geometries in which at least partial electrostatic focusing can be accomplished.

GRID-DESIGN PRINCIPLES

From the previous discussion it is clear that the most critical element in the operation of the alpha cell is the grid. Its presence is a fundamental principle of operation, but by the same token an improperly designed grid can negate the usefulness of the concept. It is the purpose of this section of the report to present the existing technology of grid design relating to the alpha cell. This can perhaps best be done by considering first-order principles for grid design and then discussing principles relating to second order effects, many of which must be evaluated experimentally.

First-Order Design Principles

To first-order principles, grid design is related to two parameters: the f-factor and the effective amplification factor (or μ-factor), which is the ratio of anode voltage to the grid voltage required to maintain this prescribed anode voltage. In the discussion which follows, it is convenient to describe grid design in terms of a coaxial cylinder geometry, with a squirrel-cage grid around the cathode, but the design principles obviously apply to other geometries.

f-Factor

As previously defined, the f-factor is the fraction of alpha particles escaping the cathode which strikes the grid. Since current losses due to the presence of the grid are proportional to $f(1 + x\,\eta_g)$, i.e., directly proportional to f, and since the magnitude of the k factor is also related to the magnitude of f, it is important that the grid have a small f-factor.

To a first approximation, the f-factor for a long squirrel-cage grid is simply the fractional area of the grid circle cylinder blocked by the grid wires,

$$f \cong \frac{N d_g}{2\pi r_g} \quad , \tag{25}$$

where N = number of grid wires

d_g = diameter of wires

r_g = radius of grid cage circle.

A more refined analysis shows that for finite cathode radius the f-factor is slightly larger than the simple area ratio of Equation (25). To a good approximation the f-factor is given by

$$f = \frac{N d_g \theta}{6\pi^2} \left[\frac{1}{(r_g - r_c)} + \frac{4}{g} + \frac{1}{(r_g^2 - r_c^2)^{1/2}} \right] , \tag{26}$$

where

r_c = cathode radius

$$\cos \theta = \frac{r_c}{r_g}$$

$$g = r_c \left[\frac{1 - \cos \theta}{2} + \left(\frac{1}{\cos \theta} - \sqrt{\frac{1 + \cos \theta}{2}} \right)^2 \right]^{1/2} .$$

This approximation is valid under the conditions that

$$\tan \left(\frac{d_g}{r_g - r_c} \right) \cong \left(\frac{d_g}{r_g - r_c} \right) \text{ and } L >> 2 (r_g - r_c),$$

where L is the length of the grid wires. It can be seen that as r_c approaches zero, the more complex relation of Equation (26) approaches the simple area ratio of Equation (25). The difference in the two equations can be illustrated by the grid used in the initial alpha cell experiments. With $N = 40$, $d_g = 0.010$ in., $r_g = 0.625$ in., and $r_c = 0.250$ in., the area ratio gives $f = 0.113$, compared with $f = 0.120$ from Equation (26); the true f-factor is about 6 per cent larger than the area ratio for this case.

For normal operating grid voltages, the f-factor is purely a geometrical factor. However, for very large grid voltages, the grid (at negative bias) attracts alpha particles and hence the f-factor increases with voltage. An approximate expression for the voltage dependency of the f-factor is

$$f = f_o \sqrt{1 + \frac{Z_o V_g}{E_o}} \quad , \tag{27}$$

where

f_o = geometric f-factor as calculated from Equation (26)

Z_o = charge on the alpha particle

E_o = energy of the alpha particle in electron volts.

Since (E_o/Z_o) is of the order of 10^6, V_g must be of the order of 10^5 volts for this correction to become significant.

Amplification Factor

The amplification factor is the magnitude of the ratio of anode voltage to the grid voltage required to maintain this prescribed anode voltage. Thus, a grid with high amplification factor requires a small bias to suppress the secondary electrons formed at the cathode in the presence of a large anode voltage. This, in turn, alleviates the problem of high voltage gradients across the electrical insulators between the grid and cathode or, alternatively, permits the grid to be located closer to the cathode (since it can operate at low voltage), resulting in a more compact device. Unfortunately, as will be shown, a high amplification factor is generally associated with a large f-factor grid, which lowers the efficiency of the device. Thus, optimum conditions must be sought in the grid design.

In an ordinary triode electron tube, the amplification factor is the ratio of the plate voltage to the negative of grid voltage for a condition of cutoff. In terms of the electric field within the tube, cutoff exists when the gradient of the potential at the cathode is zero.[4] From analysis by Spangenberg, the resulting amplification factor (or mu-factor) for a cylindrical squirrel-cage grid is[5]

$$\mu = \frac{-N \ln\left(\frac{r_p}{r_g}\right)}{\ln\left[2 \sin\left(\frac{N d_g}{4 r_g}\right)\right]} , \tag{28}$$

where r_p is the radius of the anode (plate). This equation is valid for triode tubes with screening fraction approximately 0.1 or less. [The screening fraction is the ratio of grid wire diameter to grid wire spacing, or simply the f-factor as calculated from Equation (25).] For most grid designs of interest, $\sin\left(\frac{N d_g}{4 r_g}\right) \cong \left(\frac{N d_g}{4 r_g}\right)$ so that Equation (28) can be simplified to

$$\mu = -\frac{N \ln\left(\frac{r_p}{r_g}\right)}{\ln\left(\frac{N d_g}{2 r_g}\right)} \cong \frac{N \ln\left(\frac{r_p}{r_g}\right)}{\ln\left(\frac{1}{\pi f}\right)} . \tag{29}$$

To a first-order approximation, this definition of amplification factor may be used in designing the alpha cell. The principal approximation comes about by neglecting the initial energy of the secondary electrons.

By inspection of Equation (29), it is seen that the amplification factor increases with the number of grid wires, since N appears as a linear factor in the numerator whereas it is only as a logarithmic factor in the denominator. It also increases with anode radius and grid-wire diameter. The amplification factor decreases as the radius of the grid cage increases. This equation can be used in conjunction with (25) or (26) to optimize the relation between μ and f if several of the variables are fixed by other restrictions. For example, Cranberg's criterion for voltage breakdown in vacuum[6] determines the spacing required between the grid and anode. Also, required structural strength of the grid can restrict the values of the grid-wire diameter.

Second-Order Effects Influencing Grid Design

Although the f-factor and amplification factor are critical to grid design, several other factors may have significant influence on grid design. Examples of such factors are

(1) Dependence of secondary-electron yield at the grid on grid-wire material. [Since losses are proportional to $f(1 + x\eta_g)$, in addition to minimizing f, it is desirable to choose grid wire material to minimize η_g, or hence the secondary electron yield at the grid, $\Delta_g = Z\eta_g$.]

(2) Dependence of secondary yield on electric field. For secondaries produced at the grid wires at locations exposed to the anode field, a significant increase in Δ_g might occur because of the electric field. Depending on the importance of this effect, it might be desirable to stagger the distance of the grid wires from the cathode.

(3) Gamma-induced secondary electron emission. For alpha emitters, such as polonium-210, which have very weak associated gamma radiation, the electron production due to the gamma radiation can generally be ignored. A small effect due to gamma-induced secondary emission at the grid wires might be observable for alpha emitters with appreciable associated gamma radiation, such as curium-244. The emission for metals is of the order of 0.5×10^{-16} amp/cm^2 per roentgen/hr.[7, 8]

(4) Bremsstrahlung production. The leakage current from grid to anode due to secondary-electron production at the grid constitutes a source of bremsstrahlung at the anode. The electrons leaking from the grid are accelerated by the anode field to energy equivalent to the anode voltage, and hence strike the anode with energy of the order of 1 Mev. The leakage current, and hence the bremsstrahlung production, is proporational to $(xf\eta_g)$, i.e., directly proportional to f. The radiation thus produced, in addition to presenting a possible hazard, can in turn produce secondary emission of magnitude discussed in Item (3).

(5) Structural strength of grid. At large anode voltage, the electrostatic force of attraction between anode and grid is sufficiently strong to deflect the grid wires if they are constrained only at the ends of the grid. Use of containing rings spaced along the squirrel-cage grid minimizes this deflection.

SPACE-CHARGE LIMITATION

It is to be expected that the limitation imposed on the current in the alpha cell because of space-charge effects is not a serious one since the alpha cell is basically a low-current, high-voltage device. A brief analysis of the space-charge-limited current in a simplified geometry is presented here to illustrate the magnitude of the effect.

The basic relations for charge flow at equilibrium in a space between two conductors are (in MKS units)

Poisson's equation: $$\nabla^2 V = -\rho/\epsilon_o \tag{30}$$

Continuity equation: (conservation of charge) $$\underline{\nabla} \cdot \underline{J} = 0 \tag{31}$$

Conservation of energy: $$E_o = \left(\frac{1}{2}\right) Mv^2 + Z_o V, \tag{32}$$

where the current density $\underline{J}$ is given by

$$\underline{J} = \rho \underline{v} , \tag{33}$$

and where ρ = charge density

$\underline{v}$ = alpha-particle velocity

M = mass of alpha particle (of initial energy E_o and charge Z_o)

ϵ_o = permittivity of free space

V = voltage

For simplicity the geometry used in this analysis is that of two infinite parallel-plane electrodes spaced a distance x_o apart. In this geometry, V, ρ, and v are functions of x only. The current flow per unit area from the emitter is the x-component of $\underline{J}$. Only the kinetic energy E_{ox} associated with the x-component of the velocity is transformed into potential (electrostatic) energy; the remaining energy is dissipated at the cathode.

The boundary conditions to be applied to the solution to the basic relations (30) through (32) are

$$V(0) = 0$$
$$\left(\frac{dV}{dx}\right)_{x = x_o} = 0 \tag{34}$$

This second condition is an approximation based on the fact that the large number of positive ions in the neighborhood of the collector ($x = x_o$) neutralizes the field in this region. That there is a buildup of ions near the collector is seen from the solution to Equation (31) that $J_x = \rho v_x$ = constant, and since the kinetic energy is dissipated in overcoming the potential barrier, near the collector v_x is small so that ρ must be large.

The general solution to the problem is the implicit relation

$$\left(\frac{J_x Z_o \sqrt{\frac{M}{2}}}{4\epsilon_o}\right)^{1/2} x = \frac{1}{3}\left\{\left[E_{ox}^{1/2} - (E_{ox} - Z_o V_A)^{1/2}\right]^{3/2}\right.$$

$$- \left[(E_{ox} - Z_o V)^{1/2} - (E_{ox} - Z_o V_A)^{1/2} \right]^{3/2} \Bigg\}$$

$$+ (E_{ox} - Z_o V_A)^{1/2} \left\{ \left[E_{ox}^{1/2} - (E_{ox} - Z_o V_A)^{1/2} \right]^{1/2} - \left[(E_{ox} - Z_o V)^{1/2} - (E_{ox} - Z_o V_A)^{1/2} \right]^{1/2} \right\} , \quad (35)$$

where V_A is the collector (anode) voltage. At $V = V_A$ (at $x = x_o$), Equation (35) simplifies to

$$\left(\frac{J_x Z_o \sqrt{\frac{M}{2}}}{4\epsilon_o} \right)^{1/2} x_o = \frac{1}{3} \left[E_{ox}^{1/2} - (E_{ox} - Z_o V_A)^{1/2} \right]^{3/2}$$

$$+ (E_{ox} - Z_o V_A)^{1/2} \left[E_{ox}^{1/2} - (E_{ox} - Z_o V_A)^{1/2} \right]^{1/2} . \quad (36)$$

To obtain an estimate of J_x from this expression, it is assumed that $V_A = \frac{E_{ox}}{Z_o}$. With this value of anode voltage, the cathode current density is

$$J_x = \left(\frac{4\epsilon_o \sqrt{\frac{2}{M}}}{9 Z_o} \right) \left(\frac{E_{ox}^{3/2}}{x_o^2} \right) . \quad (37)$$

This represents the maximum current density that can be obtained for a given spacing at full anode voltage, i.e., this is the space-charge-limited current. (A larger current is obtained if the anode voltage is reduced from the maximum possible value of E_{ox}/Z_o.)

The magnitude of the space-charge-limited current may be estimated by assuming the following "typical" values for the parameters

$E_{ox} = \frac{1}{3} E_o = 1.7$ Mev $= 2.7 \times 10^{-13}$ nt-m

$Z_o = 2e = 3.2 \times 10^{-19}$ coul

$x_o = 10$ cm $= 0.1$ m

$M = 4$ amu $= 6.6 \times 10^{-27}$ kg

$\epsilon_o = 8.85 \times 10^{-12}$ coul^2/nt-m^2,

which gives $J_x = 3 \times 10^3$ amp/m^2 $= 0.3$ amp/cm^2. At the assumed voltage, this is equivalent to a power density of 250,000 watts/cm^2! This large value for J_x, and hence for the power density, indicates that space-charge effects are negligible for the alpha-cell concept. A typical alpha-cell system might operate at a current density of about 10^{-7} amp/cm^2. Such conditions are seen to be a factor of 10^6 below the limitations set by space-charge effects. The limiting current for a cell with cylindrical or spherical geometry is greater than that for the parallel planes, with the same electrode spacing. Since the limiting current was so large in the case considered, the other geometries were not considered in detail.

MAGNETIC SUPPRESSION OF SECONDARY ELECTRONS

An alternative method of suppressing the secondary-electron emission accompanying the emission of alpha particles from the cathode is the application of an axial magnetic field. Such an arrangement would eliminate the efficiency loss due to the presence of the grid. However, as will be shown from the analysis summarized below, the intensity of magnetic field required for effective secondary-electron suppression in the presence of a megavolt anode potential is of the order of 1000 gauss and thus impractically large.

For concentric-cylinder electrodes with the outer electrode (anode) of diameter b and inner electrode (cathode) of diameter a, the electric field produced by anode voltage V_A is

$$\underline{E} = \frac{V_A}{r \ln \left(\frac{a}{b}\right)} \underline{e}_r \tag{38}$$

where r is the radial distance and $\underline{e}_r$ is the unit vector in the radial direction. An electron emitted at the cathode is accelerated to the anode by the force $q\underline{E}$, where q is the electron charge. Since it is desired that only the positively charged alpha particles reach the anode, to prevent electron transfer the magnetic force must oppose and exceed the electrostatic force. An axial magnetic field $\underline{B}$ will produce a force which, if sufficiently large, will curl the electrons back to the cathode. The net force on an electron is then

$$\underline{F} = q(\underline{E} + \underline{v} \times \underline{B}) . \tag{39}$$

Although the electron emission may be isotropic, the magnetic field required for complete suppression must be of sufficient magnitude to return those electrons with initial energy U_s emitted radially. Allowing for relativistic electron energies, Schock[9] derived an expression for the magnitude of the axial magnetic field required to completely turn back electrons of initial energy U_s (in ev):

$$B = \frac{2U_o}{bc\,(1-\beta^2)} \left\{ \left[\left(\frac{U_s + V_A}{U_o} + 1 \right)^2 - 1 \right]^{1/2} + \beta \left[\left(\frac{U_s}{U_o} + 1 \right)^2 - 1 \right]^{1/2} \right\} , \tag{40}$$

where

B = axial magnetic field, webers/m^2

β = a/b

c = velocity of light, m/sec

U_o = rest-mass energy of an electron, ev

V_A = anode voltage.

Since the secondary electrons have energies at birth of the order of a few ev, and nearly all have energy less than 100 ev, the initial energy U_s can be neglected with respect to V_A and U_o.* The magnetic field required to suppress zero-energy electrons (i.e., low-energy secondaries) is given from Equation (40) as

$$B(0) = \frac{2U_o}{bc\,(1-\beta^2)}\left[\left(\frac{V_A}{U_o}+1\right)^2 - 1\right]^{1/2}, \qquad (41)$$

where b, the anode diameter, is expressed in meters.

To obtain an estimate of the magnitude of the magnetic field required to suppress the secondary electrons, β^2 can be neglected compared with unity. Figure 6 is a plot of Equation (41) with this approximation. It is seen that for anode voltages of interest, the product (Bb) must lie in the range of 0.01 to 0.02 weber/m. Thus for anode diameter of 0.2 m (20 cm), an axial field of the order of 0.1 weber/m^2 (1000 gauss) is required.

To obtain a 1000-gauss magnetic field over the volume of an alpha cell is prohibitive from the standpoint of magnet weight and power loss. For these reasons, the choice of a grid to suppress secondary electrons appears to be imperative.

SELECTION OF AN ALPHA EMITTER FOR THE ALPHA-ELECTRIC CELL

Since nearly all alpha emitters occur in the range of high atomic number, the selection of a cathode coating material is limited to those radioisotopes above bismuth (Z = 83) in the periodic table. Although the number of alpha-emitting radioisotopes in this range is large, only a few have half-lives in the range dictated by power and lifetime requirements for a useful system. Assuming the minimum system lifetime of interest to be about 6 months, the lower limit of isotope half-life should be no less than 3 or 4 months. The upper limit of half-life is prescribed by maximum power output required, since these two parameters are inversely related, i.e., as half-life increases, specific power available decreases. Thus, the half-life range of interest is from about 3 months to a few hundred years. The alphas in this limited range of half-lives have similar decay energies, virtually eliminating the need for consideration of this parameter in selecting suitable isotopes for the alpha cell.

A recent survey[10] indicates that the most promising alpha emitters for the concept are polonium-210, curium-242, curium-244 and plutonium-238. Table 2 summarizes the properties and cost of these isotopes. There are several other isotopes with half-lives in the required range, notably californium-248, einsteinium-252, and plutonium-236, but these are so rare as to not be given consideration at this time. Another possible emitter, thorium-228 (half-life 1.9 years), decays as part of the thorium (4n) series and is thus a source of undesirable short-lived beta emitters. In addition it is comparatively rare.

*That the required magnetic field is nearly independent of the initial electron energy U_s is due to the fact that, in the presence of an anode potential of the order of a megavolt, most of the energy of the electron as it moves toward the anode is in the form of an increase in kinetic energy acquired from the electric field.

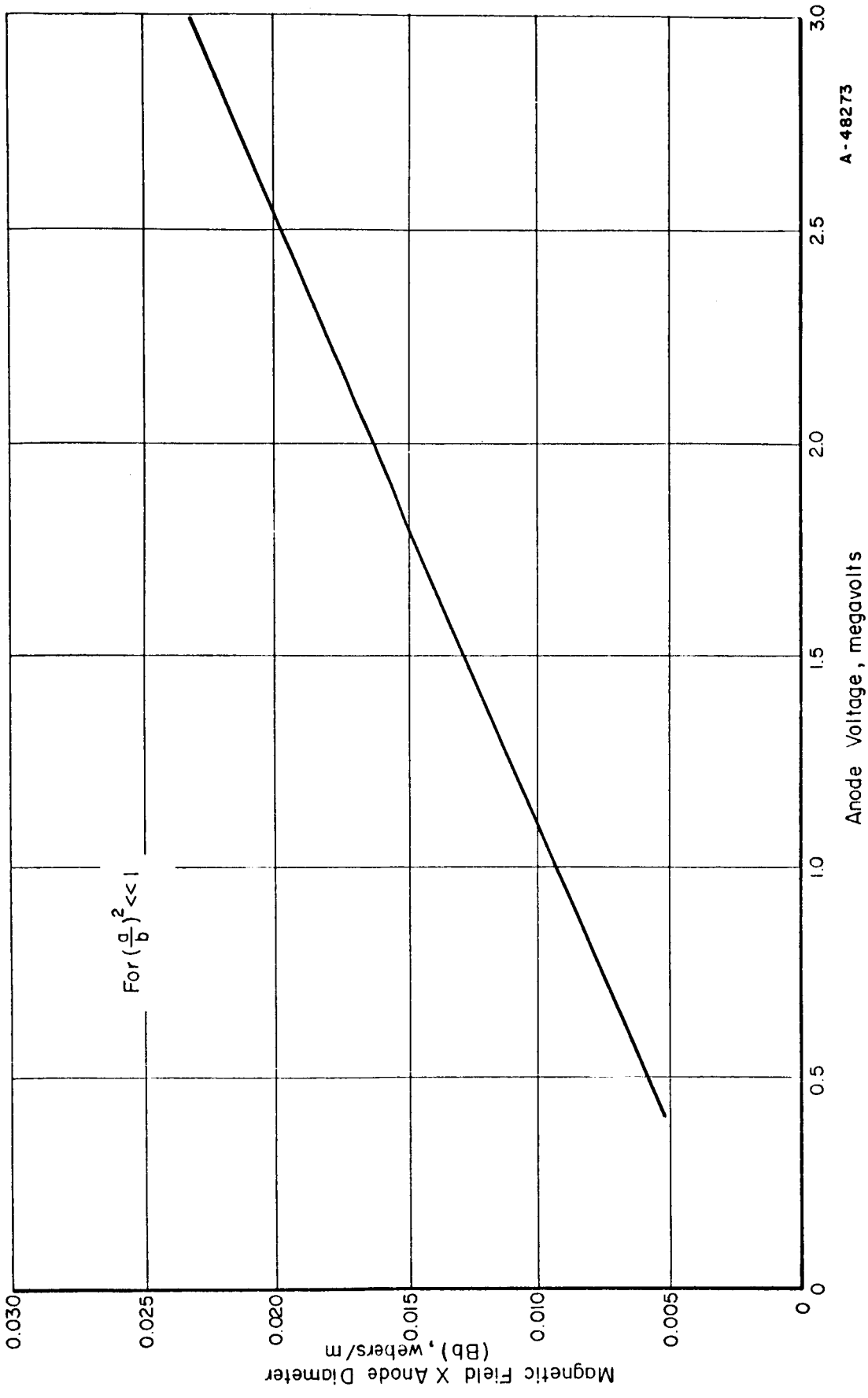

FIGURE 6. MAGNETIC FIELD REQUIRED TO SUPPRESS SECONDARY ELECTRONS

TABLE 2. ALPHA EMITTERS APPLICABLE TO ALPHA-CELL CONCEPT[a]

Isotope	Alpha Energy, Mev	Half-Life, years	Chemical Form	Thermal Power, watts/g	Projected Cost[b], $ per thermal watt
Polonium-210	5.3	0.38	Metal	140	190
Plutonium-238	5.5	90	Metal	0.48	1040
Curium-242	6.1	0.44	Oxide	120	165
Curium-244	5.8	18	Oxide	2.3	435

(a) Most data from Reference (10).
(b) Polonium-210 is the only isotope currently available in large quantity. Its present cost is $640 per thermal watt.

Along with the emergence of alpha-particles from the emitters listed in Table 2 come gamma rays, which present a low-level shielding problem. In addition secondary reactions, or in some cases spontaneous fission, provide a source of neutrons. Table 3 summarizes the radiation from 100-watt (thermal) bare alpha sources for the first three isotopes of Table 2. As seen from these data, the two short-lived isotopes have comparable radiation attendant their use. The radiation from plutonium-238 is about two orders of magnitude less.

TABLE 3. RADIATION FROM 100-WATT (THERMAL) BARE ALPHA SOURCES[a]

Isotope	Gamma Radiation, millirem/hr at 1 yard	Neutron Radiation, millirem/hr at 1 yard	Total Radiation, millirem/hr at 1 yard
Polonium-210	20.0	6.5	26.5
Curium-242	4.3	32.5	36.8
Plutonium-238	0.01	0.53	0.53

(a) Data from Reference (10).

It is apparent from this brief survey of available emitters that mission lifetime will be the principal factor in dictating the selection of alpha emitter from the four listed in Table 2. Only for the short mission is a choice really available (polonium-210 versus curium-242).

ENERGY SPECTRUM OF ALPHA PARTICLES

The energy spectrum of alpha particles emerging from the cathode was analyzed for two cases: a thin layer of alpha emitter covered by a thick metallic foil (the case applicable to experiments performed to date) and a thick layer of alpha emitter with no cover (probable case in an actual alpha-cell generator).

Case I. Thin Emitter With Thick Metallic Cover

The geometry for the calculations is shown in Figure 7. Assuming a constant stopping power, (dE/dx), to first order approximation gives the energy spectrum for a cover thickness t as

$$N(E) = \frac{N_o}{2} \frac{t}{R} \frac{E_o}{(E_o - E)^2} \qquad 0 \leq E \leq E_o (1 - t/R) \ , \tag{42}$$

where $N_o/4\pi$ is the number of particles emitted per unit solid angle per unit time (isotropic emission), E_o is the initial energy of the particles, and R is the range of an alpha particle with energy E_o in the cover material. Figure 8 is a plot of this energy spectrum for several values of t/R and for polonium-210 alphas. Of course, with no cover thickness the particles emerging from the cathode are monoenergetic. The number of particles escaping the cathode under the conditions of Case I is $(N_o/2)(1 - t/R)$ for one-sided emission.

The spectrum derived under the assumption of constant dE/dx can be compared with that derived using the experimentally determined variation of stopping power with energy. For the case of alpha particles in gold[11], the comparison of calculated energy spectrum from a 0.1-mil gold cover when using constant versus variable dE/dx is shown in Figure 9. The degree of correspondence encourages the use of a constant-stopping-power model for approximate calculations.

Case II. Thick Emitter With No Cover

The geometry for this calculation is sketched in Figure 7b. Again assuming constant (dE/dx), the calculated energy spectrum for emitter thickness t is

$$N(E) = \begin{cases} \dfrac{N_o}{4} \dfrac{t}{R} \dfrac{E_o}{(E - E)^2} & E \leq E_o (1 - t/R) \\ \dfrac{N_o}{E_o} \dfrac{R}{4t} & E \geq E_o (1 - t/R) \ . \end{cases} \tag{43}$$

Figure 10 shows this spectrum graphically for several values of t/R. The number of particles escaping the cathode in this case is $(N_o/2)(1 - t/2R)$ for one-sided emission.

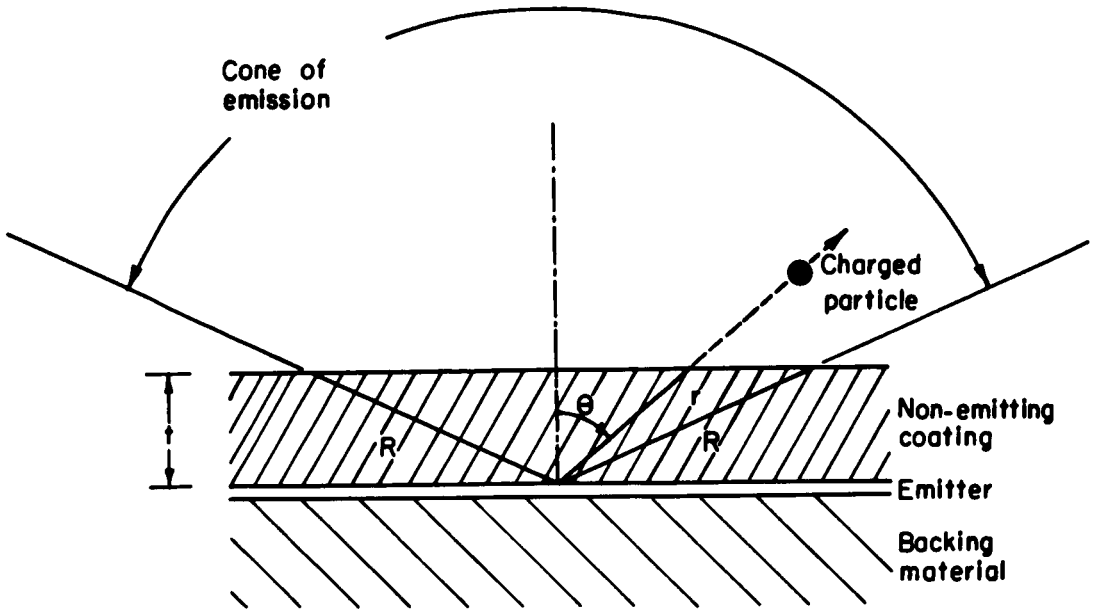

a. Case I

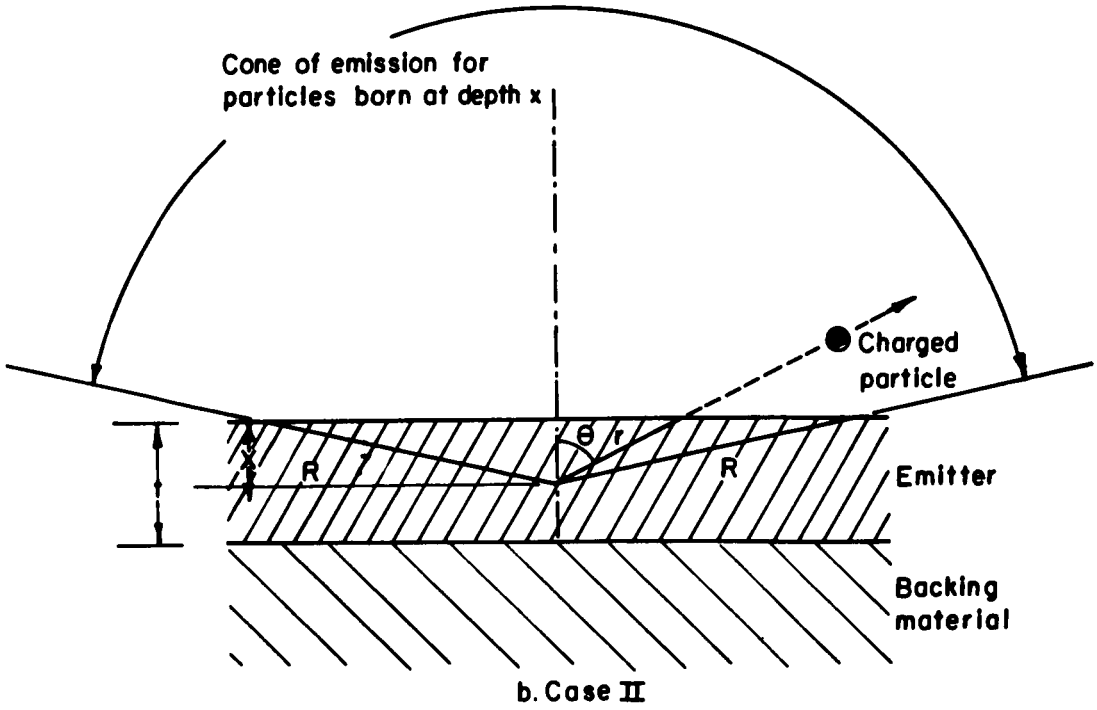

b. Case II

FIGURE 7. GEOMETRIES OF CHARGED-PARTICLE EMISSION

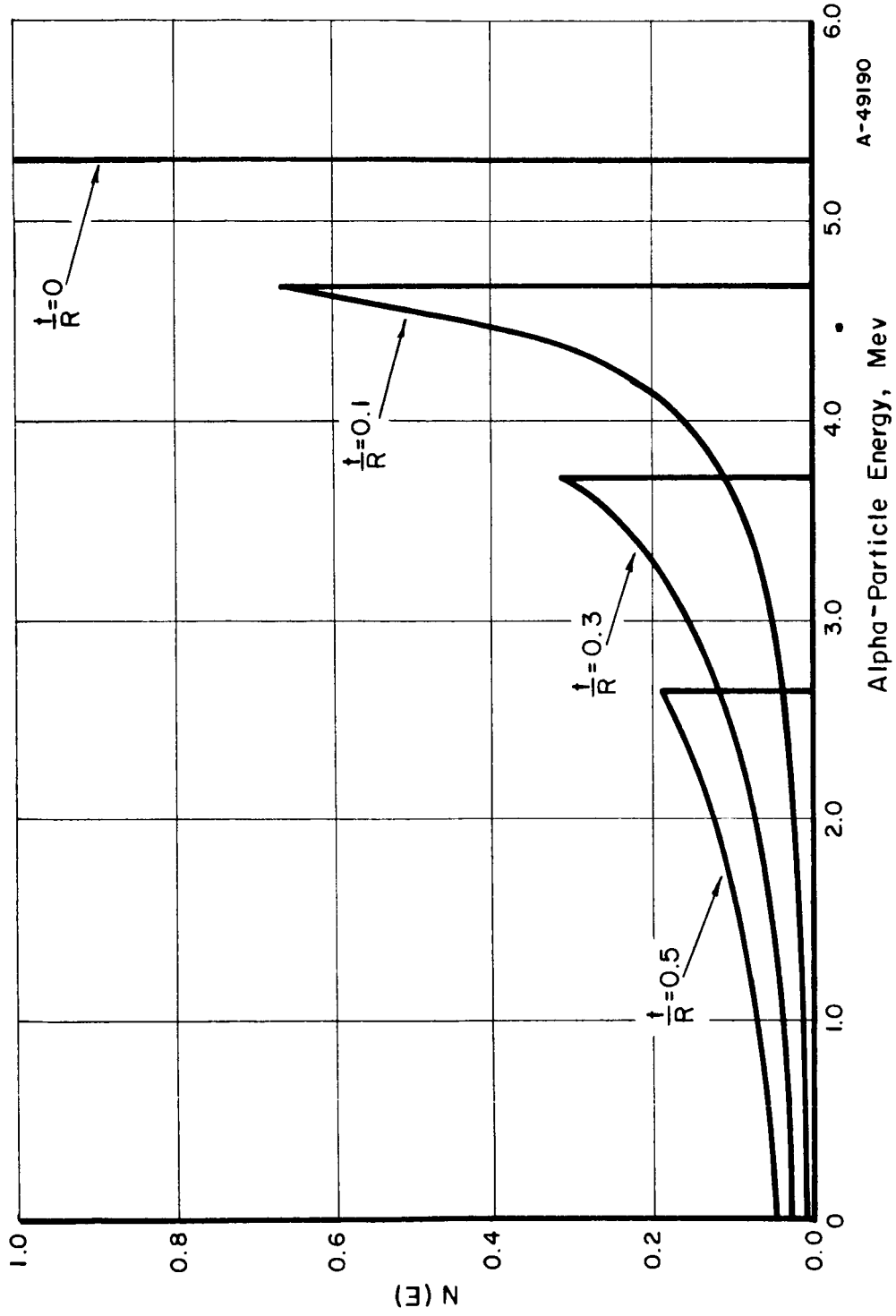

FIGURE 8. CALCULATED ENERGY SPECTRA FOR POLONIUM-210 ALPHA PARTICLES EMERGING FROM COVERING FOILS OF VARIOUS THICKNESS (CASE I)

Thin-emitter constant $\left(\frac{dE}{dx}\right)$.

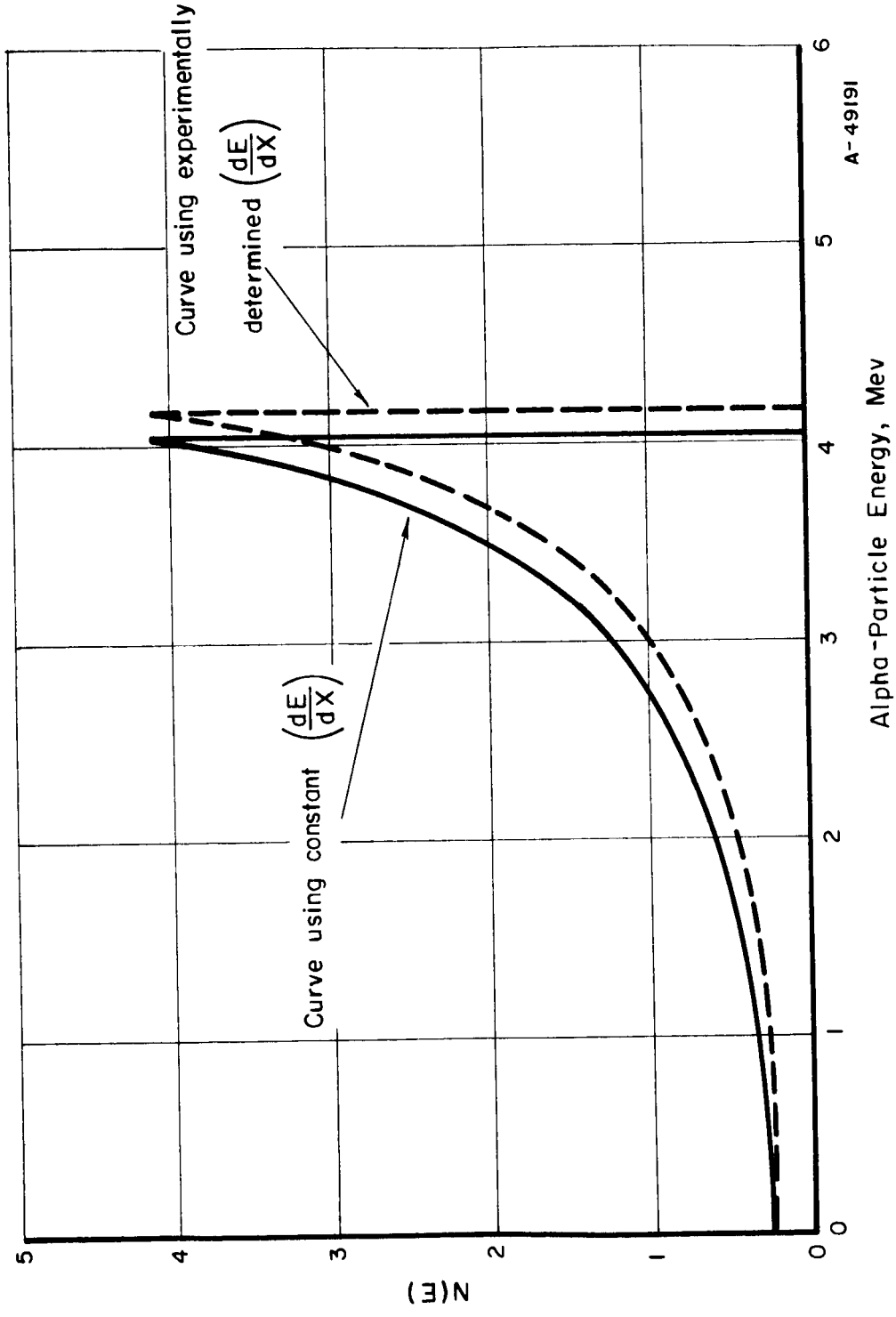

FIGURE 9. CALCULATED ENERGY SPECTRUM FOR POLONIUM-210 ALPHA PARTICLES EMERGING FROM 0.1-MIL GOLD COVER

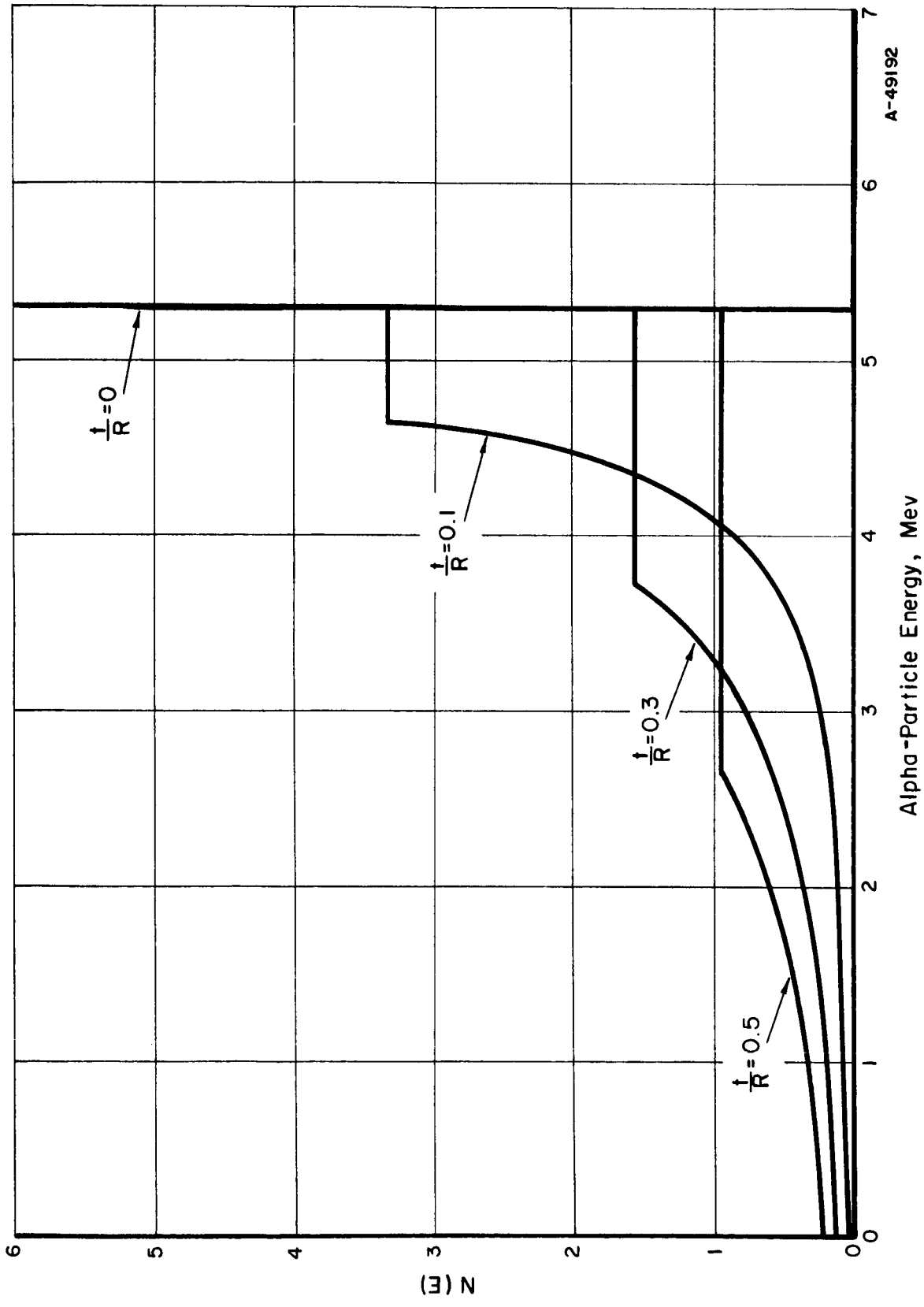

FIGURE 10. CALCULATED ENERGY SPECTRA FOR POLONIUM-210 ALPHA PARTICLES EMERGING FROM POLONIUM-210 FUEL LAYERS OF VARIOUS THICKNESS (CASE II)

EXPERIMENTAL STUDIES

This section of the report describes the experimental studies performed with the alpha cell and summarizes the results. Prior to the initiation of the study under contract with NASA, preliminary experiments aimed at demonstrating proof of principle were performed under Battelle sponsorship. These are summarized briefly to provide the background for a discussion of the more recent results.

RESULTS OF BATTELLE SPONSORED EXPERIMENTS

Preliminary Measurements of Secondary-Electron Emission

During the early conceptual stage of the development of the alpha electric cell, it was postulated that the key to efficient operation would be the use of a properly designed grid interposed between the emitter and collector electrodes. It was further anticipated that the cell simply would not work (i. e., there would be no voltage buildup) without a grid, because of an excessive number of secondary electrons emitted as each alpha particle emerges from the source material. There was no direct experimental evidence to support this belief, although results of early investigations with alpha-particle-induced secondary emission, summarized by H. Geiger[12], indicated yields in the range of 3 to 30 for alpha-particle bombardment of a metal surface. However, the foundation was still sufficiently lacking and warranted a preliminary experiment prior to design and construction of a more complex and expensive experiment in the form of an actual alpha electric cell.

For the preliminary experiment, a small polonium source (2. 5 millicuries at the time of the experiment) was placed in a vacuum chamber, and the emission current measured. The polonium was deposited on a copper backing in a circular area approximately 1 cm in diameter. The source was flashed with a thin gold coating to prevent migration of the polonium and subsequent contamination of the experiment. The secondary-electron emission as the alphas emerge from the gold coating should be similar to that produced by polonium alone (of equivalent thickness), since both elements have similar mass stopping powers for alphas. From measurement of the average energy of the alphas emerging from the source, it was estimated that the gold thickness was about 3 microns. The source was supported in the vacuum facility on an aluminum pedestal electrically insulated from the baseplate.

The emission current was measured as the source was maintained at various negative voltages with respect to the vacuum chamber dome. Data were obtained with and without the source. By subtracting the currents measured under these two conditions, leakage and other extraneous currents were eliminated. The results are shown graphically in Figure 11. With sufficiently large negative bias on the source to return secondary electrons produced at the wall of the vacuum chamber (>400 volts), the source current was measured to be 3.2×10^{-11} ampere. Scatter in the data is attributed principally to the large contribution of background current. To obtain the source current, the data above 400 volts were averaged.

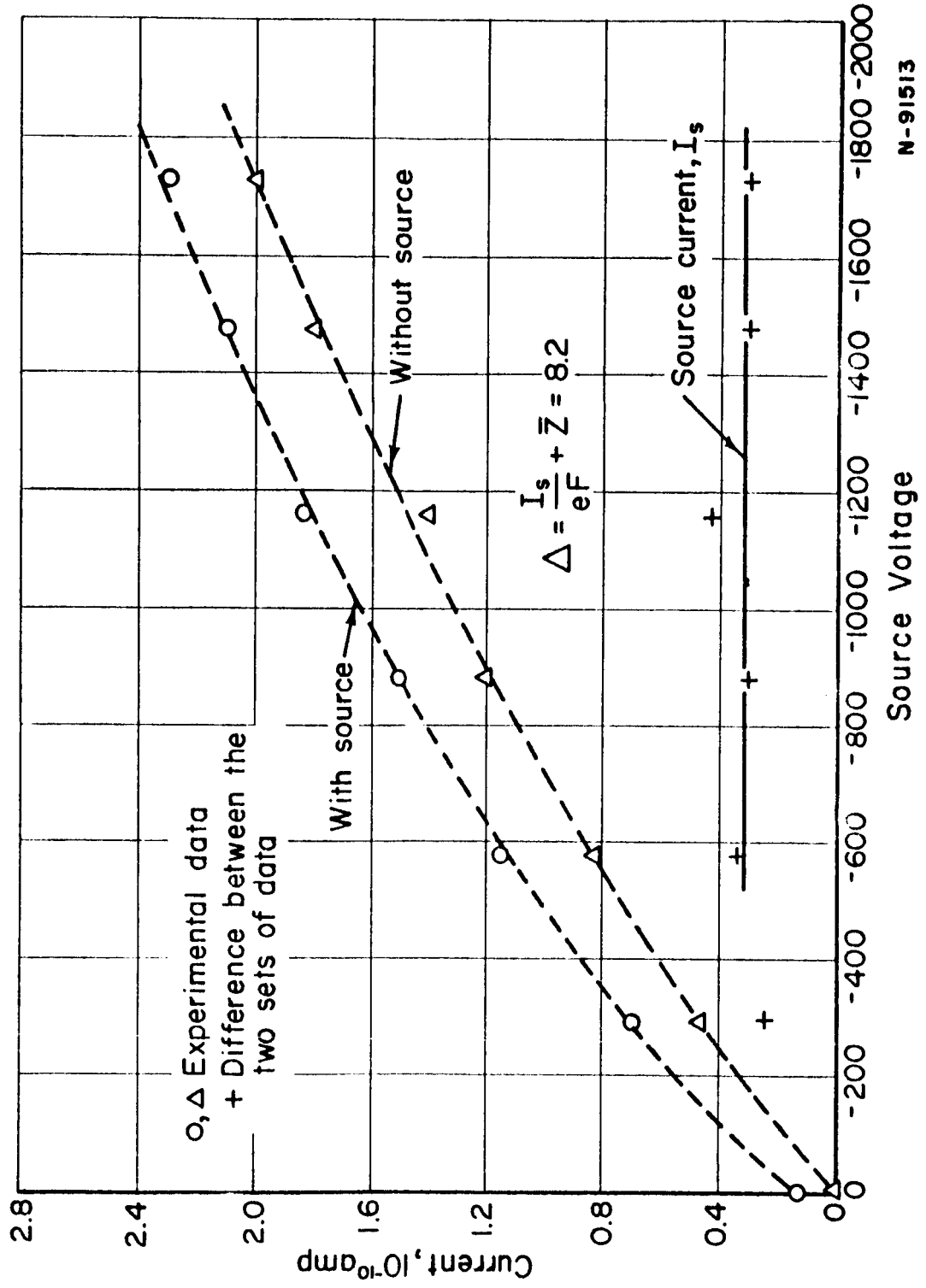

FIGURE 11. SOURCE-CURRENT MEASUREMENT FOR PRELIMINARY EXPERIMENT

Under the conditions of the experiment, the secondary-electron yield is

$$\Lambda = \frac{I_s}{eF} + \overline{Z} , \tag{44}$$

where

I_s = magnitude of the current leaving the source, amperes

$\overline{Z}$ = average charge of an escaping alpha particle

F = number of alpha particles leaving the source per unit time.

$$F = \frac{F_o}{2}\left(1 - \frac{t}{R}\right), \tag{45}$$

where F_o is the disintegration rate in the polonium, t is the thickness of gold, and R is the mean range of alpha particles in gold.* With t/R approximately 0.3, for the 2.5-millicurie source $F = 3.2 \times 10^7$ alphas/second. Since t/R is rather small, to a first approximation it may be assumed that the alpha particles retain their charge of +2. Since the first term in the yield equation is the larger term, the fact that the average charge may be degraded does not seriously affect the results. With these values of F and $\overline{Z}$, and the measured value of $I_s = 3.2 \times 10^{-11}$ ampere, the secondary-electron yield was determined to be 8.2, i.e., on the average 8.2 secondary electrons are emitted as each alpha particle emerges from the surface.

From this preliminary experiment it was concluded that the charge carried by the secondaries is larger than the opposing charge carried by the alphas, verifying the statement that a grid is essential to the operation of the device. On the other hand, the yield is not so large as to magnify the problem of current loss due to secondary-electron production at the grid. (As discussed previously, loss in alpha-particle charging current is proportional to $(1 + x\Lambda_g/\overline{Z})$, where Λ_g is the secondary-electron yield due to a small fraction of alpha particles striking the grid, and x is the fraction of secondaries formed at the grid which escape to the anode.)

The next step in the demonstration of the feasibility of the concept was to construct an actual cell and prove that with proper grid bias a voltage buildup could be obtained.

Initial Experiments With the Alpha Cell

The preliminary proof-of-principle experiments using a polonium alpha emitter were performed in late 1962. Figure 12 shows photographs of the experimental apparatus. The picture to the left shows the grid-cathode assembly used in these experiments. Several curies of polonium-210 were distributed uniformly on a cathode 1/2 inch in diameter by 12 inches long. To minimize contamination of the equipment a thin gold foil (0.0001 inch thick) was wrapped over the bare polonium surface. The cathode was surrounded by a squirrel-cage grid of 40 steel wires 10 mils in diameter equally spaced on a 1.25-inch-diameter grid circle and supported at the ends. As shown by the second photograph in Figure 12, the grid-cathode assembly was inserted

*For the source used in this experiment, the thickness of the polonium itself is much less than that of the gold layer deposited on top of the polonium. The above formula for F consequently differs from the usual relation $F = F_o/2\,(1 - t/2R)$ for a coating in which the alpha particles are born uniformly throughout the coating material.

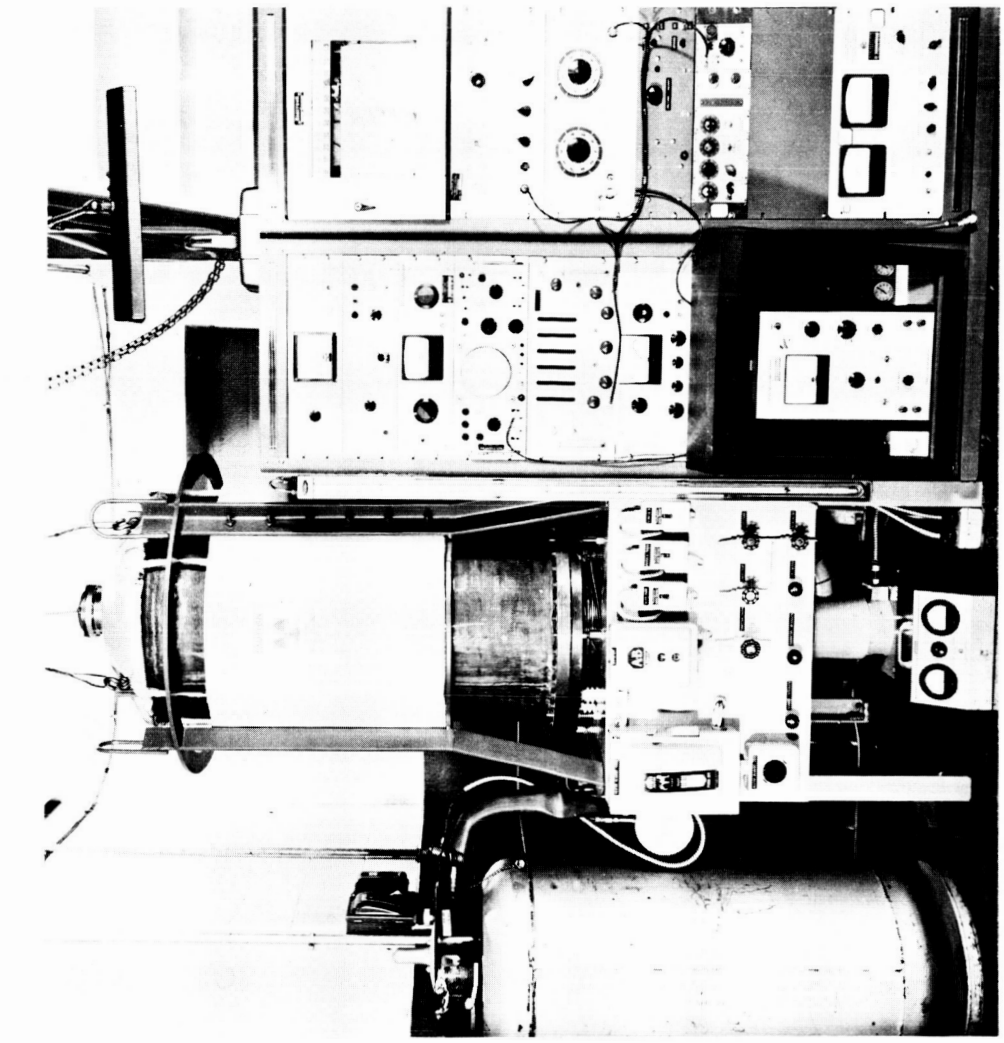

High-Vacuum Facility and Instrument Console N93983

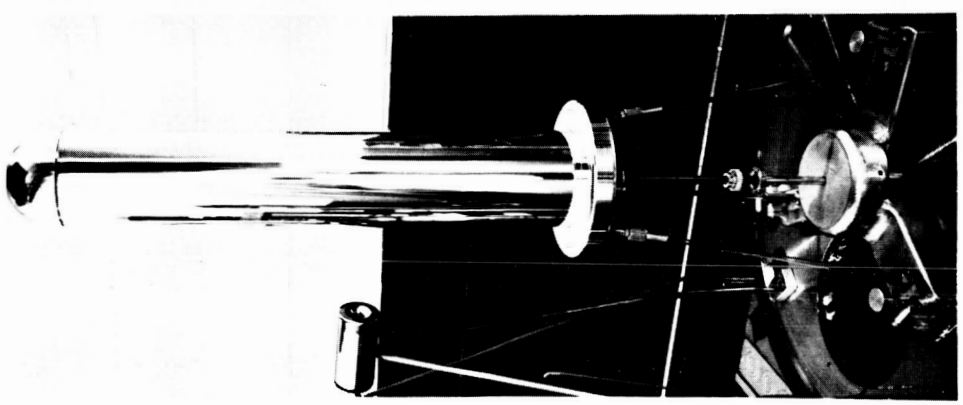

Anode

Grid-Cathode Assembly

FIGURE 12. EQUIPMENT FOR ALPHA-ELECTRIC-CELL EXPERIMENTS

in a 4-inch-ID anode cylinder electrically insulated from ground by a quartz tripod. A vacuum chamber lowers over the apparatus and fastens to the base plate. This picture also shows the components of the high-voltage measuring apparatus. The measurement of anode potential is complicated by the fact that the measurement must be made without appreciable current drain and that the voltage information must be transmitted outside the vacuum. Considerable effort was devoted to a study of different methods for voltage measurement until a satisfactory method was found. This method determines the anode voltage by measuring the increase in energy of an alpha particle accelerating through the electric field set up by the anode. Descriptions of this technique are given in the literature.[13,14]

For the measurements, a 2-millicurie polonium-210 alpha source was mounted on the outer surface of the anode. A small gas-filled chamber (with variable gas pressure) containing a thin mica window and a silicon-gold charged-particle solid-state detector was placed so that the detector could "see" the alpha source through the mica window. The small chamber was vacuum-sealed and connected by a 1/4-inch line through the test-chamber base plate to a separate evacuating system. With this arrangement the pressure in the small chamber could be varied from a few microns to 1 atmosphere without affecting the vacuum in the large test dome. Measurements with the solid-state detector as the pressure was varied in the small chamber determined the range in air of the alpha particles from the anode. From the measured range and the well-known range-energy relationships[15], the energy of the alpha particle could be determined. The anode voltage is then simply the energy at this voltage minus the energy with the anode grounded divided by the charge on the alpha particle. This technique has the advantages that the measured energy increment, ΔE, is not very sensitive to either the initial energy of the alpha particle or the physical dimensions of the detector. While it is true that the voltage determination comes from taking the difference between two large numbers, analysis of the data and techniques indicate an accuracy of better than ±10 per cent at 10^5 volts and higher. This accuracy is competitive with any other high-voltage measurement in the 10^5 to 10^6-volt range. By use of a ratemeter, the technique was converted to a continuous high-voltage measuring device.

The photograph to the right in Figure 12 shows the vacuum test chamber and the instrumentation associated with the initial alpha-cell experiment. The vacuum chamber is a stainless steel bell jar 24 inches in diameter and 56 inches high which seals to a stainless steel base plate. The chamber is evacuated by a 6-inch oil-diffusion pump backed by a 46-cfm forepump. A 6-inch chevron cold trap (liquid-nitrogen cooled) is mounted on top of the diffusion pump and sealed almost directly into the base plate. With this arrangement pressures in the 10^{-8} mm Hg range are readily attainable. A 4-inch quartz window is sealed into the top of the vacuum dome for visual observation of the experiment.

Voltage Buildup Experiments

To determine the high-voltage-buildup limits of the apparatus, prior to inserting the alpha source a special anode was installed on the quartz tripod inside the vacuum chamber with small cerium-144 – praseodymium-144 beta sources attached to the top of the anode. With beta emission, the anode charged up to 50,000 volts. At this voltage, microdischarging was initiated which abruptly termined further voltage buildup. Thus, prior to the alpha experiments, it was determined that the apparatus was capable of sustaining 50,000 volts without breakdown.

Voltage buildup with the alpha cell was measured for a variety of grid biases. A maximum of 50,000 volts was obtained in these initial experiments, which was the upper limit of the equipment and sufficient to prove the principle of operation. A grid voltage of -800 volts was sufficient to maintain this potential. It was observed that microdischarges were again responsible for the limitation in voltage buildup. Observations have shown that this microdischarging is a threshold phenomenon, i.e., essentially no microdischarges occur until the voltage attains a critical value, at which voltage the microdischarging is initiated with a frequency such that the current leakage in the discharging just matches the charging current.

Alpha-Cell Currents

Measurements in the initial experiments included a determination of cell currents as a function of grid bias at zero anode voltage. The predictions for cell currents were derived previously and illustrated in Figure 4. Below a few hundred volts on the grid, the energy distribution of the secondary electrons will affect the currents, but at high negative grid bias, the grid and cathode currents should be independent of grid bias. From the previous analysis, the cathode current would be expected to be larger than the alpha-particle current by an amount $(1 - x) f\eta_g I_o$, which represents a flow of secondary electrons formed at the grid back to the cathode. Of course, it would be hoped that the grid current is small enough that a positive net current is obtained from the device, i.e., $I_{cathode} + I_{grid} > 0$.

The measured currents are shown in Figure 13. As seen from these data, the cell currents were found to behave very nearly as expected in the ideal case. At grid bias greater than -500 volts, the currents are essentially independent of changes in grid voltage. The cathode (I_{co}) is greater than the net current (I_c), and the charging current I_c (the net from the grid-cathode assembly) is a positive current so that buildup of anode voltage could be expected.

Other Experimental Results

Energy Distribution of Secondary Electrons. The energy distribution of secondary electrons formed at the cathode as the alpha particles emerge is reflected by the grid-bias curve shown in Figure 14. As seen from these data, more than half of the secondary electrons produced by the alpha particles are collected at the grid with a positive potential of 10 volts and nearly all are collected with 100 volts on the grid. This general behavior is consistent with observations that the most probable energy of the secondary electrons is 4 to 10 ev.

Secondary-Electron Yield. From a detailed study of the currents in the alpha cell, the secondary-electron yield was determined to be 9.2 electrons for each alpha particle emerging from the thin gold layer covering the polonium on the cathode.[3] This yield determination is a refinement of the measurement performed in the preliminary study discussed previously and indicates that the early value of 8.2 was a fair approximation to the actual yield.

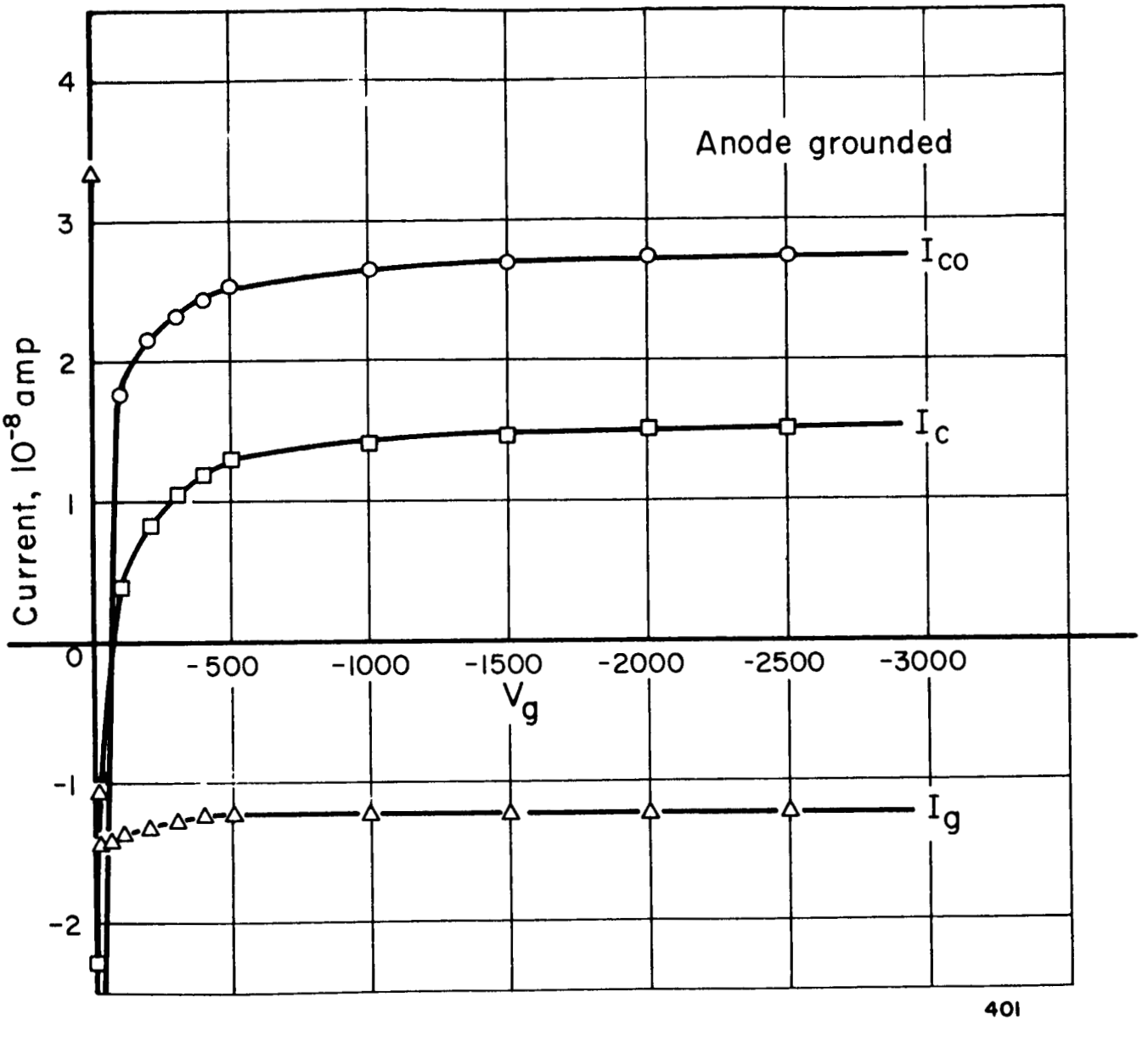

FIGURE 13. ALPHA-ELECTRIC-CELL CURRENT-VOLTAGE CURVES FOR NEGATIVE GRID BIAS

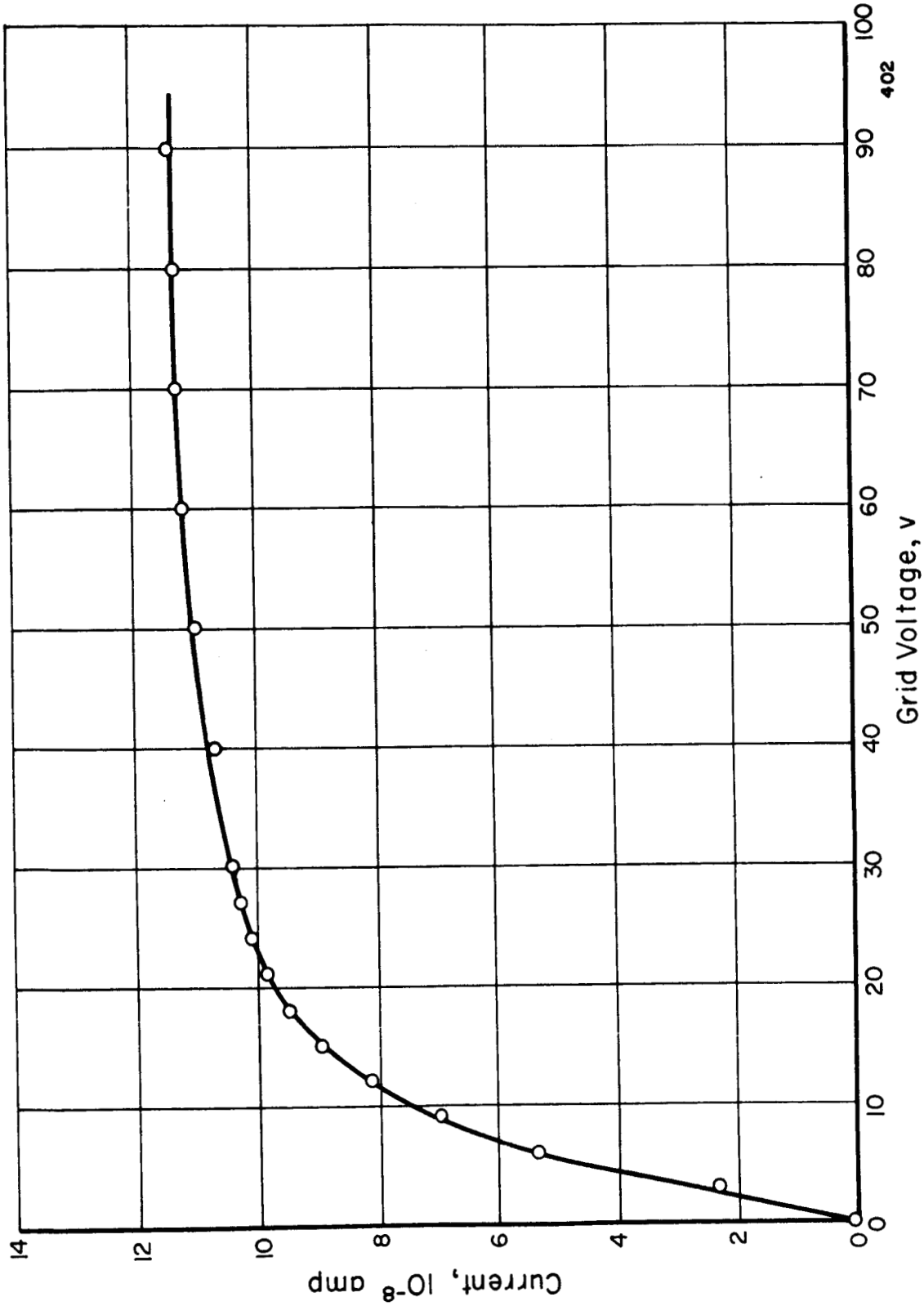

FIGURE 14. GRID CURRENT VERSUS GRID BIAS FOR POSITIVE GRID BIAS, ZERO ANODE VOLTAGE

Effect of Pressure on Voltage Buildup. The effect of test-chamber pressure on the maximum voltage buildup was briefly examined and some rather interesting phenomena observed. Figure 15 shows the effect of pressure on voltage buildup when using a beta emitter to charge up the anode. As seen from these data, the anode voltage was independent of pressure below about 10^{-4} mm Hg. Between 10^{-4} and 10^{-3} mm Hg the voltage dropped to zero. Then at 10^{-3} mm Hg it increased rapidly to about twice the high-vacuum value. Further increase in pressure caused a rapid decrease to zero voltage again. This rather anomalous behavior is roughly the same as that which was observed by Linder and Christian at RCA with a beta emitter.[2] The peak in voltage may be due to a surface-condition effect on secondary-electron and ion emission. The rapid decrease in voltage above 10^{-3} mm Hg is apparently due to ionization of the gas.

The same experiment was repeated with the alpha cell, with results as shown in Figure 16. As seen from these data, again below 10^{-4} mm Hg pressure the anode voltage was constant. The behavior above 10^{-4} mm Hg was qualitatively the same as observed with the beta device, i.e., with increasing pressure, the voltage first decreased, then peaked and finally dropped to zero above 10^{-3} mm Hg. However, near 10^{-3} mm Hg a few gross discharges were observed, and the pressure-voltage curve contained additional peaks.

Except for these studies of voltage behavior with pressure, all experiments were performed at pressures of about 10^{-7} to 10^{-6} mm Hg pressure. However, it appears from these data that only 10^{-4} mm Hg pressure is required for the operation of the alpha cell. This study was limited, of course, to the 50,000-volt range obtained in these initial experiments.

Amplification Factor of Grid. The ability of the theoretical expression for amplification factor, μ, in a triode electron tube, Equation (28), to describe the amplification factor of the grid in the alpha cell was checked experimentally during the initial experiments. The purposes of this particular experiment were twofold: to determine if grid bias was limiting voltage buildup and to obtain a measurement of the amplification factor of the grid. Maximum anode voltage was measured as a function of grid bias. The data are shown graphically in Figure 17. As seen from these data, grid bias was not limiting voltage buildup; rather, voltage buildup was limited by microdischarges as discussed previously. Over the grid-voltage range where the grid bias is the limiting factor (up to -800 volts), a rough measure of the amplification factor can be obtained. Due to the inability to accurately measure low voltages with the alpha-particle voltage-measuring technique, there is considerable scatter in the data. Although there may be a nonlinear behavior in the curve of anode voltage V_A versus grid voltage V_g, a gross measure of μ is given as $\mu = \Delta V_A / \Delta V_g \cong 50$. This value compares favorably with the value of 41 calculated from Equation (28). Although experiments at higher voltages must be relied upon to obtain a more accurate comparison, it appeared from this study that the theoretical prediction is sufficiently valid for preliminary design purposes.

Microdischarges

The data on the amplification-factor measurement shown in Figure 17 emphasize the effect of microdischarges on limiting voltage buildup in the alpha cell. The present theoretical and experimental status of high-voltage breakdown across a vacuum gap indicates that a critical current of the order of 10^{-4} amp is required to initiate

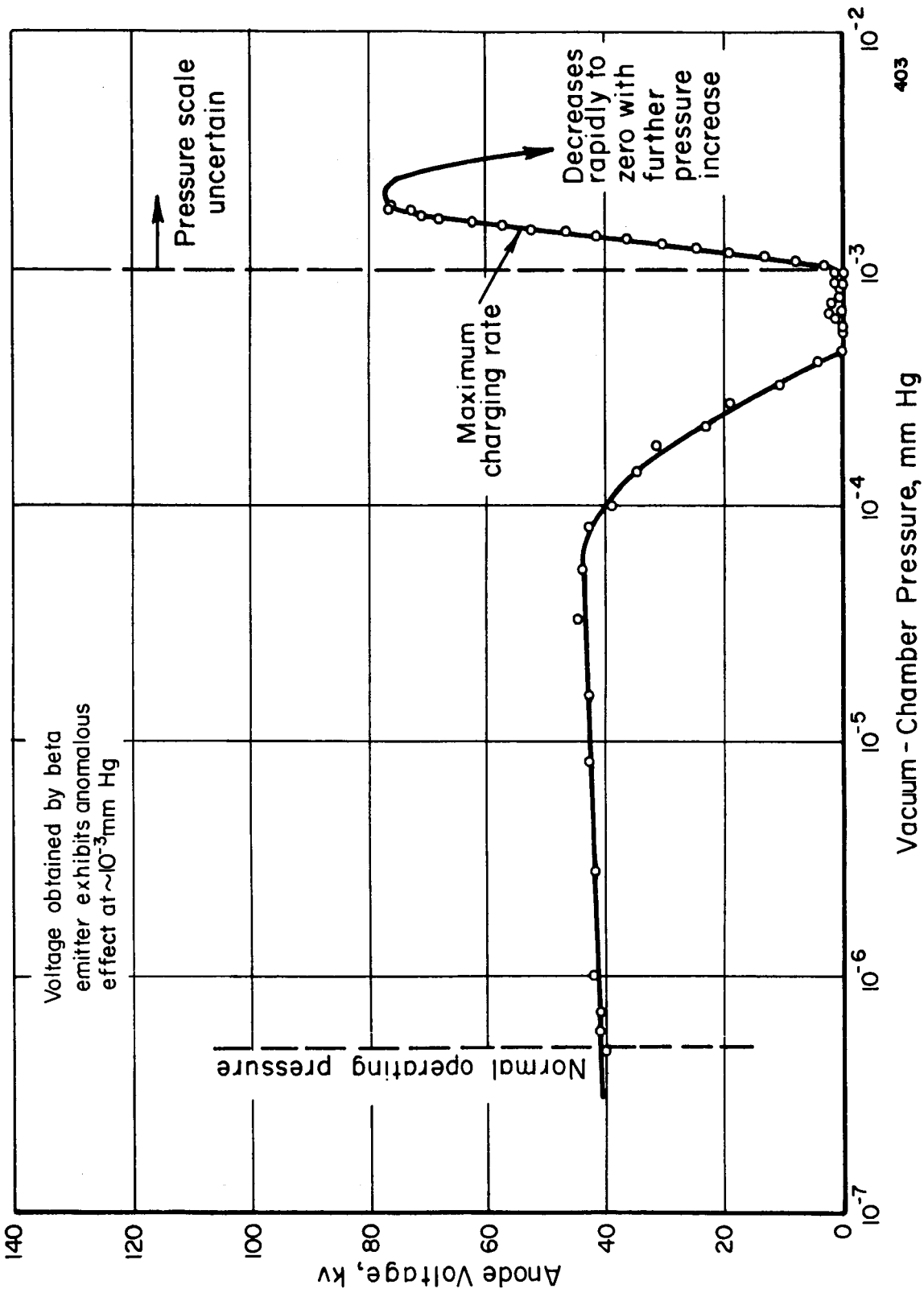

FIGURE 15. ANODE VOLTAGE VERSUS PRESSURE

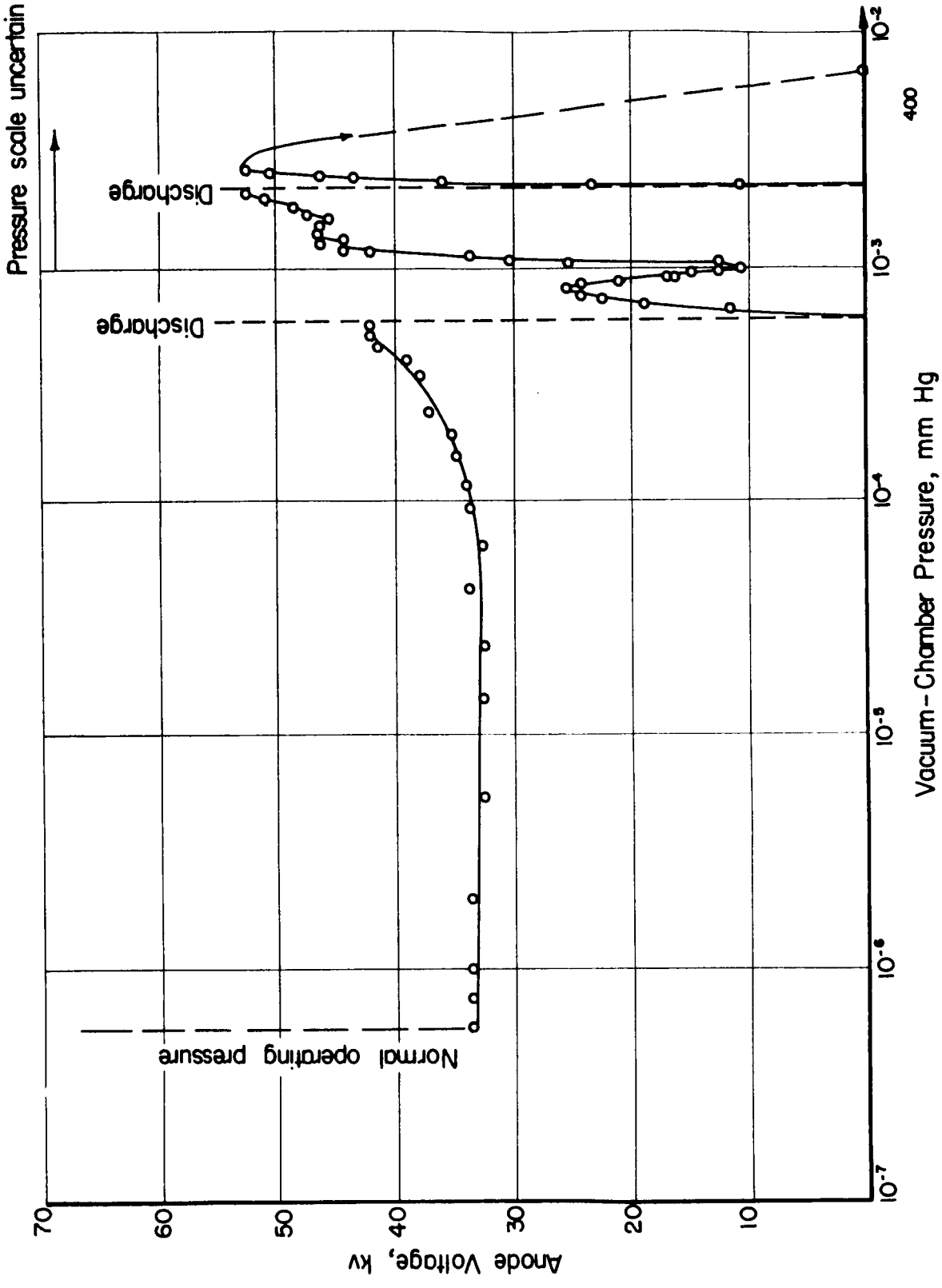

FIGURE 16. ALPHA-CELL ANODE VOLTAGE VERSUS PRESSURE

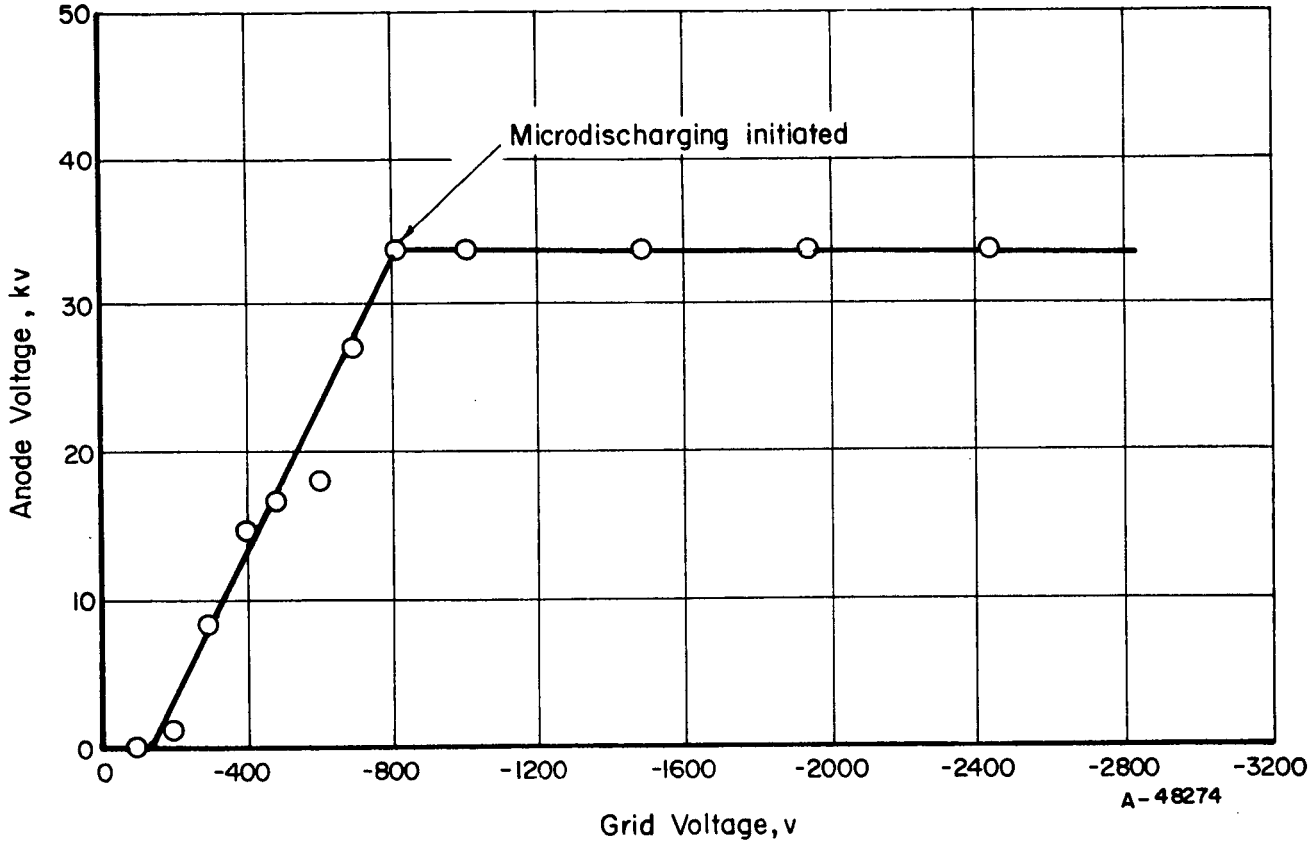

FIGURE 17. ANODE VOLTAGE VERSUS GRID BIAS

breakdown.[16] Interchange of current between electrodes at values below the critical current occurs in the form of microdischarges.[17] It has been suggested[18] that the microdischarges are due to particles or clumps of foreign material ejected from the electrode surfaces by the electric field. Whatever the mechanism, simultaneous observations of microdischarges with voltage buildup with betas indicated that the discharges first occur at about 50 kv and then occur with increasing frequency up to a limiting voltage of approximately 100 kv. Presumably, at this voltage, the leakage current contained in the microdischarges offsets the charging current. The discharge frequency as a function of anode voltage is shown in Figure 18 for an experiment using the alpha-cell apparatus but using beta emission for voltage buildup. From very crude measurements, it has been estimated that about 10^{10} electrons are contained in each microdischarge. In the initial alpha-cell experiment, the voltage never exceeded the threshold voltage for onset of microdischarging of about 50 kilovolts. The appearance of the very definite threshold voltage for microdischarging explains the sudden stop in voltage buildup with time in the initial experiments.

Summary of Battelle-Sponsored Alpha Cell Experiments

The initial experiments gave a voltage buildup of about 50,000 volts, which was very encouraging. This was sufficient to prove the principle of operation (at least in the low voltage range) and to permit extraction of preliminary values of design parameters. The experiments also vividly showed the microdischarge problem to be the main experimental obstacle to obtaining higher voltages. The big question remaining at the conclusion of the initial experiments was that of how basic a limitation the microdischarging presented. The seriousness of this problem arises from the fact that the alpha cell is inherently a low-current device.

The next logical step in the demonstration of alpha cell feasibility appeared to be to extend the voltage capability to near the 1-megavolt range, where efficient operation is possible, and to determine the characteristics of the cell under these conditions. The problem of microdischarging would be attacked through insulator design, utilizing the presently available technology. The remainder of this section of the report describes the "second generation" of experiments performed under contract with NASA with apparatus redesigned to attempt high voltage buildup.

RESULTS OF EXPERIMENTS PERFORMED UNDER NASA CONTRACT

Experimental Apparatus

The equipment for the alpha-cell experiment was redesigned on the basis of the earlier experience. The principal changes in the vacuum facility were designed to ease the loading and removal problems with the alpha emitter and to provide for a better support arrangement of the grid-cathode and anode assemblies. The principal changes in the design of the alpha-cell experiment itself were centered around the microdischarging problem and involved an increase of spacing between the cell components and a new type of insulator for the anode.

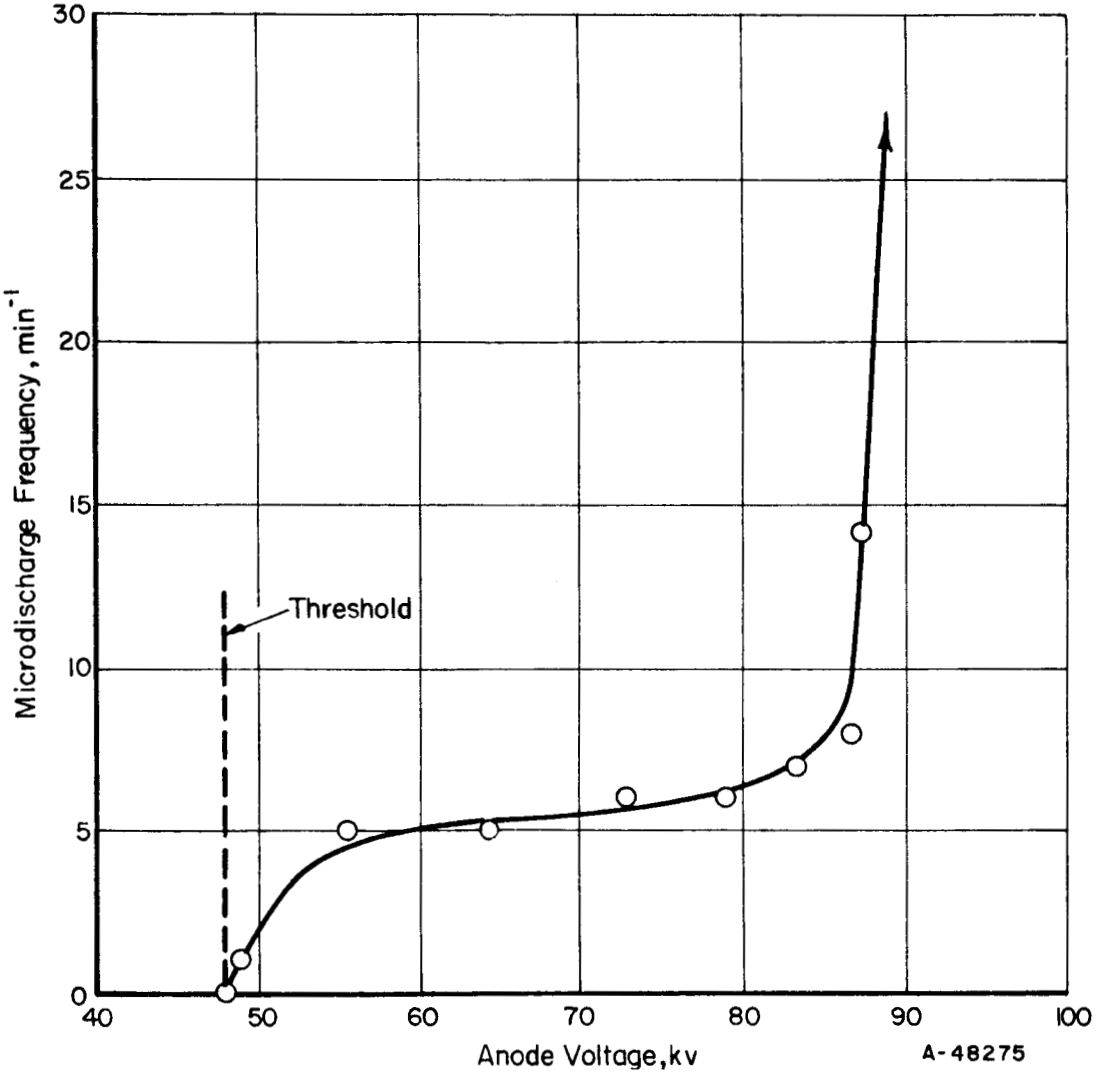

FIGURE 18. FREQUENCY OF MICRODISCHARGES VERSUS ANODE VOLTAGE

Vacuum-Facility Description

The high-vacuum system was designed to maintain a vacuum of 10^{-7} torr, a pressure shown by the initial experiments to be several orders of magnitude below that required to sustain 50,000 volts. Figure 19 is a photograph of the vacuum tank, showing the feedthroughs for the electrical connections and for the alpha voltmeter. The vacuum chamber is a 3/16-inch-thick Type 304 stainless steel bell jar 24 inches in diameter and 62 inches in height. As seen from the photograph the chamber is horizontally sectioned and flanged at approximately its midplane, providing unrestricted admittance for insertion of the experiment. Viewing ports on both halves of the chamber provide visual access to the experiment.

A 6-inch oil-diffusion pump having a maximum unbaffled pumping speed of 1440 liters/sec at 10^{-3} torr, backed by a 26-cfm mechanical compound pump maintains the vacuum at 10^{-6} to 10^{-7} torr without bakeout. An optically dense cold trap (Freon cooled) located immediately above the diffusion pump minimizes the back streaming of pumping fluid vapors. A 6-inch line with pneumatic valve connects the pumping complex with the vacuum chamber. The pneumatic valve in the 6-inch line together with a 2-inch pneumatic valve in the foreline protects the pumps and alpha-cell experiment against gross oil migration in the event of pump failure. Because of possible air-borne contamination from the alpha emitter, the exhaust vapor from the forepump exits into a leaktight exhaust stack through a Cambridge absolute filter. A cold trap in the exhaust line condenses oil vapors to prevent saturation of the absolute filter.

To expedite experiments determining the dependency of the cell currents and voltage on pressure, the vacuum chamber is equipped with a "variable leak". Conductance of the leakage is variable from 100 cm^3/sec to 10^{-10} cm^3/sec. Dry air is admitted to the chamber through the leak by passing room air through a 24-inch column of desiccant.

Alpha-Cell Experiment Design and Description

This section of the report describes the four principal components of the experiment: anode, cathode, grid and anode insulator. Figure 20 is a sketch of the alpha cell components installed in the vacuum facility which shows the arrangement of the various components.

Anode Design. The anode and anode-insulator assembly are shown in the photograph of Figure 21. The anode consists of a 6-inch-diameter aluminum tube which is highly polished, as seen from the photograph (average depth of surface irregularities estimated to be 1 to 10 microinches). The length of the straight portion of the anode is approximately 22 inches. At the bottom, the anode joins smoothly to a spherical dome which is supported by the anode insulator. The top end of the anode is open to receive the grid-cathode assembly. A lip arrangement is fitted onto the top end of the anode to reduce the electric field at the edges. The circular depression shown in the side of the anode is the holder for the small auxiliary alpha source used for the alpha voltmeter.

Insulator Design. Because of the microdischarging problem encountered in the Battelle sponsored experiments, particular emphasis was placed on insulator design. The quartz tripod arrangement used in the earlier experiments was abandoned,

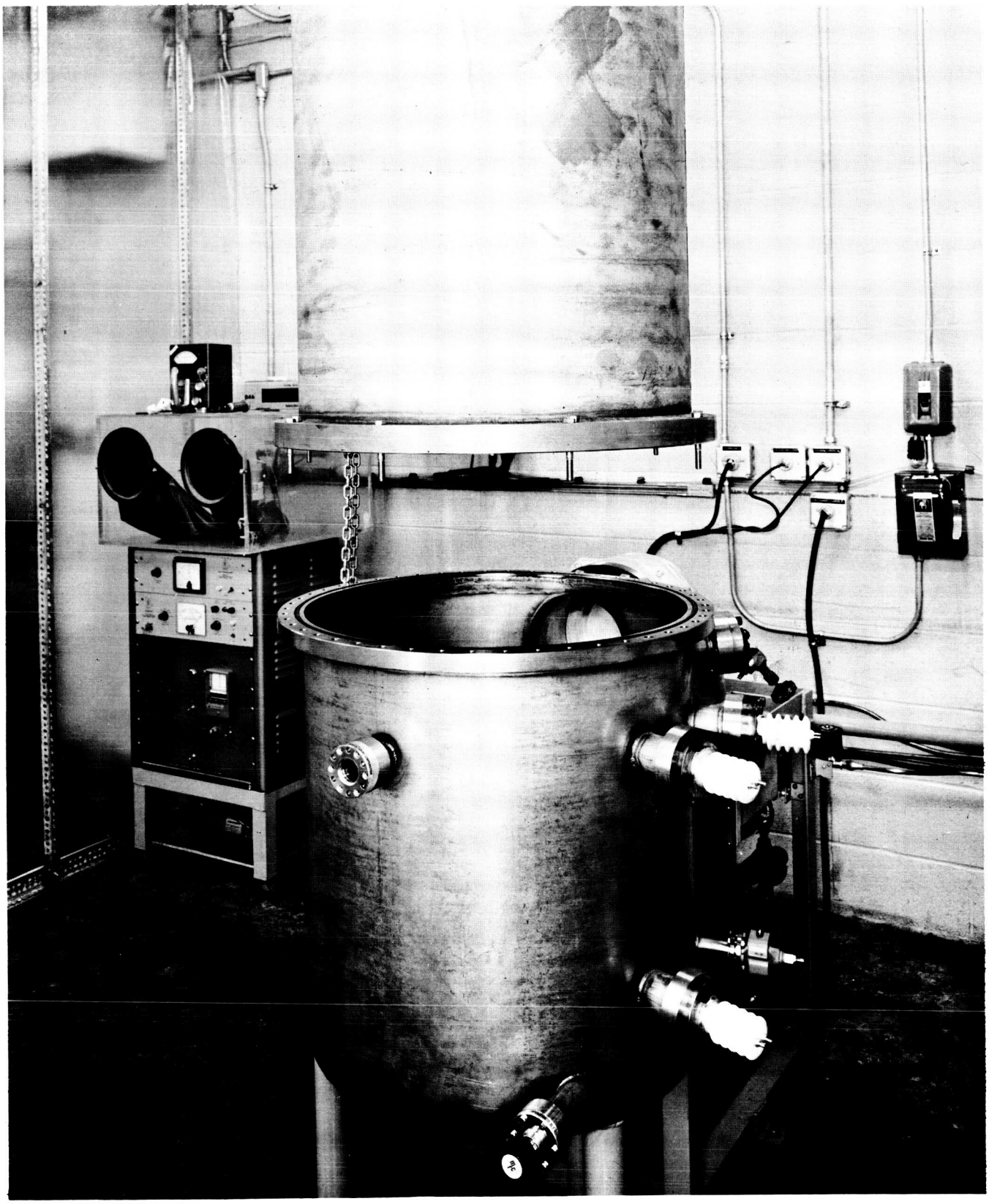

10419

FIGURE 19. VACUUM FACILITY FOR ALPHA-CELL EXPERIMENT

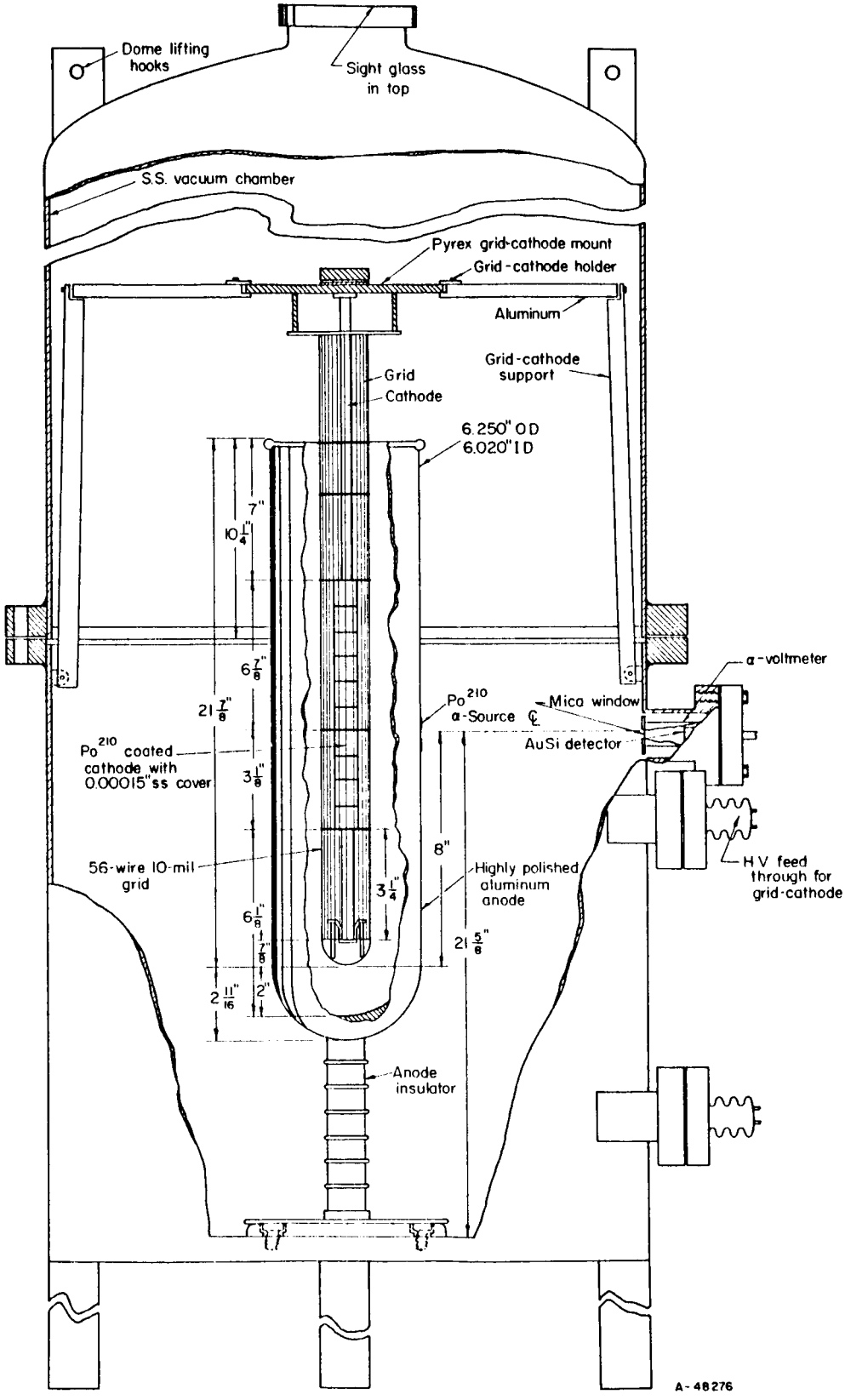

FIGURE 20. SKETCH OF ALPHA CELL EXPERIMENT ARRANGEMENT

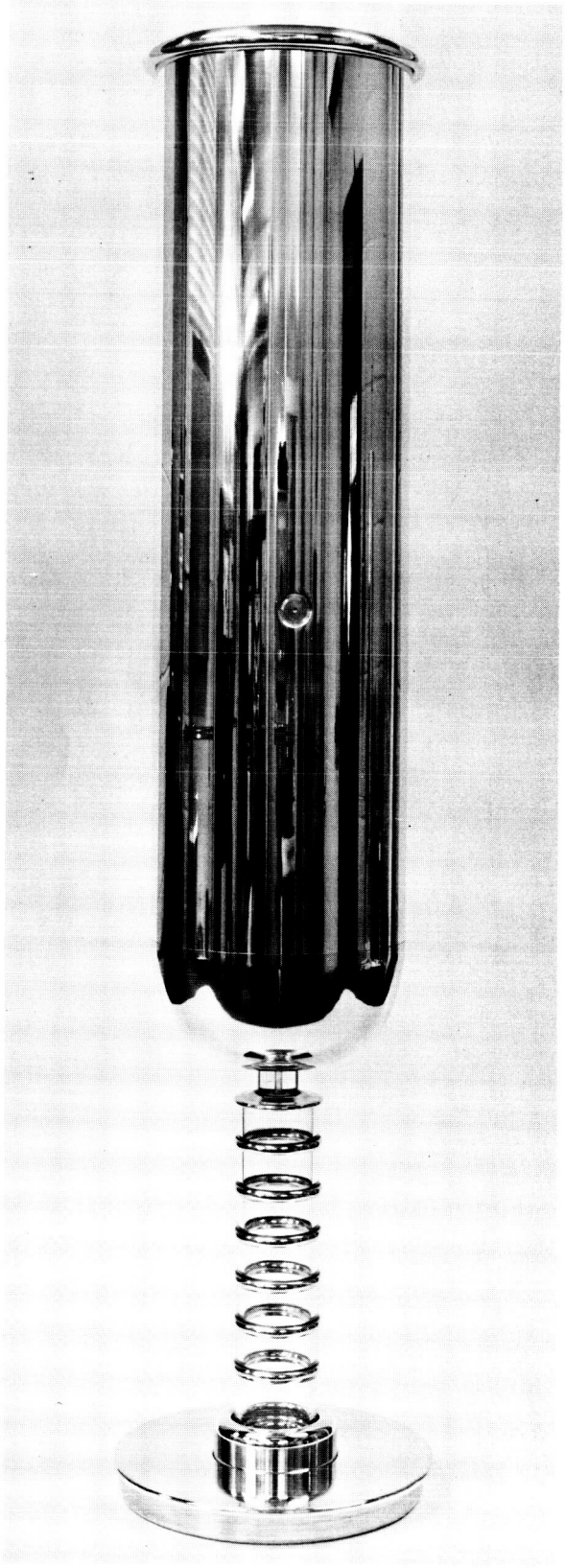

10418

FIGURE 21. ANODE AND ANODE-INSULATION ASSEMBLY

principally for structural reasons, in favor of a simple cylindrical geometry, shown in Figure 21 and sketched in detail in Figure 22. Pertinent information was gleaned from the literature to serve as a guide in insulator design. The principal observations and design reasoning are stated below.

(1) In the use of high-voltage insulators in vacuum, electrons and negative ions are preferentially emitted at, or in the immediate vicinity of, the negative junction. These gain energy in traversing the evacuated space toward the positive electrode and upon striking solid material liberate X-rays, secondary electrons, and ions. These secondary particles further the voltage-breakdown process. By recessing the insulator into the base making the negative junction, the breakdown voltage can be significantly increased.[19,20]

Referring to Figure 21, the metal-to-dielectric junction, at the bottom of the insulator, was constructed with an undercut recess in the aluminum base. The insulating glass was attached with an epoxy resin. This recessing of the insulator combined with the use of epoxy resin reduces the high fields between the insulator and aluminum base.

(2) Although it has been observed that surface resistivity and certain other factors affect vacuum-breakdown voltages, each of these factors alone generally has a less striking effect than the junction phenomenon.[19] Since the insulator resistance must be greater than 10^{14} ohms, the readily available candidate materials are the glazed ceramics and hard glasses. Since both of these materials have similar surface resistivity, this parameter was not a factor in insulator design.

(3) The voltage at which electrons are released at the negative junction and the breakdown voltage both appear to be lower for materials of higher dielectric constant.[20,21] Since hard glasses generally have lower dielectric constant, quartz was selected over a glazed ceramic as the insulator material.

(4) Voltage grading provides a uniform electric field along the insulator, thereby preventing a localized accumulation of charge and consequent flashover.[22]

The design of the anode insulator as a series of quartz rings separated by aluminum rings was based on the results of experiments performed at the Ion Physics Corporation.[22] The glass was bonded to the aluminum with epoxy. The available data indicate that each ring should be capable of sustaining about a 60-kv potential difference; the total stack therefore should support 400 to 500 kv. It should be noted that these design factors apply strictly only to the case of true high-voltage breakdown where currents are available of sufficient magnitude to cause flashover. It is assumed that these factors also apply in at least a general way to the micro-discharge problem where the total current available is of the order of 10^{-8} amp.

Cathode Design. The principal changes in cathode design over that used in the earlier experiments were an increase in the diameter of the emitting layer from 1/2 in. to 1.0 in. (to reduce the local electric field) and in the use of a covering of stainless

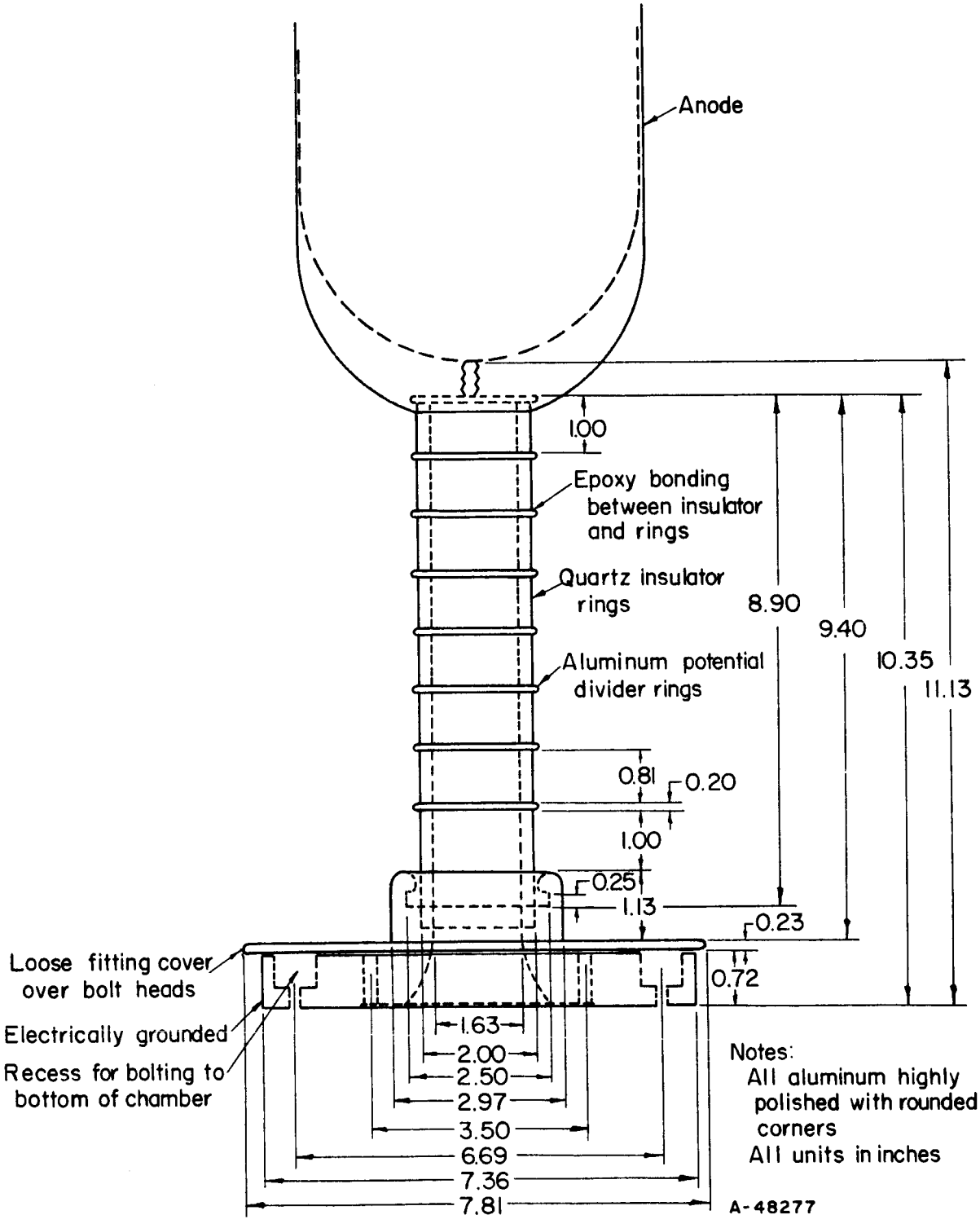

FIGURE 22. ANODE-INSULATOR DESIGN DETAILS

steel foil rather than gold. This latter change was made in an attempt to reduce gross contamination of the experimental apparatus due to migration of the alpha emitter. Polonium-210 was again selected as the alpha emitter for the purposes of the experiment because of its high specific activity (short half-life). The cathode was fabricated by the Monsanto Research Corporation.

The fueled portion of the cathode is 10 in. long and consists of three copper cylinders, each 3-1/3 in. by 1-in. OD. The copper was flashed with a thin coating of gold and then plated with a total of 8.85 curies of polonium-210 (June 4, 1964). Source strength at the time of the experiment was approximately 6 curies. Variation of the polonium content between the three cylinders was determined to be less than about 2 per cent. The source material was wrapped with a 0.00015-in.-thick stainless steel foil which extends the entire length of the cylinders. The end-point energy of the alpha particles leaving the foil is approximately 3.5 Mev, and the resolution of the energy-spectrum peak is between 10 and 15 per cent.

Grid Design. Grid design was based on the first-order principles stated previously in the discussion of the theory of operation of the alpha cell. With the dimensions of the cathode and anode given by other considerations, e.g., vacuum-facility dimensions, voltage breakdown, and end losses, the objective of the grid design was to achieve an amplification factor of 50 and an f-factor (screening fraction) of 0.1 or less. The amplification factor of 50 was based on the anticipated ability of the grid insulation to maintain a potential of 10 kv and on the anode insulator to support 500 kv. With given values for the grid-circle radius (1 in.), cathode radius (1/2 in.), and anode radius (3 in.), from Equations (26) and (28), the product (Nd_g) is determined, where N is the number of grid wires and d_g is the diameter of the wires. Figure 23 shows the grid constructed on the basis of the curves of Figure 24, which show the f-factor and number of grid wires required versus wire diameter to achieve the desired amplification factor with the given dimensions. As the graph shows, to obtain an f-factor of less than 0.1, the grid-wire diameter must be less than 11 mils. Selecting a 10-mil diameter to coincide with commercially available wire, the number of wires selected was 56, which is the even number closest to that indicated by the analysis. Using these values, the calculated f-factor and amplification factor of the grid are 0.0955 and 48.5, respectively.

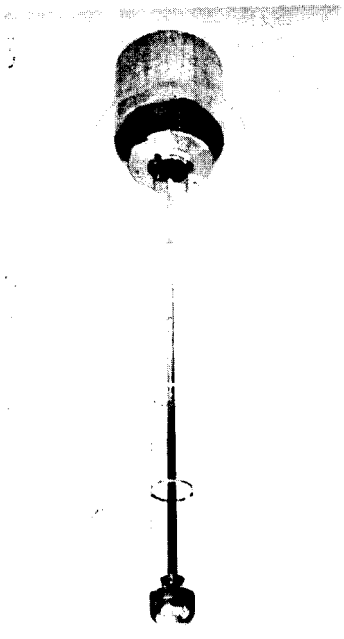

FIGURE 23. GRID USED IN ALPHA-CELL EXPERIMENTS

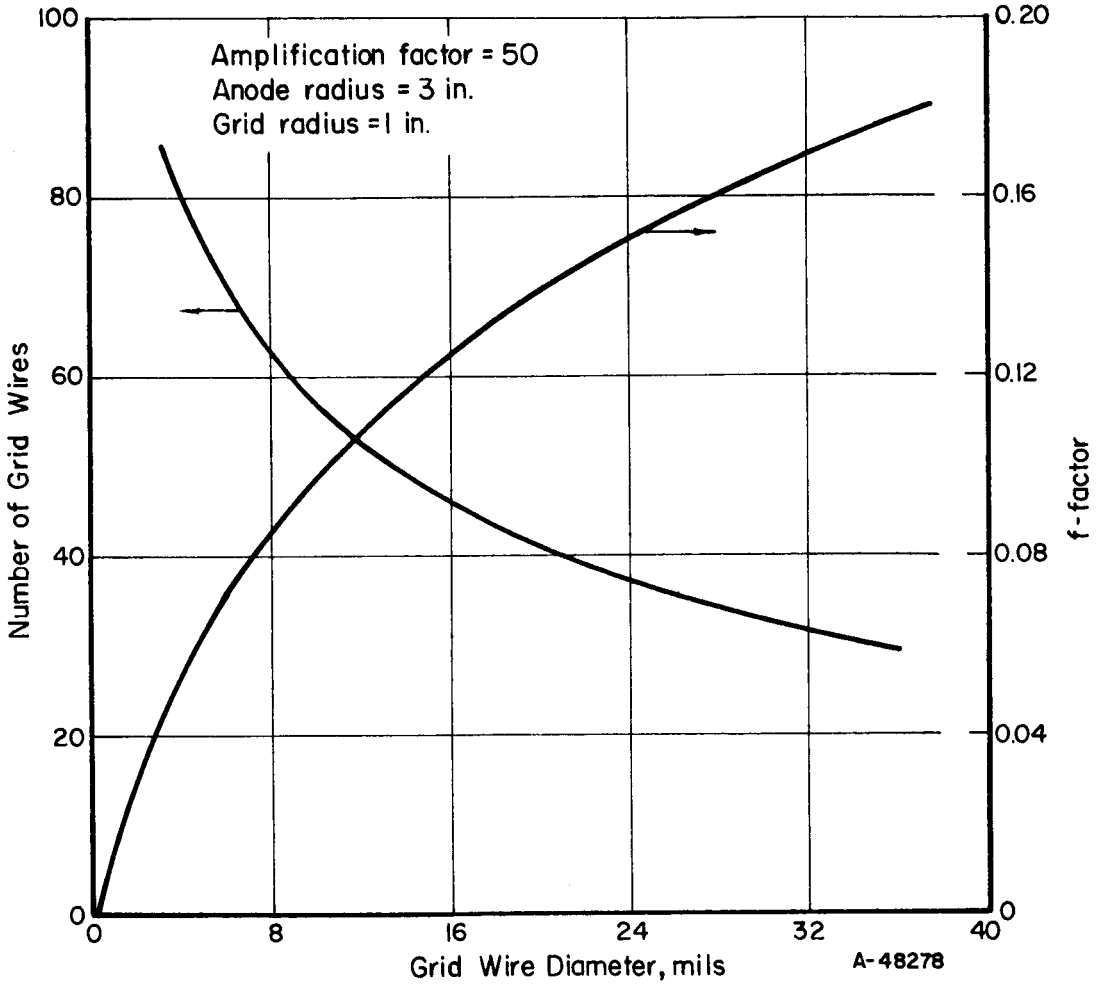

FIGURE 24. GRID DESIGN PARAMETERS VERSUS GRID WIRE DIAMETER

Figure 25 is a photograph of the alpha cell experiment installed in the vacuum chamber.

Instrumentation

The alpha cell is instrumented for measuring anode voltage, grid and cathode currents, and chamber pressure.

Anode voltage is measured using the previously described alpha-particle voltmeter. Figure 26 is block diagram of the complete measuring circuit. The alpha particles emerging from the small anode source are detected through an air-filled chamber by a surface-barrier detector in conjunction with a charge-sensitive preamplifier and low-noise amplifier. The signal is then fed into a single-channel differential analyzer. With the analyzer in the differential mode (calibration channel), the signal is fed into a scaler-timer unit for determination of the range of the alpha particles in the small air-filled chamber in front of the detector. In the integral mode of operation (recording channel), the signal is directed to a ratemeter and then to a recorder for a direct anode-voltage reading.

Grid voltage is supplied by a 0 to 10-kv battery power supply. The grid and cathode currents are measured through Keithley Model 410 micromicroammeters. These currents can also be recorded directly to study transient effects.

Pressure in the small alpha-voltmeter air chamber is determined from a mercury manometer. Pressure in the high-vacuum chamber is measured by a Hughes cold-cathode gage and control unit.

Preliminary Measurements and Calibrations

Prior to installing the polonium-coated cathode, anode capacitance, insulator resistance and background currents were measured, and the alpha voltmeter calibrated. These results are briefly summarized below.

Capacitance and Resistance Measurements

The anode capacitance to ground was determined from a capacitance-bridge measurement to be 62 $\mu\mu$f. This value compares favorably with the calculated value of 55 $\mu\mu$f treating the grid, anode, and vacuum chamber arrangement as a segment of an infinite triaxial system.*

Because of the extremely high resistance of the anode insulator, the magnitude of its resistance could not be determined. However, time-constant determinations showed its value to be much greater than 10^{14} ohms, which is sufficiently large to produce a negligible drain on the anode during operation of the experiment.

*The coefficients of capacitance and inductance listed as Equation (44) in the midpoint report were found to be in error.

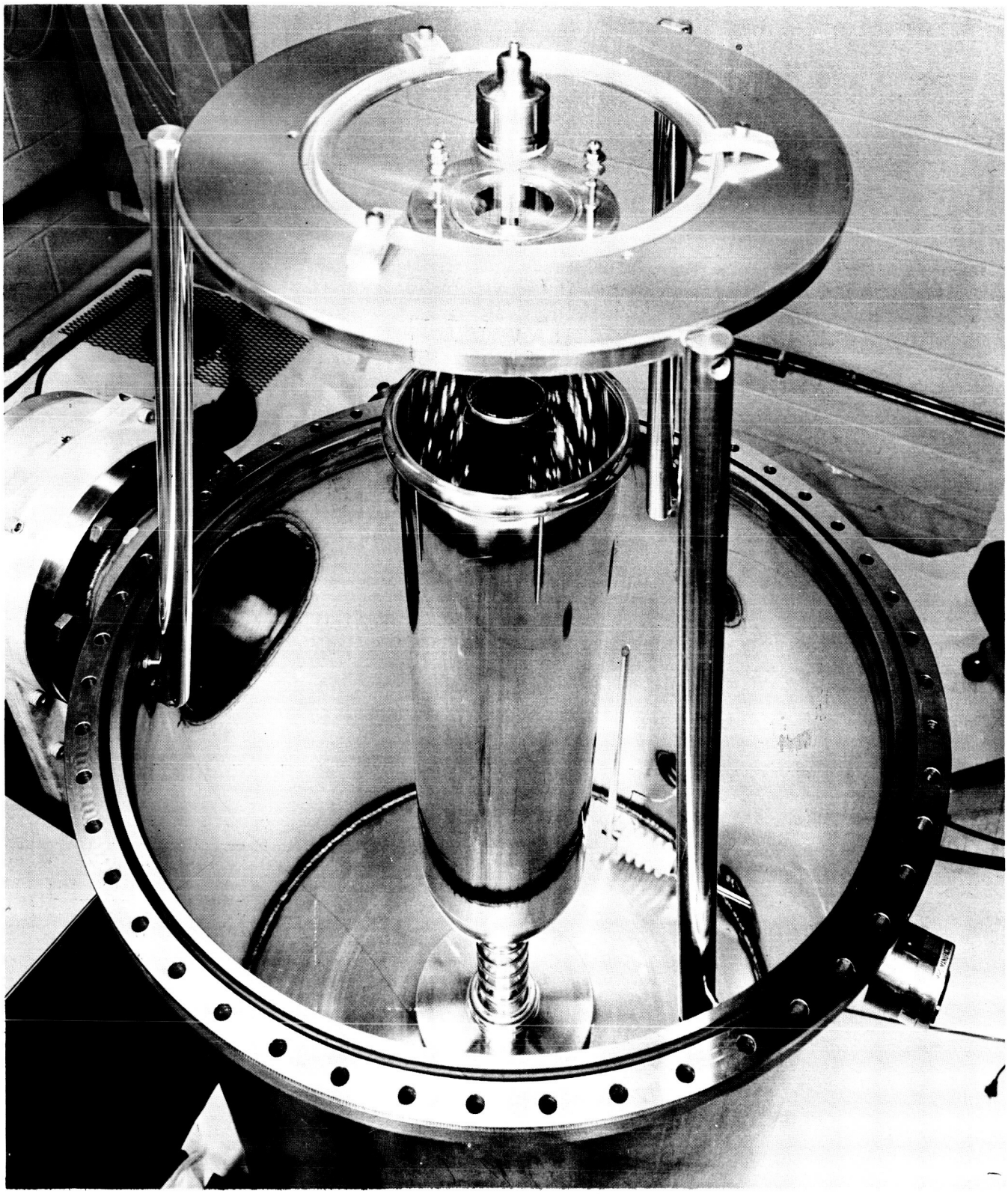

12670

FIGURE 25. ALPHA-CELL EXPERIMENT INSTALLED IN VACUUM CHAMBER

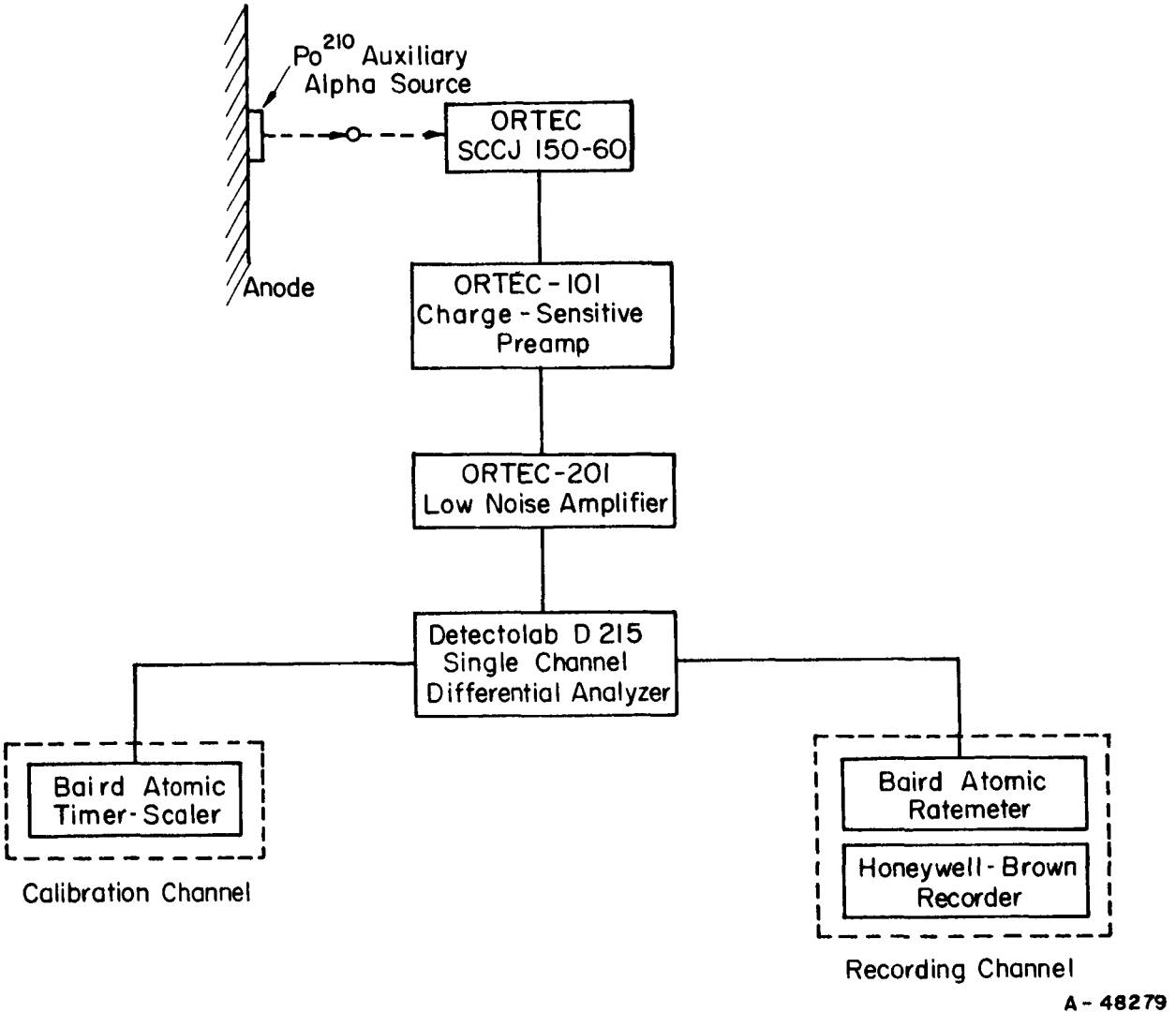

FIGURE 26. ALPHA-VOLTMETER CIRCUITRY

Grid and Cathode Currents With No Alpha Emitter

The grid and cathode currents were determined to be of the order of 10^{-11} amp with no alpha emitter on the cathode. As will be seen from later data, these currents are several orders of magnitude below the currents present with the fueled cathode (10^{-8} to 10^{-7} amp), and thus no correction to the fueled data is required for background currents. The principal source of the small residual grid current is leakage in the battery power supply.

Alpha-Voltmeter Calibration

As mentioned previously, the alpha voltmeter operates on the principle of change of alpha-particle range in air with alpha-particle energy. Figure 27 shows the total (integral) count rate detected by the surface-barrier detector as a function of air pressure in the thin-windowed chamber interposed between the detector and a small (23 millicuries) polonium-210 source mounted on the anode (at the position shown in Figure 21). The lower curve is the base-line curve obtained with the anode grounded. Although this voltage-measurement technique is rather inaccurate below about 50 kilovolts, a check on the voltmeter performance was obtained by applying 30 kilovolts to the anode from an external power supply and observing the shift in the count-rate curve. These data were then compared with the predicted shift based on the alpha particle range-energy relationship. The results, shown in Figure 27, indicate excellent agreement.

For a fixed pressure, the range of linearity of voltage with count rate is limited. The nonlinearity can be accounted for by measuring the shift in energy spectrum of the alpha particles striking the surface-barrier detector. (This method, in fact, can be used over the entire range of interest but is experimentally inconvenient.) The peak shift is determined by a multichannel analyzer substituted in the calibration channel of the alpha-voltmeter circuit (see Figure 26). The channel shift was calibrated in terms of energy change by determining the channels at which the peaks of known alpha emitters occurred. For this calibration, plutonium-239 (5.14 Mev) and polonium-210 (5.30 Mev) bare, thin sources were used, with typical results as shown in Figure 28. Also shown in this figure is the zero-voltage energy spectrum of the alpha particles seen by the surface-barrier detector through the mica window of the voltmeter chamber. Assuming linearity of the channels with energy, the polonium-210 and plutonium-239 calibrations both yield 0.0248 Mev/channel. A rough check on the assumption of linearity was made by comparing the channel shift between the two calibration sources. This comparison yields 0.027 Mev/channel, with at least 15 per cent error, which is in good agreement with the linear value of 0.0248 Mev/channel.

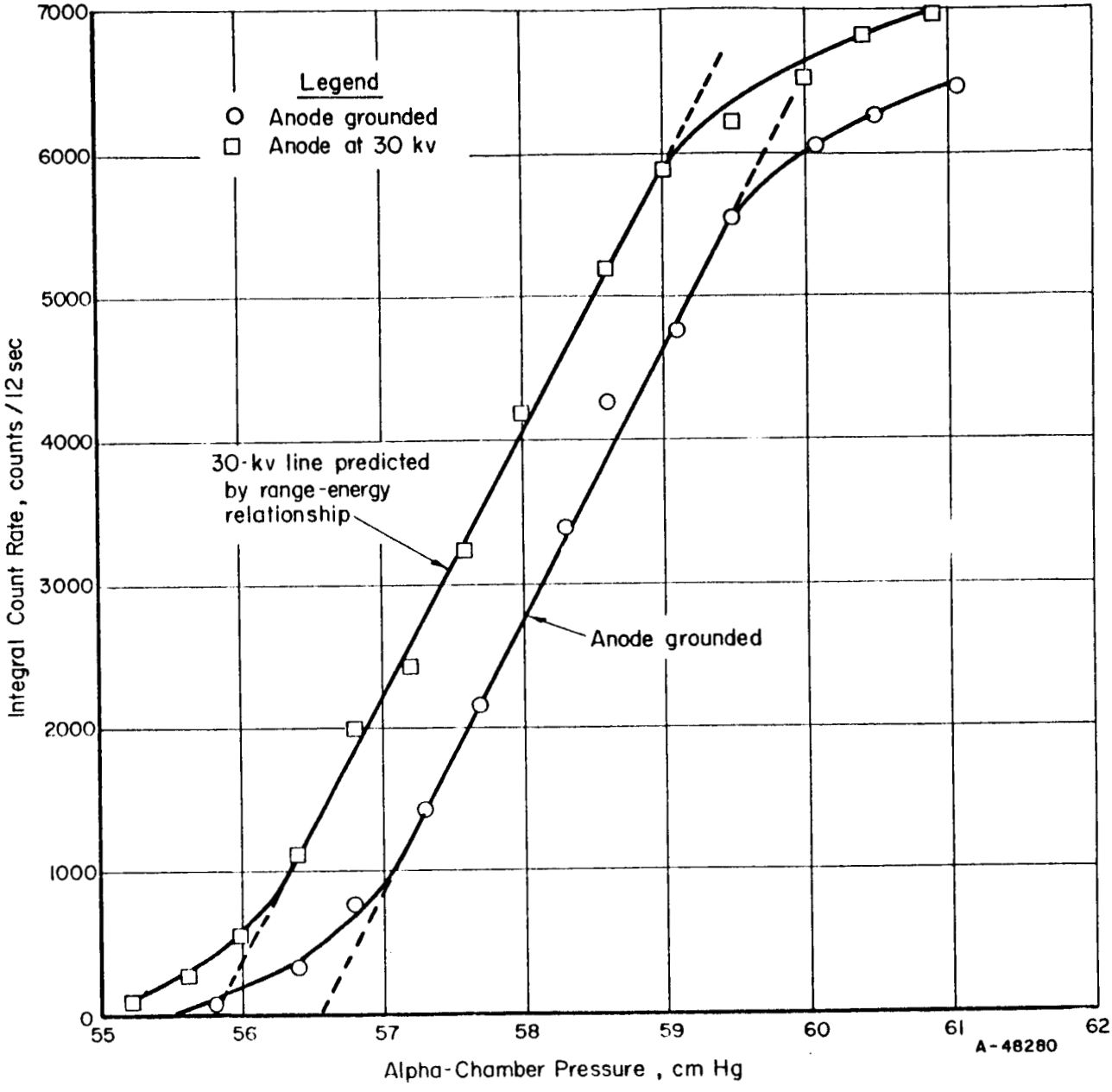

FIGURE 27. LOW-VOLTAGE INTEGRAL COUNT RATE VERSUS PRESSURE FOR ALPHA VOLTMETER

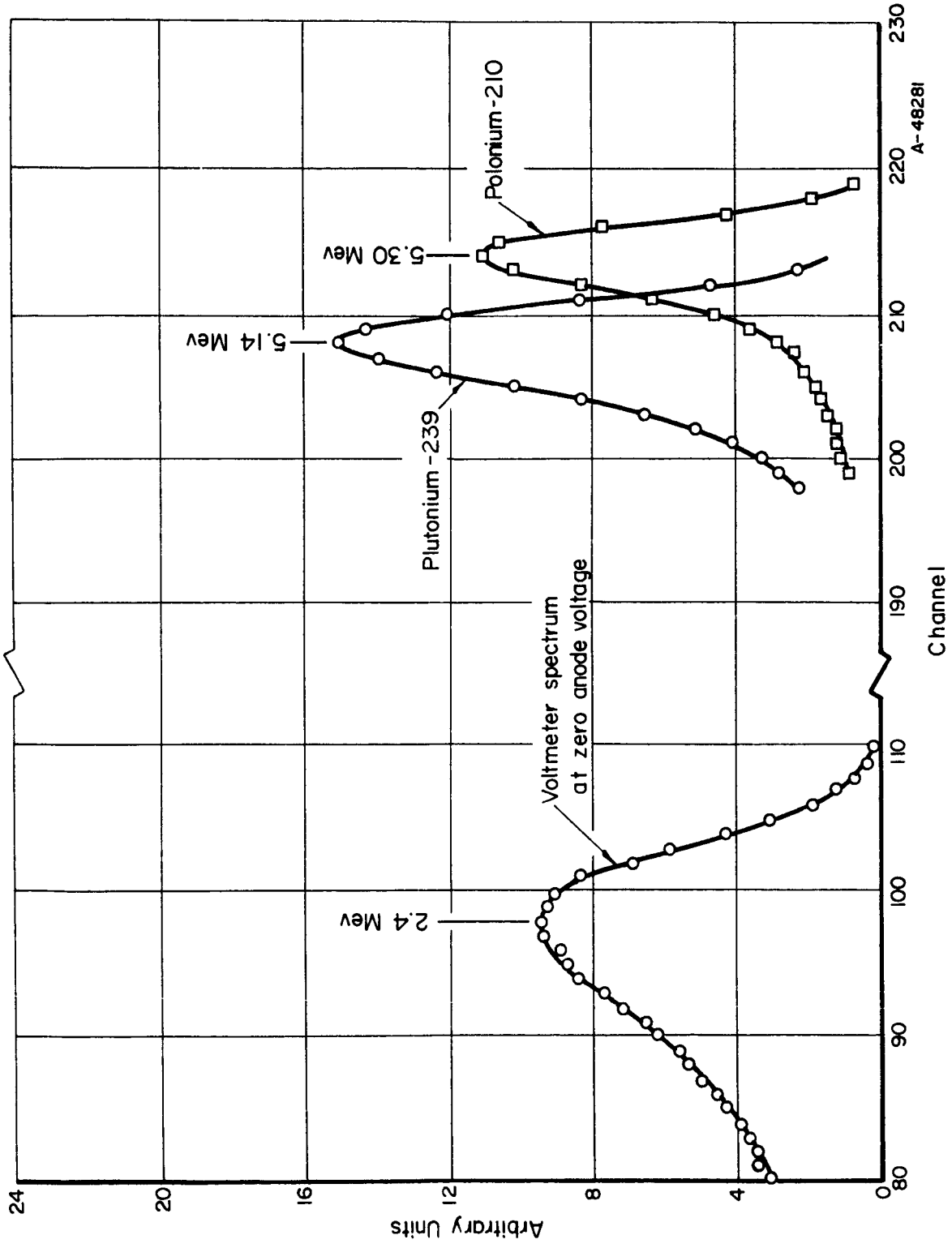

FIGURE 28. ENERGY SPECTRUM OF VOLTMETER ALPHAS AND ENERGY CALIBRATION OF ANALYZER

Experiments With the New Alpha Cell

Upon completion of the measurements and calibrations with no alpha emitter present in the experiment, the polonium-coated cathode described previously was inserted into the vacuum chamber and data obtained from the new experiment. The results are presented below along with analyses of the data.

Cell Currents With Anode Grounded

The first important result required from the experiment was to demonstrate that a net positive current flows upon application of large negative voltage to the grid. To obtain this information, the cathode current I_{co} and grid current I_g were measured as a function of negative grid bias with the anode grounded. These data are shown in Figure 29. The results show that the net current I_c from the grid-cathode assembly, which is the algebraic sum of the grid and cathode currents, is indeed positive; thus, voltage buildup can be expected when the anode is ungrounded. The currents nearly reached their limiting value with -500 volts on the grid, and there is no leakage current between the electrodes.*

The detailed behavior of the grid current at small grid bias is shown in Figure 30. This current-voltage curve reflects the energy spectrum of the secondary electrons present in the cell. As was observed in the earlier experiments (see Figure 14), more than half of the secondary electrons are collected at the grid with a positive bias of 10 volts, and nearly all are collected with 100 volts. At large positive bias, the grid collects all secondary electrons, both those emitted at the cathode by the emerging alpha particles and those emitted at the anode by the impinging alpha particles. Secondaries formed at the grid by the small fraction of alpha particles striking the grid are retained at the grid with large positive bias. On the other hand, at negative bias, the grid suppresses secondary-electron emission at the cathode and anode, and the grid current is that due to secondary electron production at the grid. Thus, except for a small contribution to grid current from the positively charged alphas striking it, the difference between the saturated values of I_g at positive and negative bias represents the total secondary electron current generated in the device, which is approximately 10^{-7} amp compared with an alpha-particle charging current of about 10^{-8} amp. This comparison emphasizes the task of the grid in the alpha cell. Of course, it is the current at negative grid bias which is most important to cell operation.

Figure 31 shows the detailed behavior of the cathode current at small grid bias. At positive grid voltage, all secondaries formed at the cathode escape along with the emitted alpha particles, which are not affected by grid bias. Note that with no bias on the grid, the cathode current is a large negative current. Also note that for positive bias it requires several tens of volts to reveal all the cathode secondaries – there is an exchange of electrons between electrodes which is not completely suppressed at voltages near zero. At large negative grid bias all secondaries formed at the cathode are suppressed, and a fraction $(1 - x)$ of the secondaries formed at the grid arrives at the cathode, appearing as a positive addition to the alpha-particle current. It is also seen in Figure 31 that the cathode current approaches its limit more slowly when grid bias is negative than when grid bias is positive. This reflects the fact that it is easier to attract electrons from the cathode than to suppress their emission (turn them back).

*A small leakage observed in preliminary data presented in the midpoint report was found to be in the external circuitry and was eliminated.

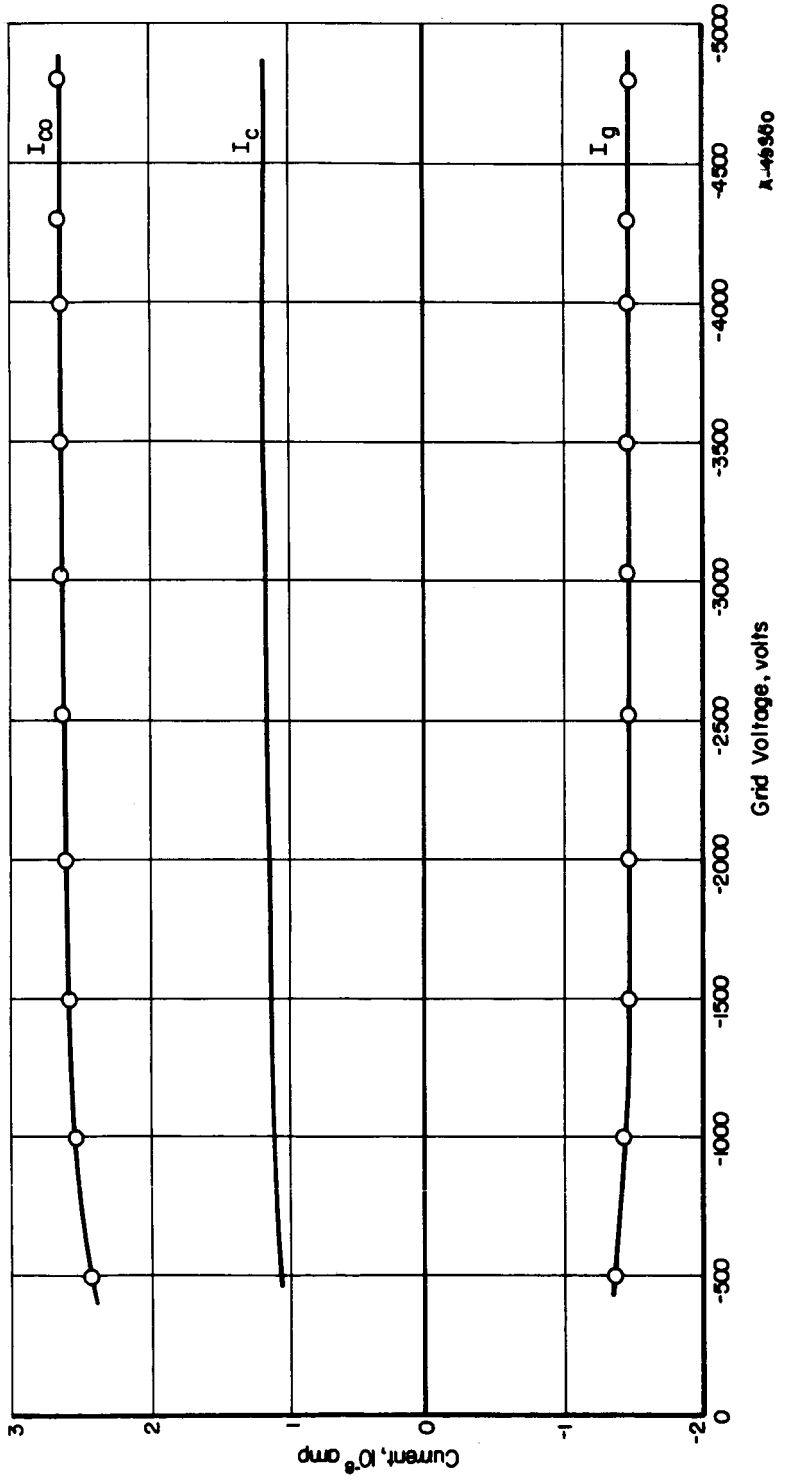

FIGURE 29. CELL CURRENTS AT LARGE NEGATIVE GRID VOLTAGE

Anode grounded.

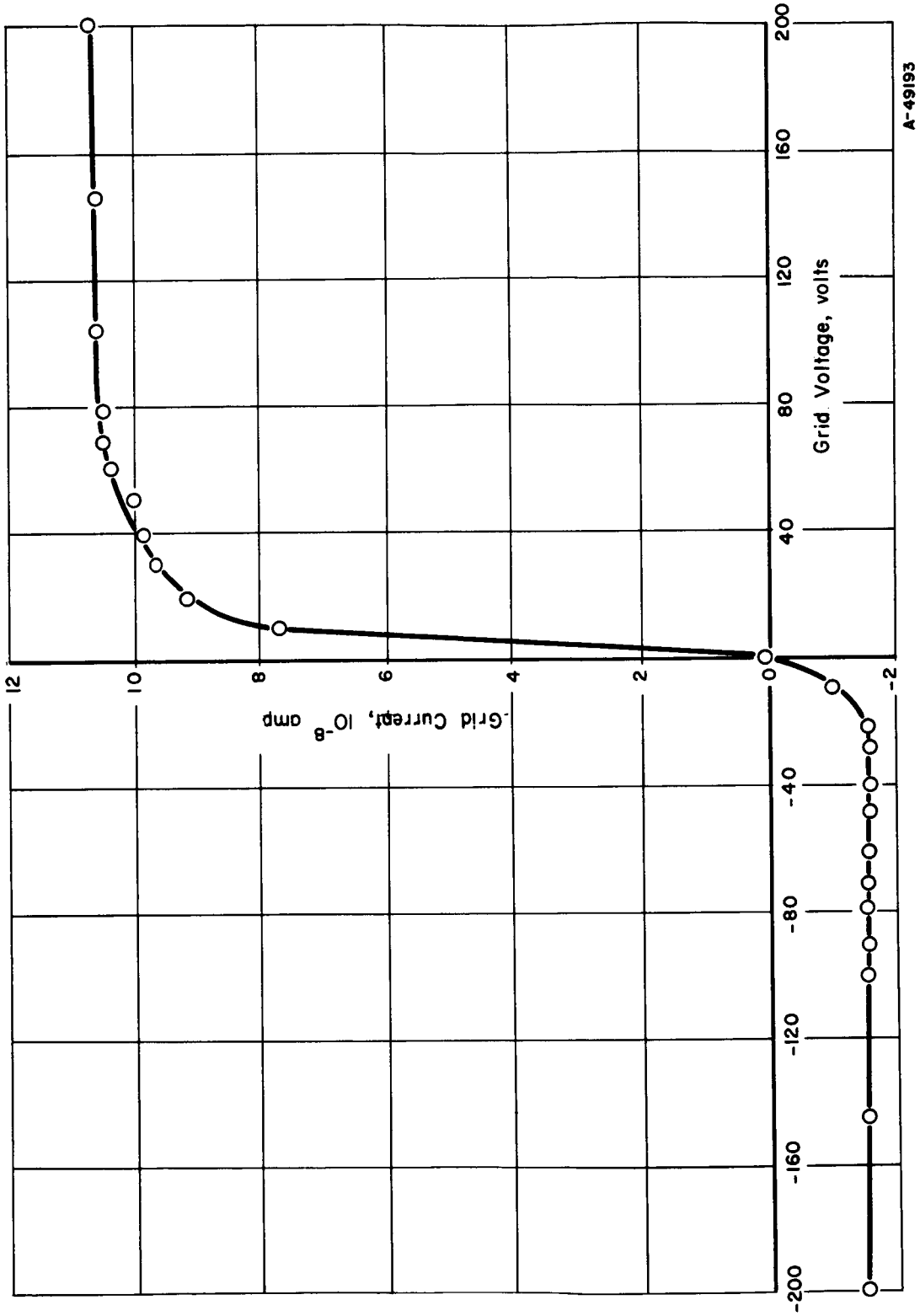

FIGURE 30. GRID CURRENT AT LOW GRID VOLTAGE

Anode grounded.

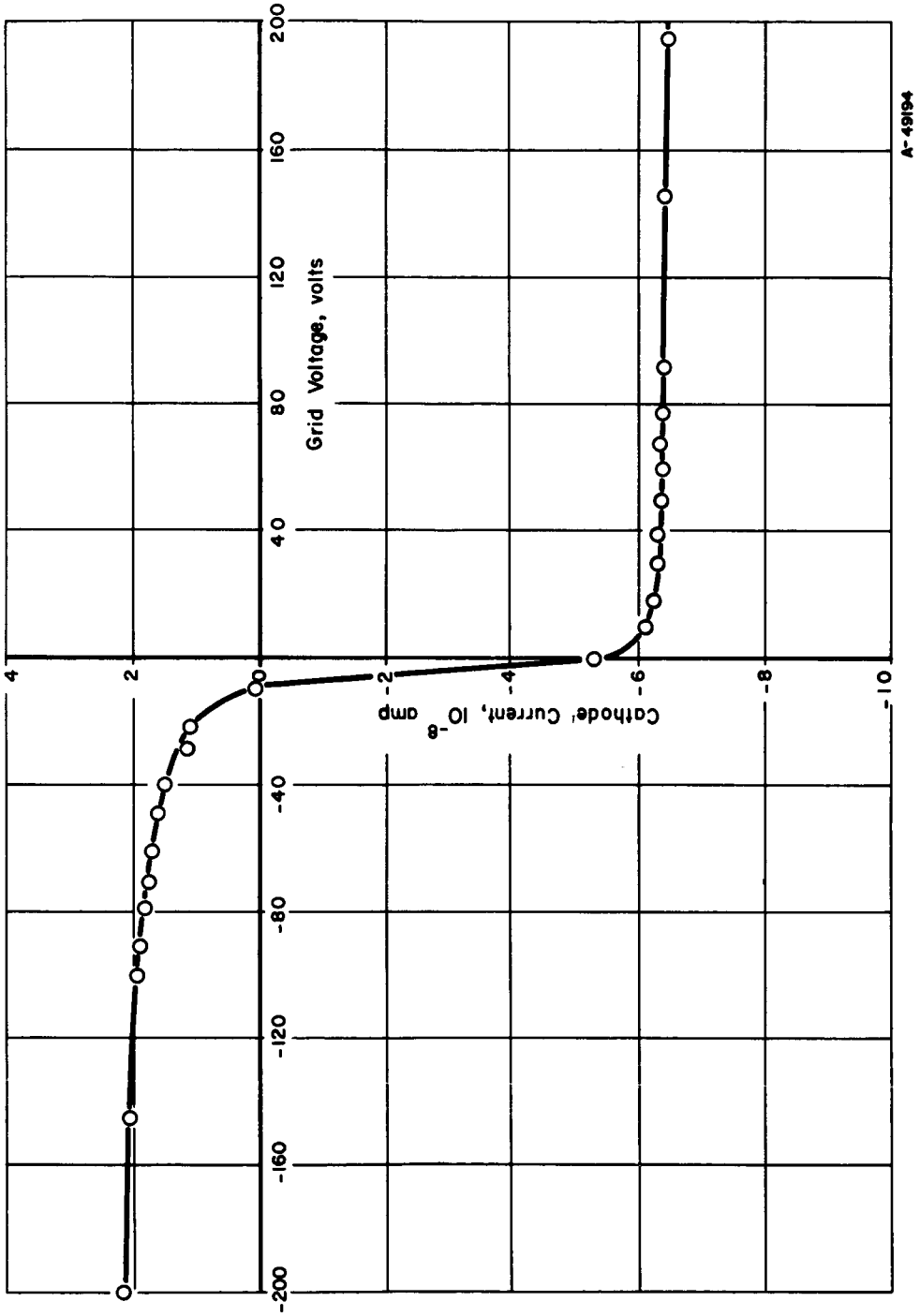

FIGURE 31. CATHODE CURRENT AT LOW GRID VOLTAGE

Anode grounded.

Cell Parameters When Anode is Grounded. Using the previously derived relations for the cell currents at large negative grid bias [see Equations (8) and (9)], we have

$$I_{co} = [1 + f\eta_g - xf\eta_g]\, I_o$$

$$I_g = -f(1 + \eta_g)\, I_o \quad .$$

By using calculated values of the alpha-particle current I_o and of the f-factor, these two equations permit evaluation of η_g and x to a first-order approximation. The data for this evaluation and for comparison with results of the previous experiments are given in Table 4. To calculate I_o from the source strength, one must consider both the alpha-particle loss and the charge degradation due to the presence of the metallic foil wrapped over the polonium-210. These corrections were estimated by replacing the observed variation of mean alpha-particle charge, $\overline{Z}$, with particle energy[23] by a step function:

$$\overline{Z} = \begin{cases} 0 & E < 0.65 \text{ Mev} \\ 2.0 & E > 0.65 \text{ Mev} \end{cases} \quad .$$

The range of alpha particles in the covering material was then taken as that length, R_{eff}, which reduced the alpha particle energy to 0.65 Mev. The stopping power was assumed to be constant over the energy interval 0.65 Mev $\leq E \leq$ 5.30 Mev, and deviations of particle paths from straight lines were neglected. The alpha particle current is then given as

$$I_o = 1/2\ DeZ_o\ (1 - t/R_{eff}) \quad , \qquad (46)$$

where D is the disintegration rate in the emitter (determined from the reported curie content), e is the electronic charge, Z_o is the alpha-particle charge at birth, t is the thickness of the metallic foil covering the polonium, and the factor of 1/2 accounts for the fact that only half of the alpha particles are emitted radially outward from the fuel layer.

The resulting parameters obtained from combining the calculations with the current measurements are listed in Table 5 for the two experiments. This comparison shows several unexpected results. The secondary-electron production at the grid as reflected by η_g* is more than a factor of two larger in the new experiment, whereas the x-factor (the fraction of secondary electrons formed at the grid which escape to the anode) is considerably smaller. As a result, the net fractional loss in charging current, δ, is the same in the two cases, where

$$I_c = I_{co} + I_g = [1 - f(1 + x\eta_g)I_o = (1 - \delta)\, I_o \quad .$$

Presumably, the change in x is due to the differences in geometry in the two experiments, since the grid-wire diameter and material were held constant. The change in η_g was not understood until the experiment was opened for visual observation at the conclusion of the experimental studies. It was then observed that the steel wires were partially oxidized. Presumably, they were in this condition at the time of inserting the grid-cathode assembly into the chamber, but the oxidation had gone unnoticed. Generally an oxide layer on a metal increases the secondary electron emission.[24]

*The secondary-electron yield Λ is related to η by $\Lambda = \eta\,\overline{Z}$, where $\overline{Z}$ is the average charge on an alpha particle striking the grid. Hence the yield is approximately twice the magnitude of η.

TABLE 4. SOURCE STRENGTHS AND SATURATED CURRENTS IN ALPHA-CELL EXPERIMENTS

	Source Strength at Time of Experiment[a], curies	Correction Factor For Losses in Covering Foil	Calculated Alpha-Particle Current, I_o, 10^{-8} amp	Measured Grid Current, I_g, at Large Negative Grid Bias[b], 10^{-8} amp	Measured Cathode Current, I_{co}, at Large Negative Grid Bias[b], 10^{-8} amp
Previous experiment	7.01	0.624	2.59	-1.23	2.80
New experiment	6.05	0.545	1.95	-1.46	2.64

(a) Obtained from manufacturer's reported curie content, corrected for radioactive decay to the time of the current measurements.
(b) From data given in Figures 13 and 29.

TABLE 5. SECONDARY-ELECTRON EMISSION AND GRID PARAMETERS

	Calculated f-Factor	Charge Ratio at Grid, η_g	Charge Ratio at Cathode[a], η_c	x-Factor	δ-Factor[b]
Previous experiment	0.120	2.96	3.82	0.772	0.394
New experiment	0.0955	6.84	3.95	0.458	0.395

(a) Data at large positive bias extrapolated to zero voltage.
(b) $\delta = f(1 + x\eta_g)$ and represents the fractional reduction in charging current due to the presence of the grid.

It should be pointed out that these parameters derived from the data are sensitive to the calculated values of f and I_o and should be considered as preliminary results. The x-factor obtained in this manner appears to be much larger than would be expected and is particularly sensitive to the choice of f and I_o. However, the ratio of the η_g's in the two experiments is less sensitive to the choice, and even if x is taken to be zero, the η_g in the new experiment shows up to be a factor of two larger than in the previous experiment.

The charge ratio of secondary electrons to alpha particles at the cathode, η_c, is obtained from the cathode current with positive bias on the grid,

$$I_{co}^{+} = - (\eta_c - 1) I_o \quad . \tag{47}$$

As previously observed[3], the secondary emission from the cathode is slightly dependent on the grid voltage in a manner similar to the Schottky effect. This effect predicts a change in surface work function of

$$\Delta\phi = (eE/4\pi\epsilon_o)^{1/2} \tag{48}$$

where E is the electric field at the emitter which is proportional to the applied grid voltage. Although this effect is usually associated with thermionic emission, the change in work function is independent of a thermionic model of emission. On the other hand, the effect of the change in work function on the secondary yield appears to be the same as that for thermionic emission, i.e., the yield is related exponentially to the change in work function. Figure 32 presents a Schottky plot of the data above 100 volts, where the grid bias is sufficient to cut off interchange of secondary-electron flow between anode and cathode. The yield at zero voltage is found by extrapolation and is listed in Table 5. Since the cathode geometries are not radically different in the two experiments and since the secondary-electron emission is not strongly dependent on material[24], it would be expected that η_c would be approximately the same in the two experiments (gold versus stainless steel cover over the polonium). The comparison in Table 5 shows this to be the case.

After the alpha cell experiment had been in continuous operation in the vacuum chamber for a month, the secondary-electron emission from the cathode was again measured as a function of grid voltage. In this experiment the grid voltage was varied up to 10,000 volts, producing a maximum electric field at the cathode of the order of 10^6 v/m. (This experiment also demonstrated that the grid design would sustain 10,000 volts without breakdown.) The results are shown graphically in Figure 33. The data appear to fit a Schottky plot over the extended grid-voltage range. From extrapolation of a least-squares fit to the data, the charge ratio at zero electric field was determined to be 3.32. This value is about 10 per cent smaller than that obtained a month earlier. This difference is probably due to a change in cathode surface condition with time.

Discussion of Results of Analyses. A general observation to be made from the measurements of cell currents is that their qualitative behavior with grid voltage is in accord with the reasoning behind the development of the detailed expressions for the currents leaving the individual electrodes. That the grid current is independent of grid voltage at large negative bias further shows that there are no unexpected second-order electron-emission effects. [This is a particularly significant fact in view of the presence of such effects in a cell using fission fragments as the charging particles.[25]]

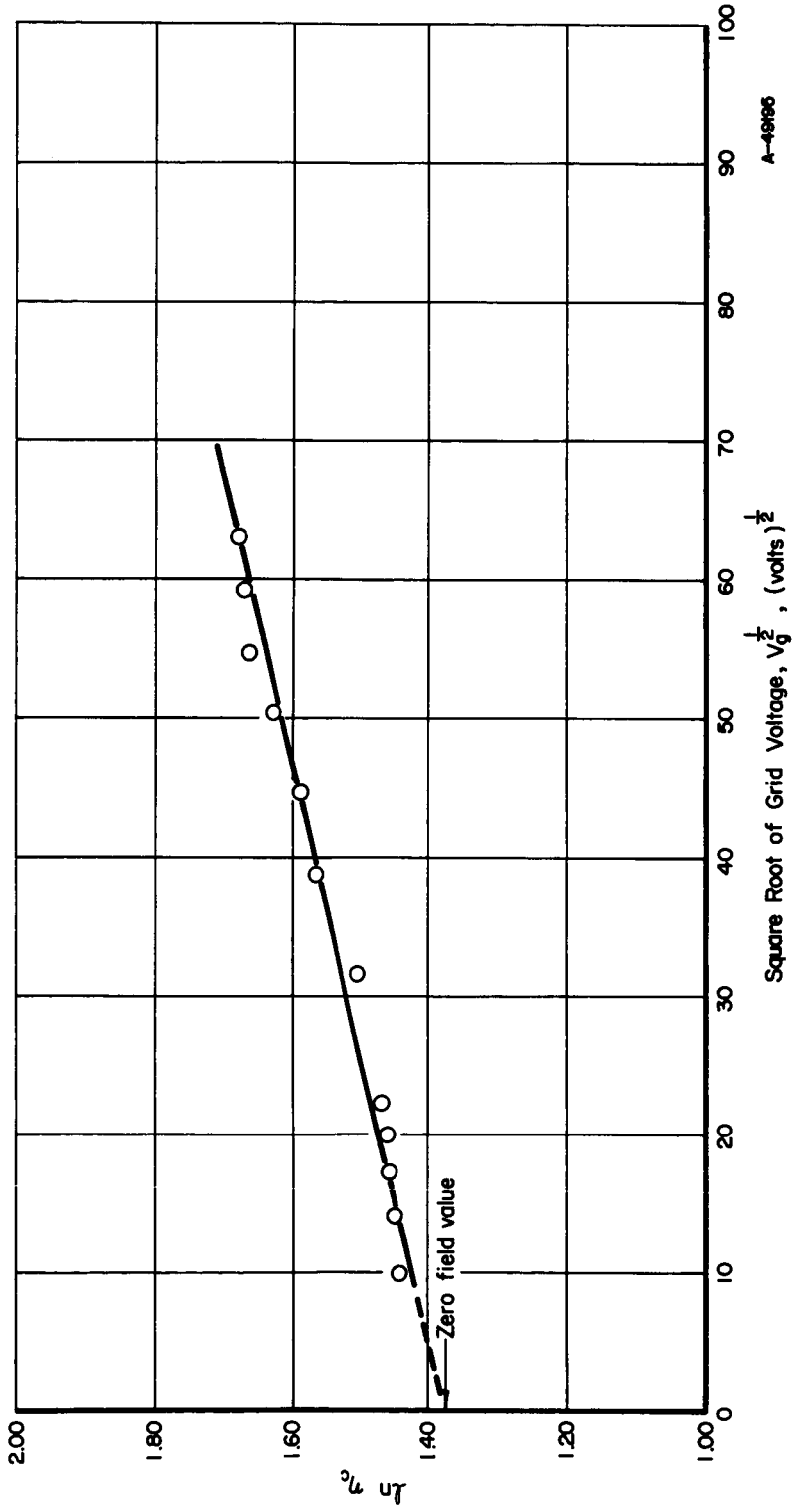

FIGURE 32. SCHOTTKY PLOT OF CHARGE RATIO AT CATHODE

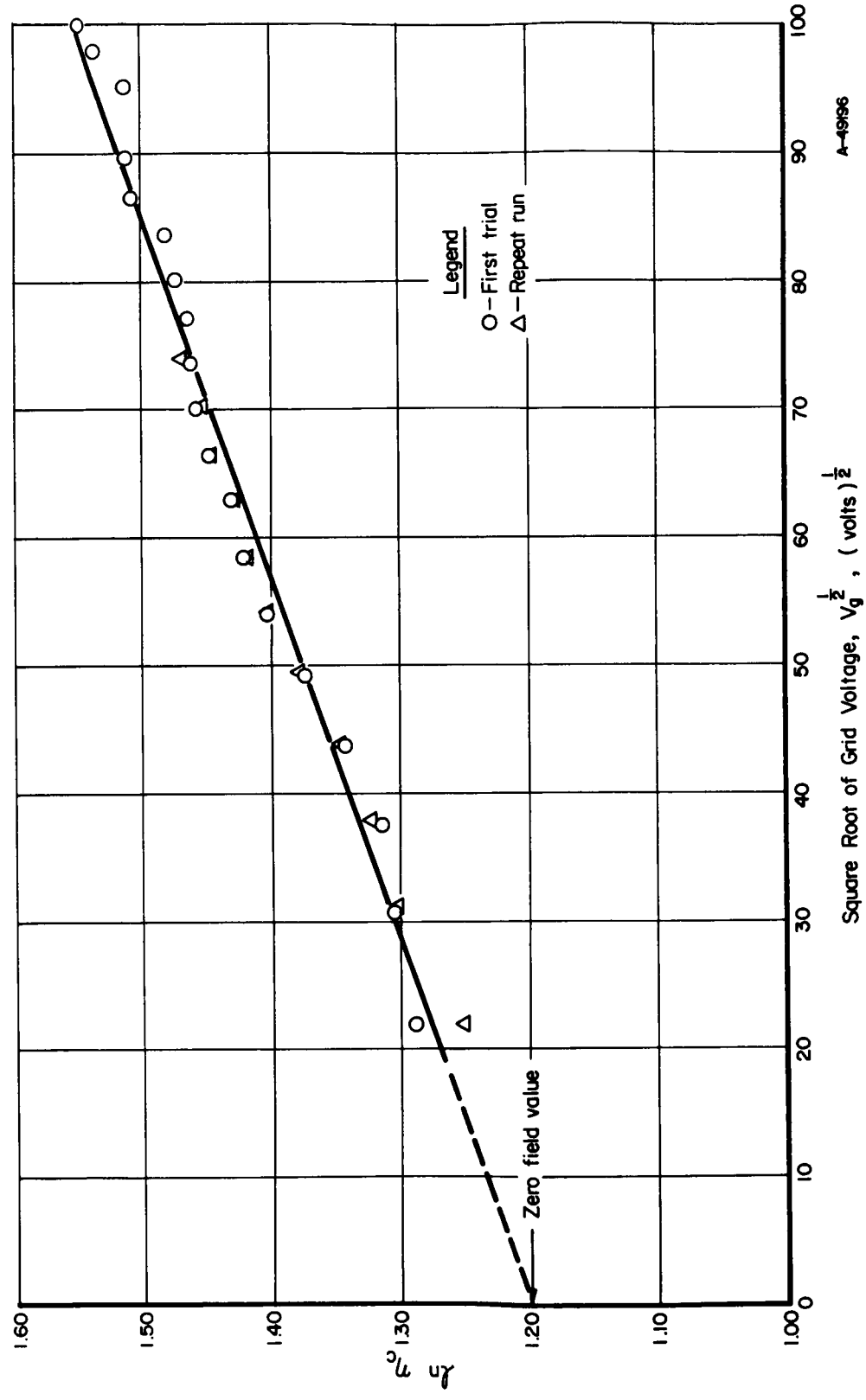

FIGURE 33. CHARGE RATIO AT CATHODE AFTER 1 MONTH'S OPERATION

The analysis shows that the two different grids are equal in their reduction in the charging current (they have the same δ-factor), in spite of the design differences. Although this striking constancy of the δ factor in the two cases raises the possibility that δ is a more fundamental characteristic of the cell (that is, within limits one obtains the same δ-factor regardless of geometry), it is believed at present that the agreement is fortuitous.

By comparing the grid design parameters derived from two experiments, it was found that the fraction x of secondaries formed at the grid which are released to the anode is apparently quite sensitive to geometry changes. Figure 34 summarizes the differences in the two experiments.

Without attempting to explain the differences in the magnitudes of the x-factors in the two experiments, the fact that x is large can possibly be explained as shown in Figure 35. It is known that the dependency of the secondary-electron yield on the angle between the incident particle and the normal to the surface is

$$\Delta(\theta) = \Delta_n \sec \theta \quad , \tag{49}$$

where Δ_n is the yield at normal incidence.[26,27] Thus, the secondary-electron yield would be expected to be very large for the few alpha particles just grazing the grid wires. The large x-factors would indicate that many secondaries are being formed in a position to be released to the anode. Possibly the few grazing collisions, with their exaggerated yield, are causing most of the losses.

These grid design parameters, it appears, will require repeated confirmation in order to gain confidence in their magnitudes. Their importance, of course, is that they are related directly to the efficiency attainable with a gridded device.

The value of η_c is important only in demonstrating that some means of suppressing secondary electron emission from the cathode is required. (It is possible that its magnitude will also have bearing on the high-voltage conversion technique.) That an increase in η_c occurs with electric field is incidental to the cell performance. However, it is significant to note that the Schottky-type enlargement of secondary-electron yield at the cathode with grid voltage is not present on the secondary yield at the grid wires, i.e., increase of negative grid bias on the grid fortunately does not result in a larger grid current. This somewhat puzzling difference may be related to the fact that the alphas are emerging from the cathode but impinging on the grid wires. It is plausible that the concentration of secondary electrons near the cathode surface is much greater than the concentration near the grid wire surface on a per alpha particle basis; hence, an applied field has a more significant effect on the emission at the cathode.*

Initial Voltage Buildup

The approach to high-voltage operation was initiated with the new emitter installed. This approach involved a series of steps with appropriate data at each voltage level. The first level, 100,000 volts, was achieved at high vacuum (less than 10^{-6} torr) with approximately -2000 volts on the grid. Microdischarging was observed at 100 kv and prevented further increase in voltage buildup under high vacuum.

*The situation appears to be different with fission-fragment primaries, in which case the grid current has been observed to increase as the grid voltage becomes more negative. This Schottky-type effect on secondary-electron emission may explain the failure to obtain appreciable voltage buildup in a gridded device when using fission-fragment primaries.[25]

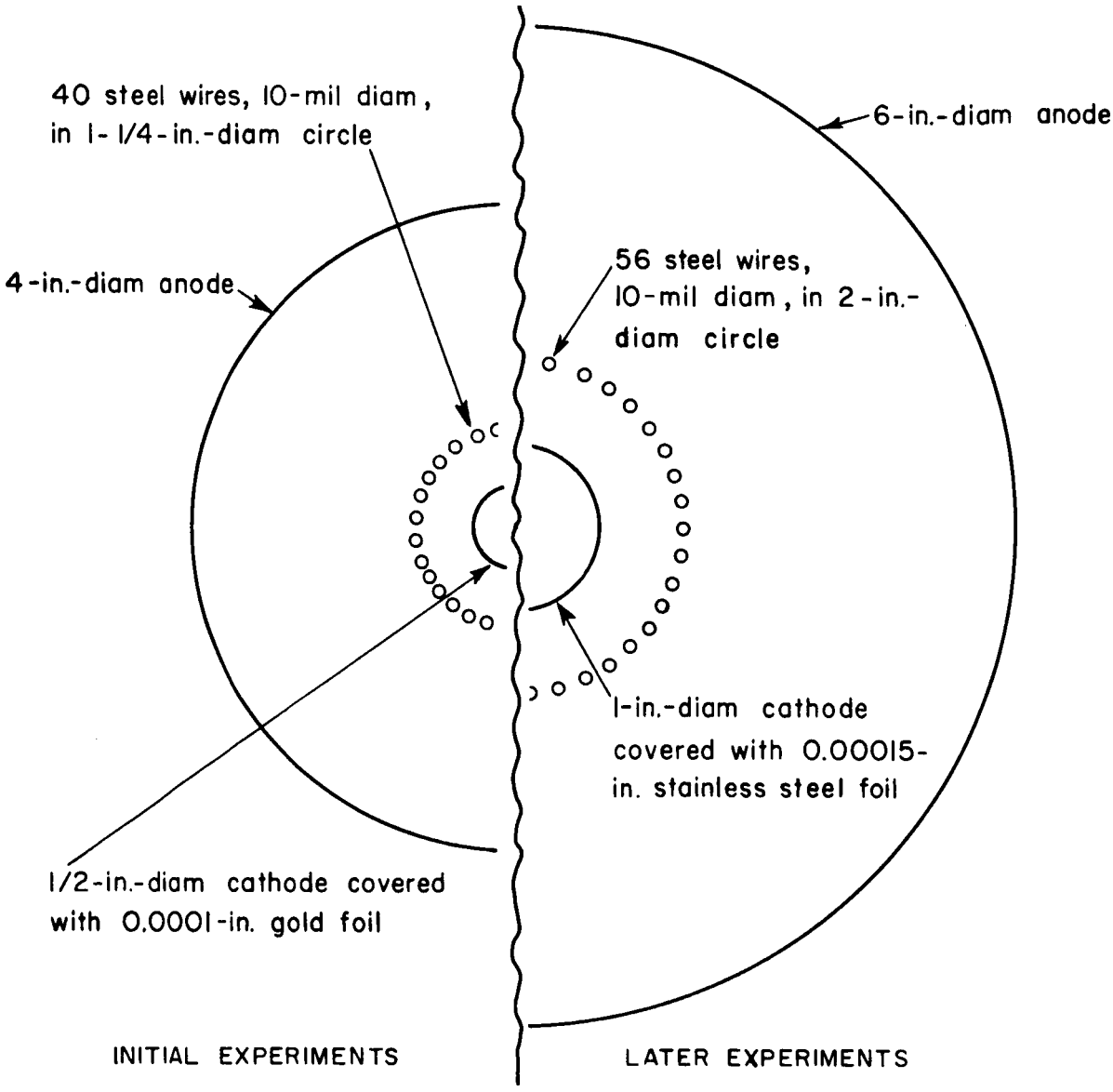

FIGURE 34. COMPARISON OF CELL GEOMETRIES IN TWO ALPHA-CELL EXPERIMENTS

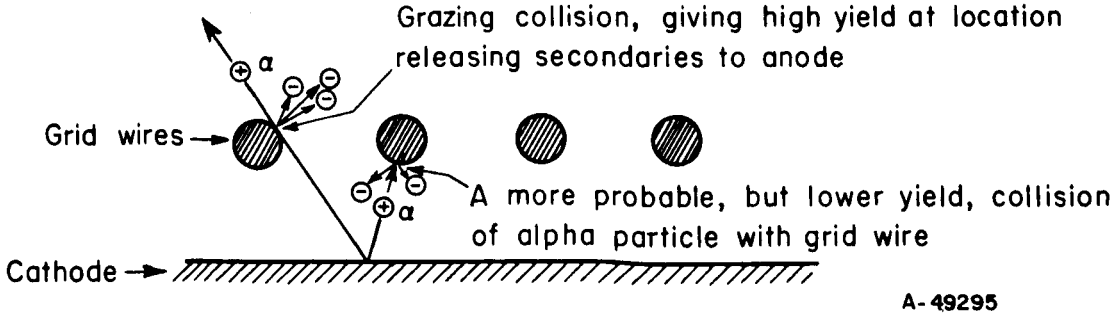

FIGURE 35. POSSIBLE EXPLANATION FOR LARGE x-FACTOR

After several hours' operation at the 100-kv level at high vacuum, the maximum voltage attainable under the initial conditions appeared to decrease to near 50 kv*, i.e., some sort of conditioning effect appeared to be present. This general behavior was observed previously in the operation of a beta high-voltage generator (see Figure 18 and the accompanying discussion).

Measurement of the voltage buildup with time permitted an independent check on the charging current to the anode,

$$I_C = C(dV_a/dt)_o \quad , \tag{50}$$

where C is the anode capacitance and $(dV_a/dt)_o$ is the slope of the curve of anode-voltage buildup with time evaluated at t = 0. From a slope of 206 volts/sec and measured anode capacitance of 62 $\mu\mu$f, the charging current was determined to be 1.28×10^{-8} amp, in good agreement with the current measurements presented in Figure 29. (It is estimated that only 3 per cent of the current leaving the grid-cathode assembly flows out the end of the anode cylinder; the remainder flows directly to the anode as the charging current.)

Grid Control of Anode Voltage

Figure 36 shows the net cathode current as a function of grid bias at low voltages. It is seen that in both the previous and in the new experiments the net current becomes positive between -40 and -50 volts. (This comparison further emphasizes that both grid designs have similar electron-caging characteristics.) Thus, voltage buildup on the anode is possible whenever the grid voltage exceeds about -50 v. Under high-vacuum operation the grid was again found to control the anode voltage below the voltage limit set by microdischarging. Figure 37 shows the anode voltage obtained as a function of the grid bias. The scatter in the data reflects the fact that it is more difficult to determine voltages with the alpha voltmeter in the low voltage range. However a least-squares fit of a straight line to these data produced an intercept at -40 volts' grid bias, in agreement with the data presented in the previous graph. As indicated previously, a gross measure of the effective amplification factor $\mu = \Delta V_a/\Delta V_g$ can be obtained from the slope of this line, neglecting possible nonlinearities. Table 6 presents a comparison of μ obtained in this fashion with the value calculated from the triode-tube formula, Equation (28), for both experiments. This comparison shows that the measured amplification factor in both cases is within about 20 per cent of the calculated value, but the measured value is not consistently higher or lower than the calculated value. This agreement is probably an indication both of the accuracy of the voltage determination at the lower voltages and of the validity of applying the triode-tube formula to the alpha cell system. These data are interpreted as showing that the amplification factor of the alpha-cell grid design can be predicted to a first order approximation.

*These observations of the initial behavior of anode voltage with time were complicated by instrumentation malfunctioning and by the fact that voltage was not monitored nor maintained continuously during this initial period to allow for a prearranged series of experiments (voltage buildup with time, grid-control studies, etc.)

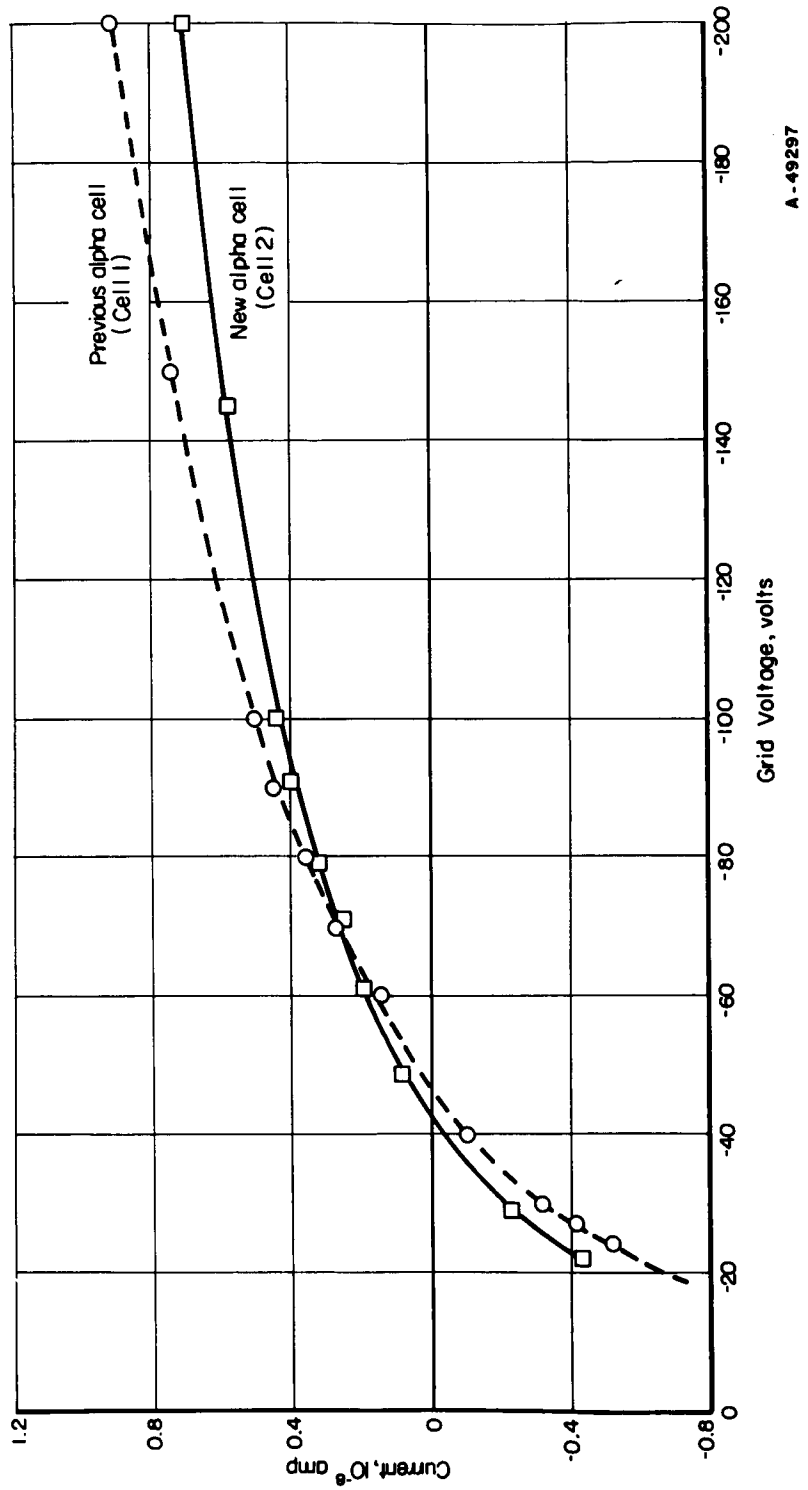

FIGURE 36. NET CURRENT FROM GRID-CATHODE ASSEMBLY

$I_C = I_{CO} + I_g$.
Data not corrected for differing source strengths.
$\left(I_{02} \cong \frac{3}{4} I_{01}\right)$.

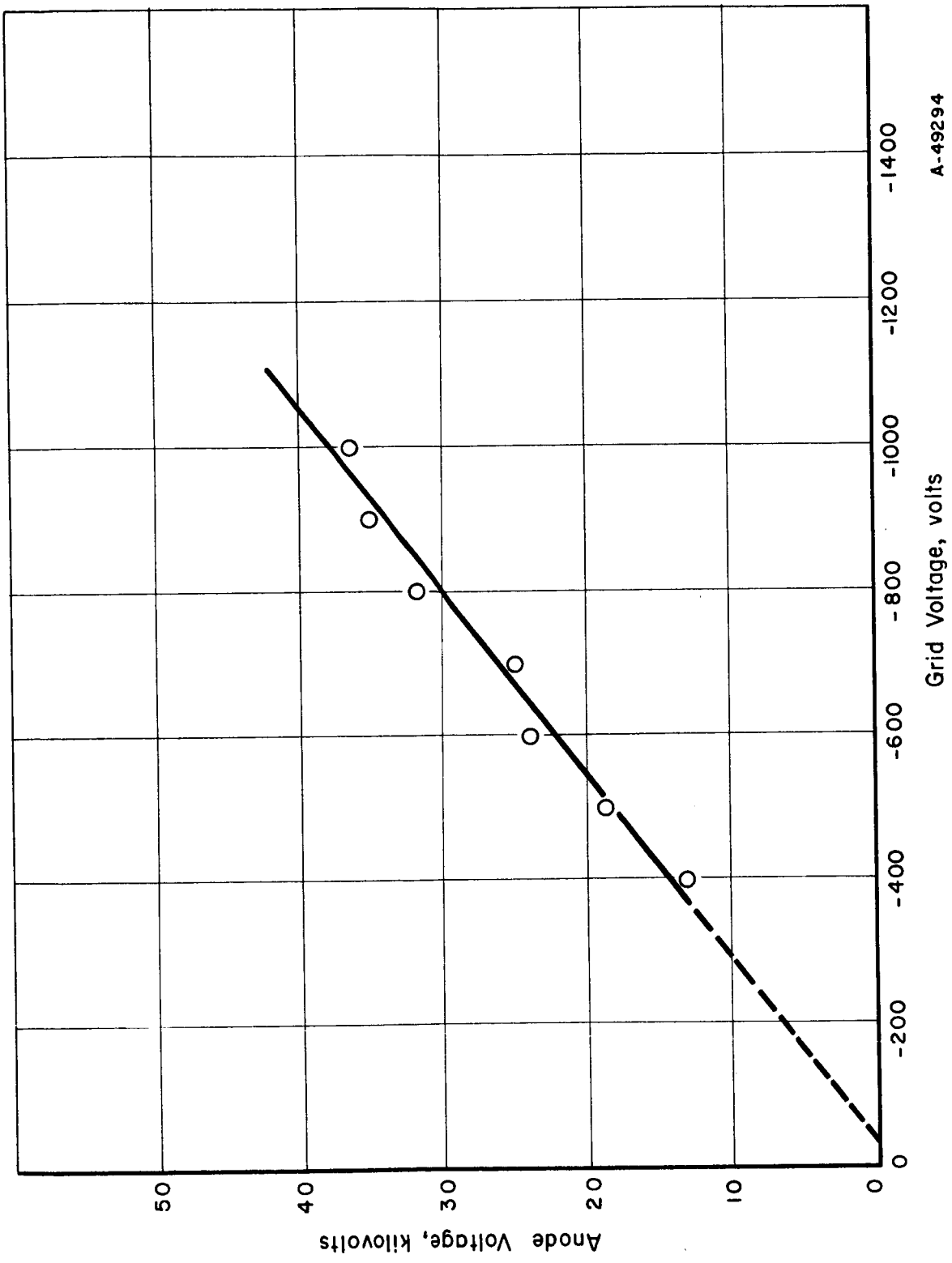

FIGURE 37. VARIATION OF ANODE VOLTAGE WITH GRID VOLTAGE

TABLE 6. CALCULATED AND MEASURED GRID-AMPLIFICATION FACTORS

	Calculated μ	Measured μ(a)
Previous experiment	41	50
New experiment	48.5	40

(a) Assumes linearity of anode voltage V_a with grid voltage V_g so that $\mu = \Delta V_a / \Delta V_g$ is simply the slope of the V_a versus V_g line.

Behavior of Cell Currents With Anode Voltage

The variation of the charging current to the anode with anode voltage is reflected by the behavior of the voltage buildup with time. A typical curve is shown in Figure 38, which was obtained from the average of several trials in order to eliminate fluctuations in the count-rate output from the voltmeter. The approximately linear buildup from 0 to 30 kilovolts indicates constant charging current over this range. Above 30 kilovolts, the rate of buildup decreases, indicating a decreasing charging current. As will be discussed later, this decrease is presently attributed to a voltage-dependency of the x-factor, since at this voltage range no significant effect on alpha-particle trajectories is to be expected. At the time of the measurements, microdischarging was being initiated as low as about 40 kilovolts, abruptly terminating any further voltage buildup. *

The transient behavior of cell currents with anode voltage is shown in Figure 39. Voltage buildup is initiated by removing a grounding bar from contact with the anode. Looking first at the grid current, it is seen that immediately upon release of the grounding bar the current flow to the grid increases in magnitude stepwise and then remains constant up to about 30 kilovolts. This step increase is due to the current induced to the grid by the changing anode voltage, i.e.,

$$I_g = (I_g)_\alpha + C_{ga} \frac{dV_a}{dt} \quad , \tag{51}$$

where $(I_g)_\alpha = -f(1 + \eta_g)I_o$ is the grid current produced by alpha particles and secondary electrons, and C_{ga} is the coefficient of inductance between the grid and anode. The second term, responsible for the step increase in I_g, produces a charge accumulation on the grid and does not represent a physical exchange of current between the grid and the other electrodes. Note that at about 30 kilovolts, where dV_a/dt breaks from a constant value as shown in Figure 38, the current to the grid decreases. At the voltage where microdischarging is initiated, the grid current attains a value equal in magnitude to the cathode current but of opposite polarity, resulting in a zero net charging current. That the step increase in I_g is indeed due to the changing anode voltage was checked by measuring I_g for several steady voltages (up to 20 kv) applied to the anode by an external power supply. These data, also presented in Figure 39, show that the steady-state grid current is constant with anode voltage and maintains the value measured with the anode grounded.

*It should be emphasized that microdischarging is a threshold phenomenon. For example, at voltages below the threshold where the grid controls the anode voltage (Figure 37), no microdischarges are observed.

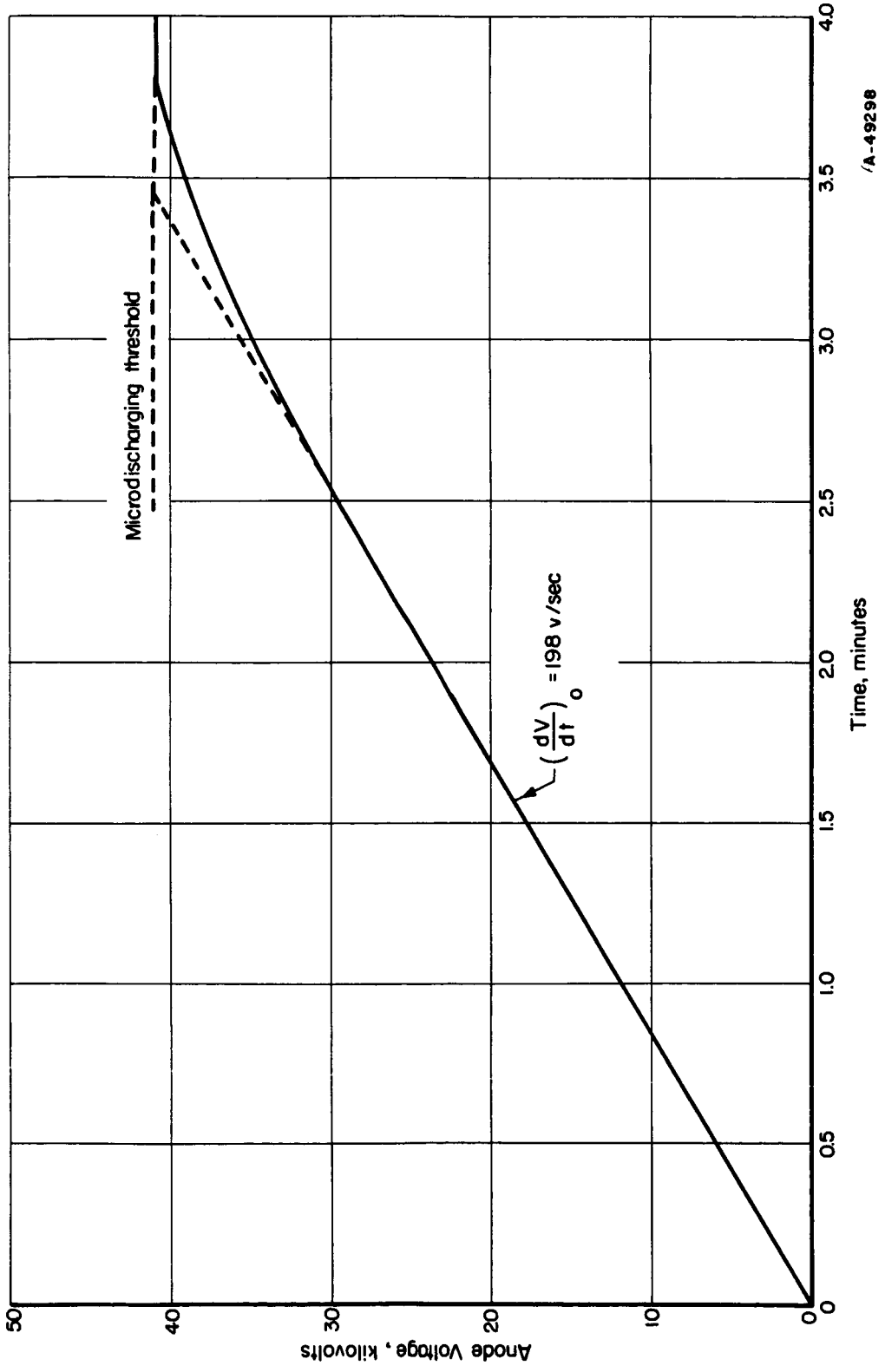

FIGURE 38. TYPICAL VOLTAGE BUILDUP WITH TIME

-2000-volt grid bias.

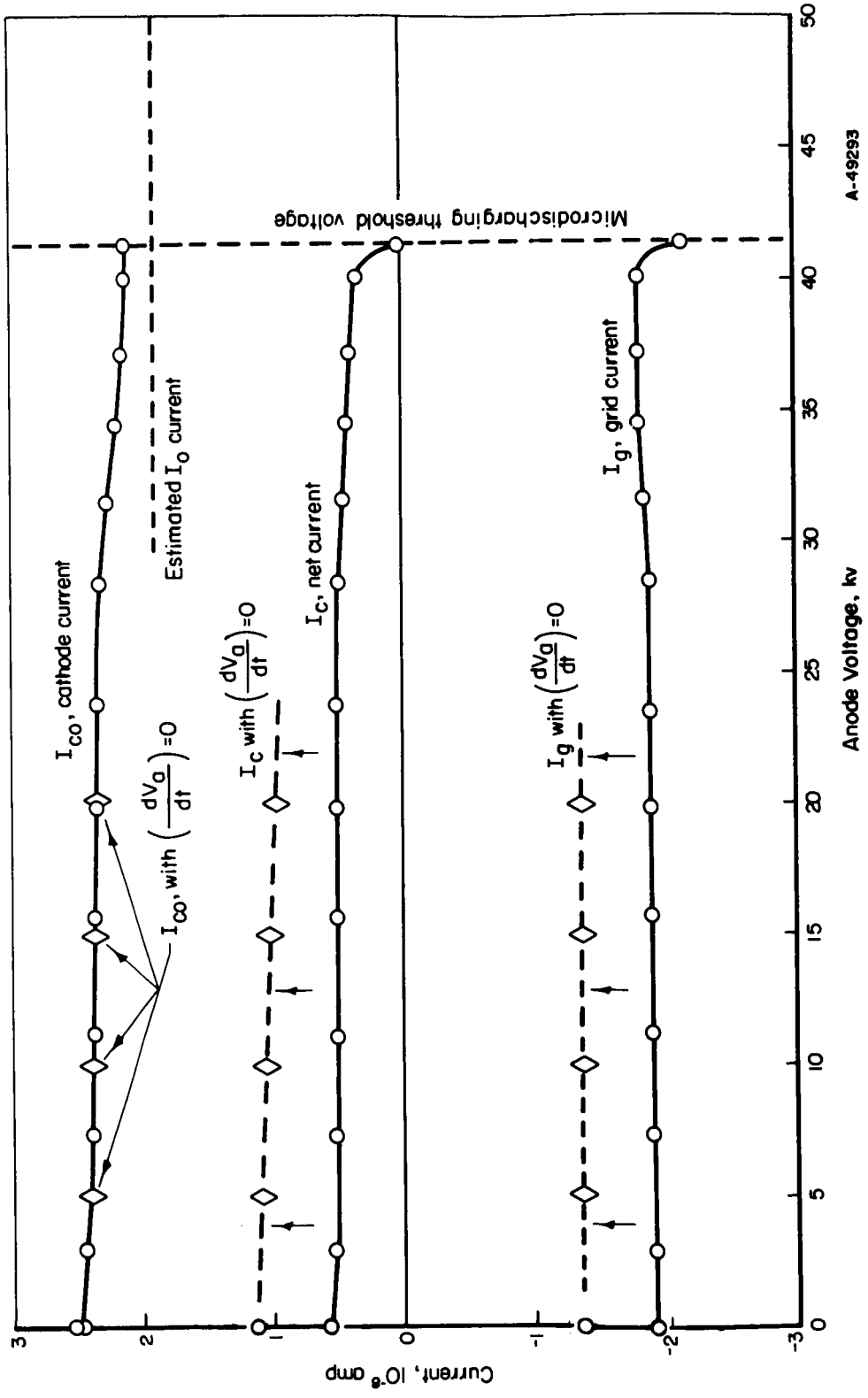

FIGURE 39. TRANSIENT BEHAVIOR OF CELL CURRENTS WITH ANODE VOLTAGE

-2000-v grid bias.

Because of the weak interaction between the anode and cathode, the changing anode voltage produces only a slight shift of cathode current, as shown in the graph. Recalling that the cathode current is

$$I_{co} = [1 + (1 - x)f\eta_g]I_o$$

the observed change in I_{co} with anode voltage is interpreted as a possible variation of the x-factor with anode voltage, i.e., the fraction of secondary electrons formed at the grid which escapes to the anode appears to increase with anode voltage, as would probably be expected. With this interpretation, $x(V_a)$ can be obtained from the I_{co} variation. The results are shown in Figure 40 for the data from Figure 39 with the grid at -2000 volts and also for several other grid voltages. It is seen that with -2000 volts on the grid, x apparently increases from about 0.5 to 0.8 as the anode voltage increases from 0 to 40 kilovolts. This interpretation is consistent with the previously discussed conjecture that many of the grid secondaries are formed by alpha particles striking the grid wires at grazing angles in locations where they can escape to the anode. Figure 40 also shows that the x-factor variation with anode voltage is dependent on grid voltage. Above 25-kilovolt anode voltages, the data indicate that with higher grid voltage the change in x-factor is less at a given anode voltage, which would be expected.

Returning to the current-voltage curves of Figure 39, it is seen that the measured net current to the grid-cathode assembly reflects the step change in grid current due to the changing anode voltage. The actual net current to the anode decreases slightly from 0 to 20 kilovolts. This decrease is interpreted as resulting from the change in x-factor, since $I_c = [1 - f(1 + x\eta_g)]I_o$. Presumably, the decrease continues at higher anode voltage, assuming the I_{co} behavior above 20 kilovolts to be due to a changing x-factor. At the voltage where microdischarging is initiated, the net current goes to zero.

Discussion of the Results of Analysis of Cell Current-Voltage Behavior. The large (dV_a/dt) in the alpha cell generates induced currents which mask the actual current-voltage behavior of the charging current to the anode. This fact prevents direct observation of the transient behavior of the cell charging current. However, the current to the cathode, which is shielded from the anode by the grid, is nearly free from induced currents and may be used to study changes in cell parameters with anode voltage. Attributing the change in I_{co} to a change in the x-factor indicates that the x-factor increases appreciably with anode voltage. In terms of cell design, this means that for high-voltage operation it must be assumed in the design that nearly all secondaries formed at the grid will escape to the anode. This tentative conclusion further emphasizes the necessity for a small f-factor, since charging current losses are proportional to $f(1 + x\eta_g)$. Alternatively, the data suggest that different grid designs be sought in which the fraction of secondaries released to the anode can be reduced, possibly by staggering the grid wires with respect to distance from the cathode so that some of the wires suppress the electron release from other wires.

Microdischarges

The frequency of microdischarging at 42-kv anode voltage (vacuum chamber pressure 4×10^{-7} torr) was observed by viewing the grid current with an oscilloscope. A typical scope picture of the discharging is shown in Figure 41, with a sweep of 1 sec

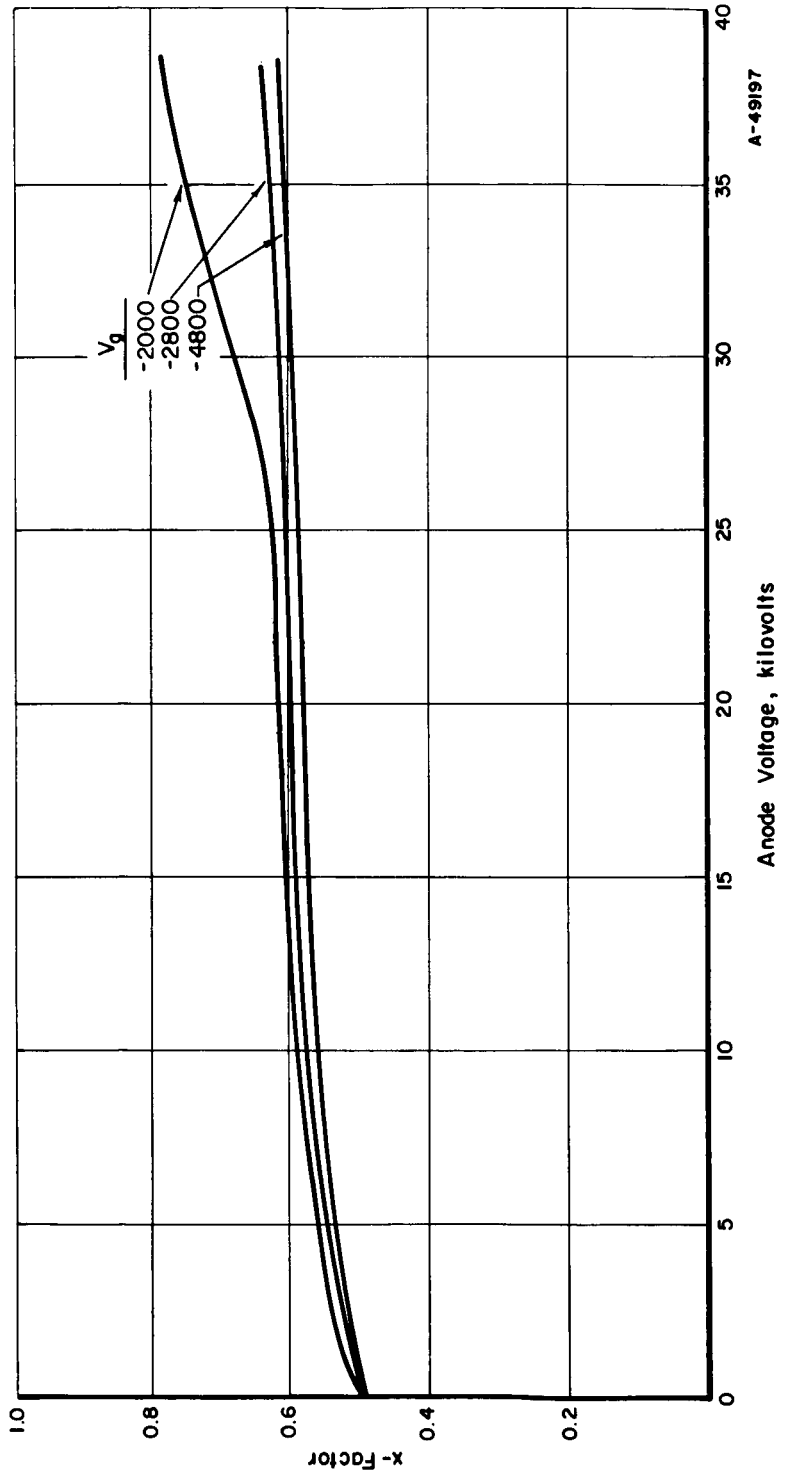

FIGURE 40. VARIATION OF x-FACTOR WITH ANODE VOLTAGE FOR SEVERAL GRID VOLTAGES

Assumes I_{co} variation with V_a due to change in x-factor.

per cm (per large division). The observed frequency was 90 per minute, in approximate agreement with the 110 min^{-1} frequency observed in the previous Battelle-sponsored experiment. With a charging current of about 0.75×10^{-8} amp at the limiting voltage, the average charge carried in each microdischarge is estimated to be 5×10^{-9} coul, or about 3×10^{10} electrons. This estimate assumes that the grid current is monitoring all microdischarges in the system and hence is probably an upper limit to the average charge per microdischarge. A probable lower limit of 2×10^{9} electrons per microdischarge was estimated by examining the waveform of the discharges on faster scope sweep.

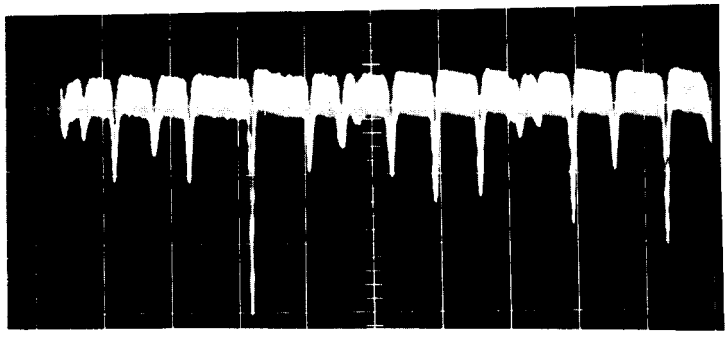

FIGURE 41. OSCILLOSCOPE PICTURE OF MICRODISCHARGING AS VIEWED ON THE GRID CURRENT

"Lifetime" Tests

With -2000 volts on the grid, the anode voltage was allowed to build up to the microdischarging limit (about 42 kv), and this voltage was observed for several hours to determine if any gross discharges would sporadically occur. The observation was terminated after 5-1/2 hours at full voltage. No gross discharges were observed; the voltage remained constant within the ability to determine the voltage by the voltmeter (about ±5 kv). Pressure during the measurements was steady at 4×10^{-7} torr.

After the alpha cell had been in continuous operation in the vacuum chamber for 6 weeks, the "lifetime" test was repeated, this time for a 60-hour period. Again, no instabilities were observed, although drift in the alpha voltmeter due to pressure changes in the voltmeter chamber precluded observation of slow anode voltage variations.

This brief study showed that the alpha cell was quite stable at the maximum voltage attained.

Variation of Anode Voltage With Chamber Pressure

Anode voltage was measured as the pressure in the vacuum chamber was varied from the normal operating pressure of 4×10^{-7} torr up to 2.5×10^{-2} torr. With the variable leak built into the system, the pressure could be held constant at any desired pressure in this range by admitting a controlled amount of gas to the system continuously as it was being pumped. This was done for several points in each decade

pressure range, with continuous recorder monitoring of anode voltage between the fixed points. At each point, the pressure was held constant sufficiently long to determine if a significant change in voltage was occurring. It was anticipated that a curve similar to that obtained previously (Figure 16) would be obtained showing a significant voltage increase near 10^{-3} torr, and it was planned to seek the maximum voltage attainable with this pressure effect by making small variations in pressure in this range and by adjusting grid voltage. However, as seen from the results presented in Figure 42, the anticipated anomalous behavior of anode voltage with pressure was not found. Instead, the anode voltage dropped sharply to zero at pressures between 10^{-5} and 10^{-4} torr. As observed previously, the anode voltage was constant with pressure below the drop off.

The data plotted in Figure 42 represent five different experiments. The data for the upper three curves were obtained within a few hours' span. These data show that there is no difference in cutoff pressure for various gases introduced into the chamber and for different grid voltage. The "wet" air curve is for ordinary room air, whereas the dry air curve is for room air passed through a dessicant. No large significance is attached to the small changes in the anode voltage at the high-vacuum limit associated with these various cases. Such differences are within the accuracy of the voltage determination in this range. The lowest curve was obtained 2 days before the others. For this particular experiment, the maximum voltage buildup was limited to 32 kv by microdischarging. This was the lowest voltage obtained during the course of the experiments, i.e., generally the microdischarging limited the voltage to 40-45 kv. Under the conditions of this experiment, the pressure at which the anode voltage dropped to zero was slightly higher than in the other experiments.

The reasons for the failure to obtain a higher voltage buildup near 10^{-3} torr are not fully understood. The most significant change between the new experiment and the previous one which might bear on this effect is the change in geometry, especially the change in anode diameter from 4 to 6 inches. It is possible that the changes in geometry rather critically affected the operation of the system as an ionization chamber, i.e., ionization may be occurring at lower pressures in the experiment, thereby masking the beneficial effects of a small amount of gas in suppressing undesirable charged-particle interchange between electrodes.

Variation of Cell Currents With Pressure

With the anode grounded, the cell currents were measured as the vacuum chamber pressure was varied from 2×10^{-7} to 2.5×10^{-2} torr. The measurements were made for several grid biases: -2000, -3400, and -4800 volts. Figure 43 presents a graph of the resulting variation. As seen from these data, below about 10^{-4} torr, the cell currents are essentially independent of vacuum-chamber pressure. Above 10^{-4} torr the grid and cathode currents both increase in magnitude, presumably because of ionization of the chamber gas. At 25 microns, the upper limit of the pressure range studied, the net current from the grid-cathode assembly is nearly zero.

Increase in the magnitude of the grid bias resulted in increased current magnitudes in the pressure range near 10^{-4} torr and above. The increasing grid bias also lowered slightly the pressure at which the currents deviated from the constant high-vacuum values.

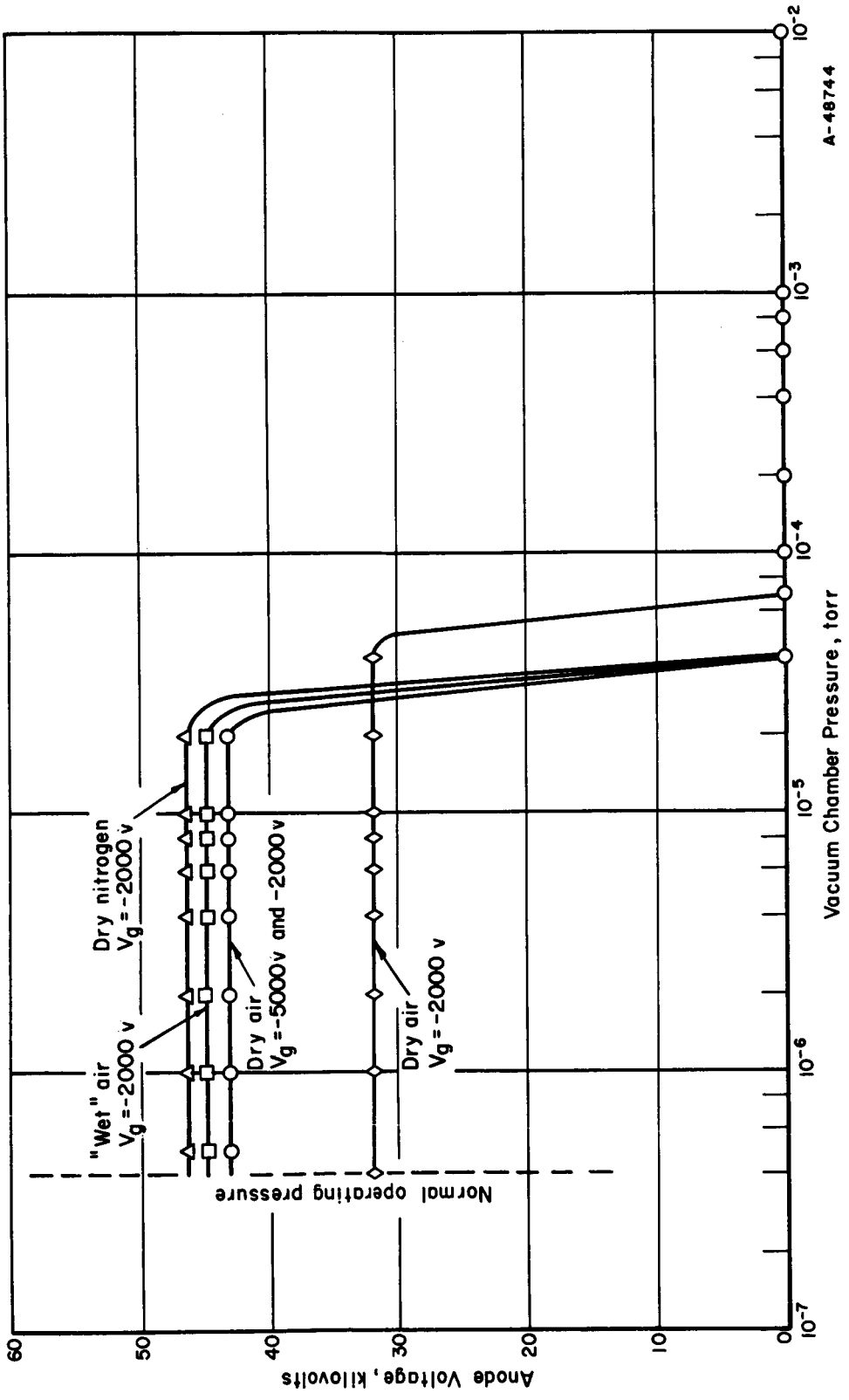

FIGURE 42. ANODE VOLTAGE VERSUS CHAMBER PRESSURE

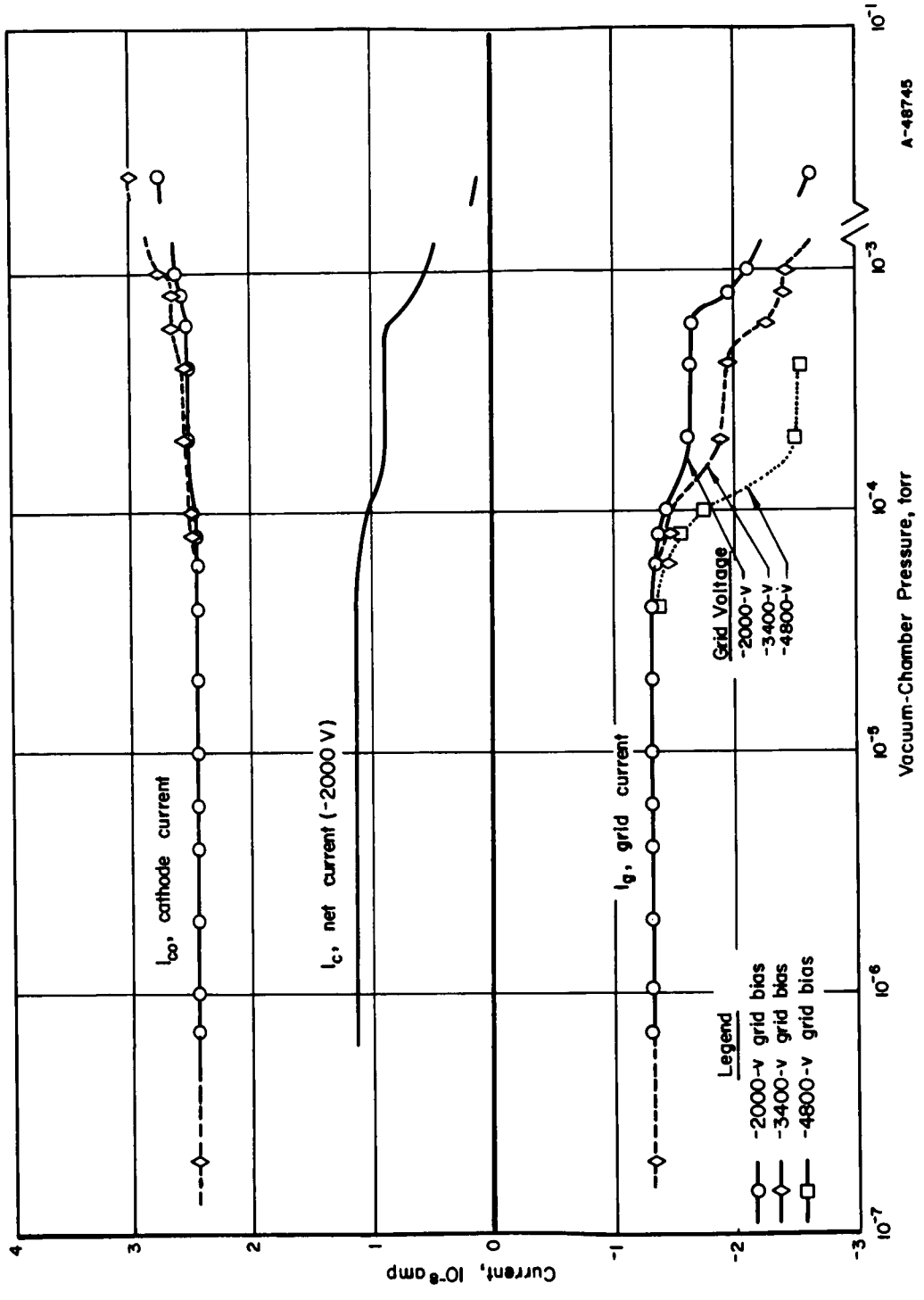

FIGURE 43. VARIATION OF CELL CURRENTS WITH PRESSURE, ANODE GROUNDED

Comparing Figures 42 and 43, it is seen that the anode voltage drops to zero near 5 x 10^{-5} torr pressure, even though the net (charging) current from the grid-cathode assembly to the anode remains approximately constant in this region. This indicates that current is leaking from the anode to the chamber walls or down the insulator, i.e., the loss in anode voltage with increasing chamber pressure is not due to leakage between the anode and grid but rather between the anode and other structures. However, charging-current losses at even higher pressure (above 10^{-4} torr) may be due to ionization between the grid and anode.

Results of Experiments With Smaller Anode

The lack of an anomalous pressure-voltage effect with the initial geometry of the new experiment (6-in.-ID anode) made it desirable to reduce the anode inside diameter to 4 in., which was used in the earlier Battelle-sponsored studies. This was accomplished by installing an insert into the existing anode assembly. The results of measurements with the smaller anode and analyses of the results are briefly summarized in the following paragraphs.

Cell Currents With Anode Grounded. Figure 44 shows the cell currents with the anode grounded as a function of negative grid bias. These curves are similar to those obtained with the 6-in. anode (Figure 29), but with the magnitudes diminished due to radioactive decay of the polonium-210 emitter. The calculated alpha-particle current, I_o, at the time of obtaining these data was 1.49 x 10^{-8} amp, compared with a current of 1.95 x 10^{-8} amp when the data of Figure 29 were obtained. The data in Figure 44 permit deduction of the secondary emission and grid parameters as discussed earlier. Table 7 summarizes the results of analyses and presents a comparison with similar factors obtained from the data with the 6-in. anode. This comparison shows that there is no large effect on these parameters associated with a change in anode diameter from 4 to 6 in. The η_c value of 3.64 lies within the variation of from 3.95 to 3.32 observed with the 6-in. anode at a 1-month interval. There may be some significance to the fact that η_g and x (and hence δ) were both slightly larger when the 4-in. anode was used, since the electric field at the outside of the grid cage is larger for the smaller anode.

TABLE 7. COMPARISON OF SECONDARY-ELECTRON EMISSION AND GRID PARAMETERS FOR 4-IN.- AND 6-IN.-DIAMATER ANODES

	Charge Ratio at Grid, η_g	Charge Ratio at Cathode[a], η_c	x-Factor	δ-Factor[b]
4-in. anode	7.01	3.64	0.489	0.423
6-in. anode	6.84	3.95	0.458	0.395

(a) Data at large positive bias extrapolated to zero voltage.

(b) $\delta = f(1 + x\eta_g)$ and represents the fractional reduction in charging current due to the presence of the grid.

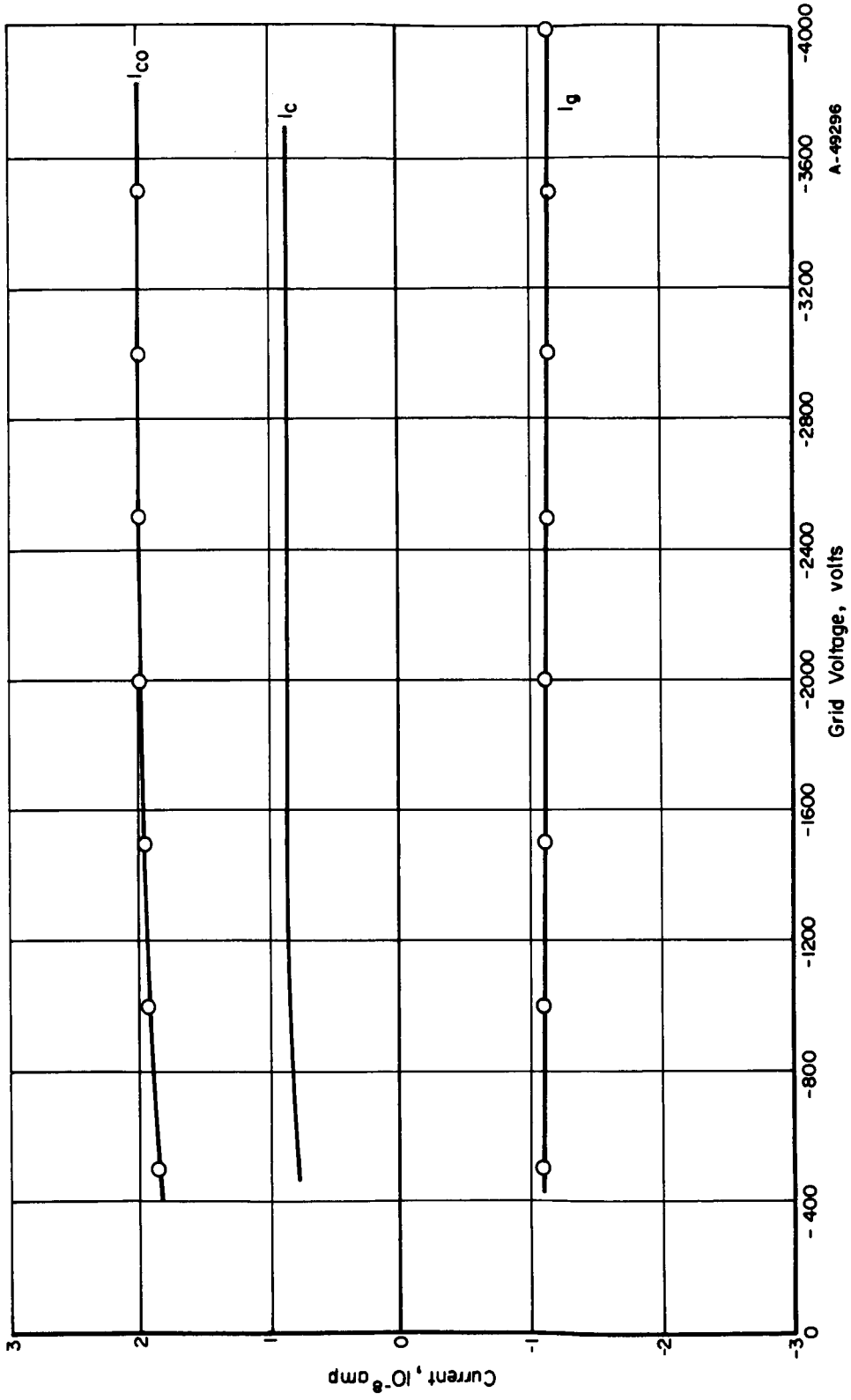

FIGURE 44. CELL CURRENTS AT LARGE NEGATIVE GRID VOLTAGE WITH 4-IN.-ID ANODE

Anode grounded.

The data presented in Figure 45 for grid current versus positive grid bias further emphasize the lack of appreciable effect on cell currents due to the change in anode diameter. After corrections for polonium decay, the current-voltage behavior was nearly identical, both in magnitude and shape, in the two cases.

Effect of Pressure on Anode Voltage. Anode voltage was measured as chamber pressure was varied from 4×10^{-7} torr up to 2.5×10^{-2} torr. The results, shown in Figure 46, were nearly identical with those obtained with the 6-in.-diameter anode: the voltage was constant up to 2×10^{-5} torr, then dropped to zero between 2 and 4×10^{-5} torr. No anomalous effect was found. From this observation, it appears that the anomalous behavior observed in the earlier experiments is quite sensitive to the detailed cell geometry and that the remaining geometry differences account for the absence of this effect.

Summary of Results of NASA-Sponsored Alpha Cell Experiments

The results of the experiments performed on the alpha cell under contract with NASA are summarized below.

(1) Cell currents with the anode grounded are affected by grid voltage in a predictable manner. A net positive current flows from the grid-cathode assembly upon application of negative grid bias larger than -40 volts.

(2) At high vacuum, microdischarging limits voltage buildup in the cell to 50-100 kilovolts. (This range is the same as that found using emission of beta particles to charge the anode, as seen in Figure 18.)

(3) The anomalous affect of vacuum-chamber pressure on anode voltage found in earlier Battelle-sponsored experiments was not present in the new experiment, with either 4-inch or 6-inch-diameter anodes.

(4) The grid controls the anode voltage, as predicted, below the limiting voltage determined by microdischarging. The triode-tube formula for amplification factor predicts the measured $\Delta V_a / \Delta V_g$ to within a precision of about 20 per cent or better.

(5) The secondary-electron emission at the cathode appears to be independent of cover material (it is the same for stainless steel and for gold) and has the value of about eight electrons per emerging alpha particle. The secondary yield at the cathode is slightly dependent on the electric field, but the secondary yield at the grid is not noticeably field-dependent.

(6) The secondary-electron emission at the grid appears to be sensitive to the surface condition of the grid wires, being approximately a factor of two larger for oxidized steel than for clean steel.

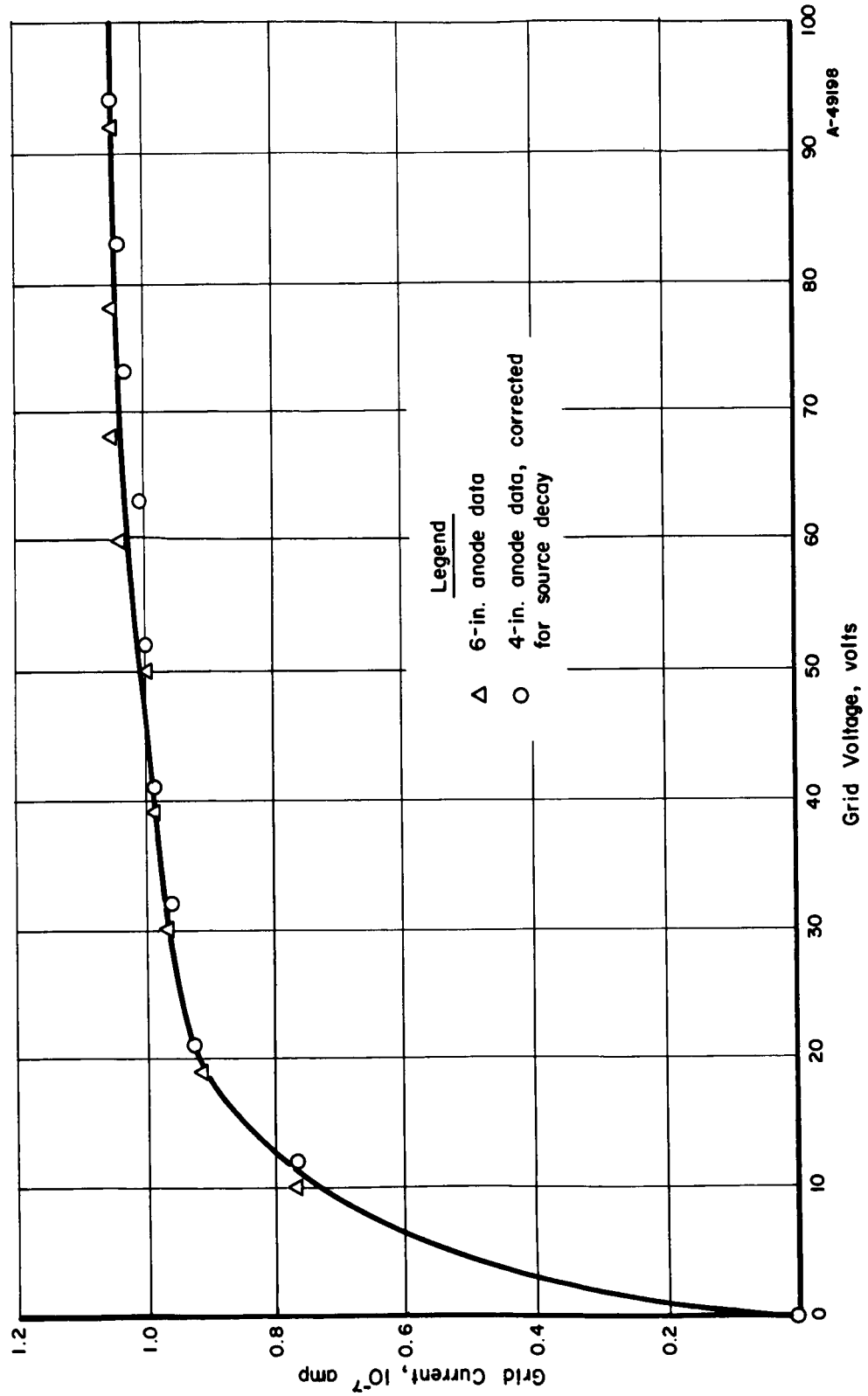

FIGURE 45. GRID CURRENT VERSUS POSITIVE GRID BIAS

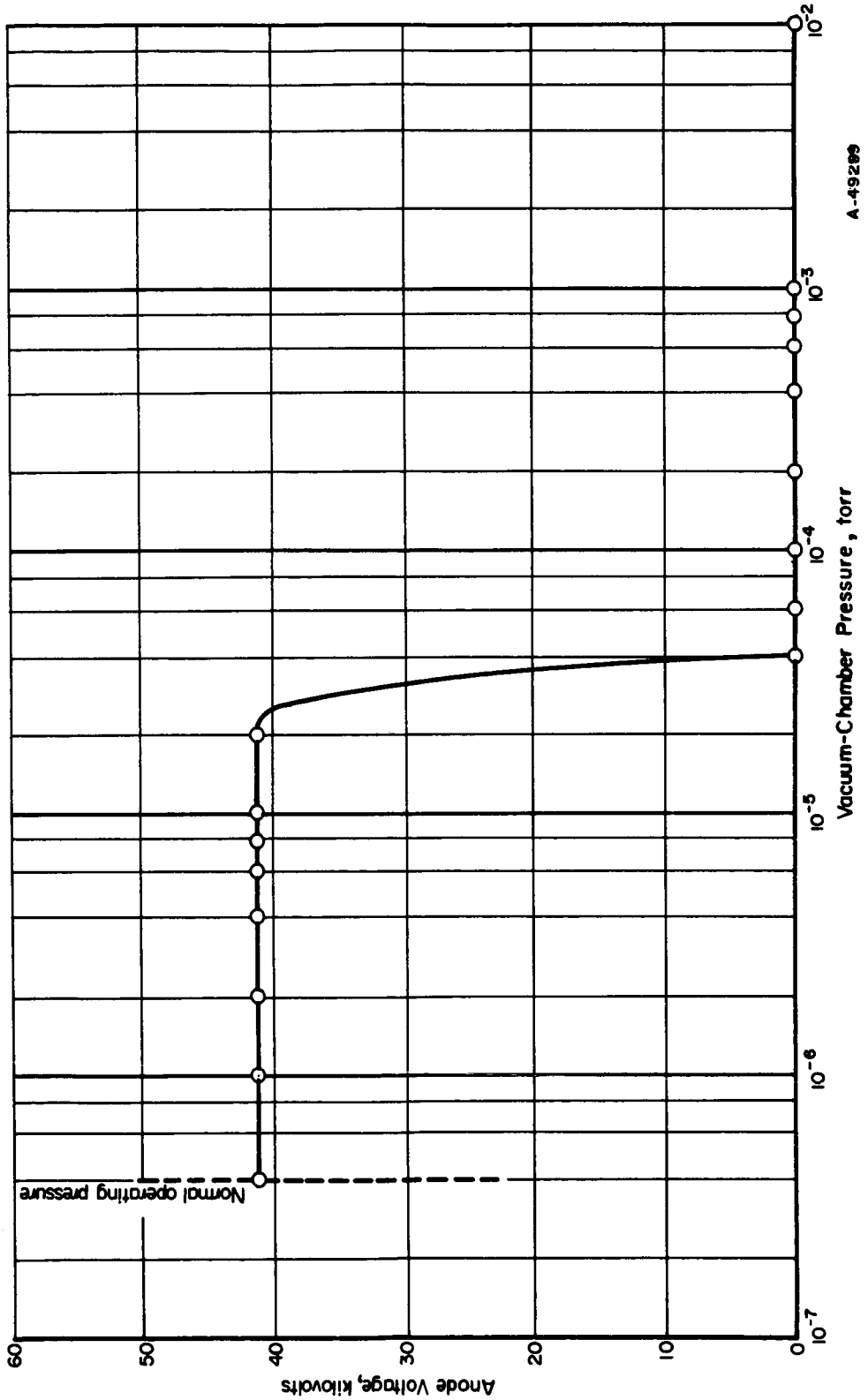

FIGURE 46. ANODE VOLTAGE VERSUS CHAMBER PRESSURE

4-in. -diam anode.
V_g = -3000 volts.

(7) The grid current is independent of anode voltage to at least 30 kilovolts. The dependency of cathode current on anode voltage indicates that the x-factor (fractional release of grid secondaries to anode) increases with anode voltage.

(8) The x-factor has magnitude of the order of 0.5 or more at zero anode voltage.

(9) A change in anode geometry from 6-inch diameter to 4-inch diameter had only a small effect on the grid design parameters η_g and x.

(10) No instabilities were observed in anode voltage at the microdischarge limit; during a 60-hour test there were no gross discharges or significant voltage variations.

INVESTIGATION OF METHOD OF ELECTRICAL-POWER CONVERSION

Several methods of converting the high voltage output of the alpha cell to a lower voltage have been investigated. The objective of these studies has been the conceptual design of a conversion system that would provide an output in the kilovolt range with a reasonable conversion efficiency. Conventional methods do not meet the requirements of this application because of the very high voltage and relatively low current of the alpha-cell generator. Two approaches to the problem have been taken: ballistic methods, which produce the desired output by control of the cell charging current, and external circuit methods, which accomplish the conversion through circuit components external to the cell. From these studies, it appears that the particular requirements for the converter are best met by a piezoelectric device which is an external circuit but which also takes advantage of the grid-control characteristics of the alpha cell.

Design Considerations of the Piezoelectric Converter

Alpha-Cell Characteristics

The first step in the design of the conversion system is the characterization of the alpha cell itself. The assumed equivalent circuit for the alpha cell is shown in Figure 47. The source voltage, E_o, represents the open-circuit voltage equivalent of the energy of alpha particles emerging from the cathode. The source impedance, R_o, is just E_o/I_o, where I_o is the short circuit or alpha-particle charging current. The charging current and, hence, the source impedance are a function of the emitter source strength. It is important to note that even with a source of high disintegration rate, R_o represents a relatively high resistance. This means that the output impedance must also be high if the anode voltage is to be maintained in the region of maximum collection efficiency.

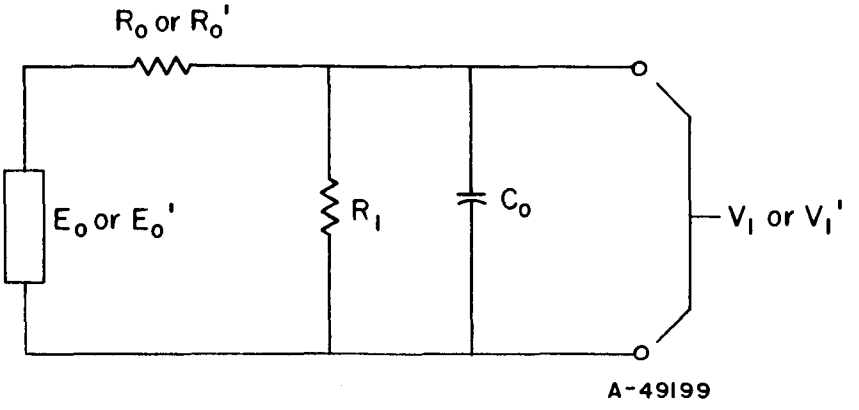

FIGURE 47. ALPHA-CELL EQUIVALENT CIRCUIT

In the equivalent circuit, the alternate source voltage, E_o', is the open-circuit voltage under conditions which allow a net negative (electron) current to flow to the anode. This characteristic is important to the conversion system that is to be described because it permits the cell to operate both as a positive and negative source, depending on the grid bias.* The source resistance associated with the negative voltage source, R_o', is equal to E_o'/I_o'. In this case the current I_o' not only is a function of the disintegration rate of the source but also is a variable controlled by the grid bias voltage. The capacitance C_o is the anode-to-cathode capacitance, and R_1 is the anode-to-cathode leakage resistance, which may be assumed to be large compared to R_o and R_o'.

The equivalent circuit of Figure 47 has been verified by analysis of cell current and voltage data obtained in previously described experiments. For the purposes of conversion-system analysis, it is assumed that the characteristics of the cell at high operating voltages are the same as those observed in the experiments in the kilovolt range. While this assumption may not be strictly valid, it is reasonable to assume that the high-voltage characteristics in the absence of microdischarging will be similar to those already observed.

The characteristics of the alpha cell are summarized in Figure 48. Power and current curves are normalized since they depend on the alpha source strength. The voltage scale shown is that for an unattenuated source, i.e., a bare source, of 5-Mev alpha particles. The collection efficiency curve is that of Figure 3 for coaxial cylinders, which has been repeated here to compare the voltage at maximum power (at $E_o/2$) with the operating voltage for maximum collection efficiency.

If the load connected to the alpha cell has a resistance comparable to R_1 and a capacitance much less than C_o (assumptions that are reasonable for the circuit to be considered), the operation of the alpha cell is independent of the load parameters and is described by the equation

$$\frac{dq_1}{dt} + \frac{1}{R_o C_o} q_1 = \frac{E_o}{R_o} \quad , \tag{52}$$

*In a sense, the grid in the alpha cell acts as a high-vacuum, high-voltage switch.

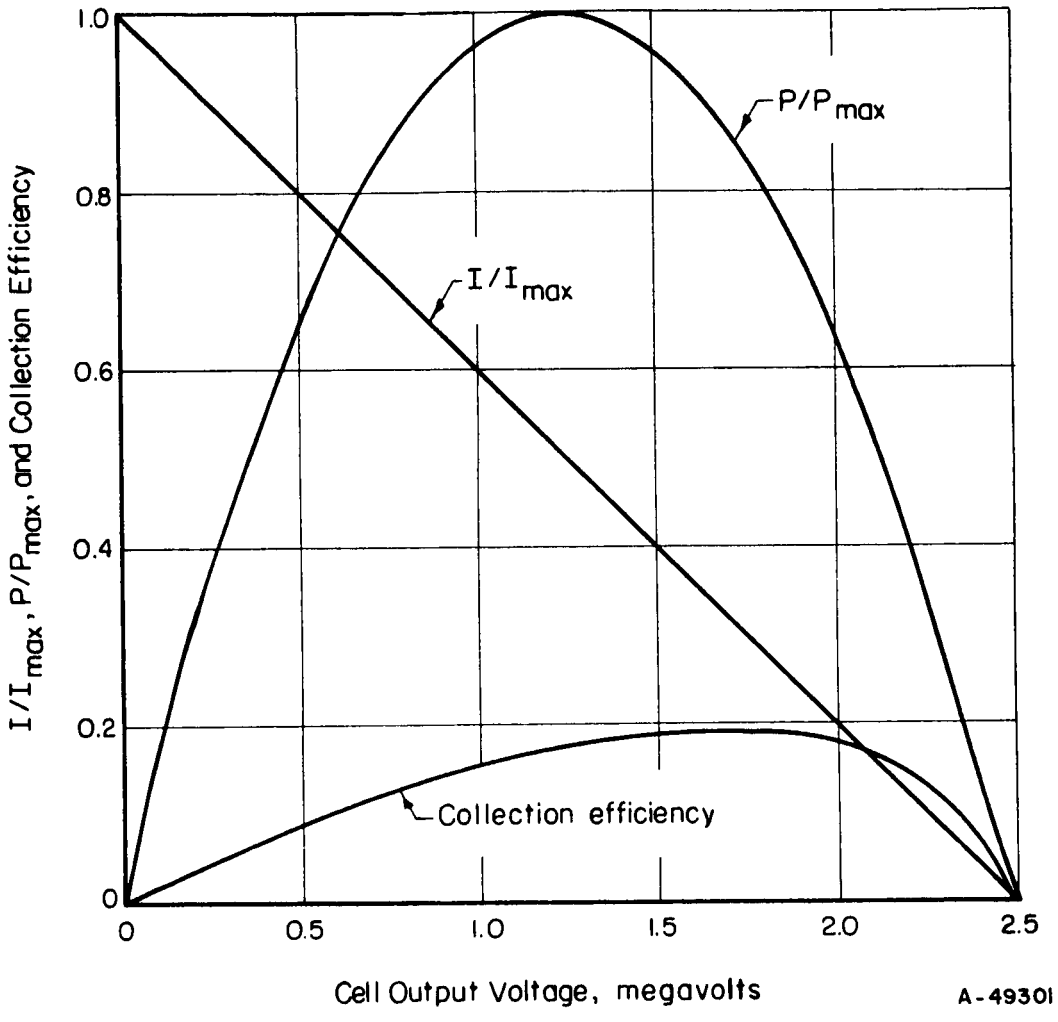

FIGURE 48. CELL CURRENT, POWER, AND COLLECTION EFFICIENCY

where the subscript 1 refers to cell, or primary circuit, variables. Equation (52), however, describes operation in only one mode. This mode is taken to be the charging mode, in which the net current to the anode is an alpha particle or positive current.

The mode in which the anode current is an electron or negative current is referred to as the discharging mode, and its operation is described by

$$\frac{dq_1'}{dt'} + \frac{1}{R_o'C_o} q_1' = E_o'/R_o' \quad , \tag{53}$$

where the primed factors are those associated with the discharge mode.

With the initial conditions that V_{10} is the anode voltage at the beginning of the charging part of the cycle and V_{10}' is that at the beginning of the discharge part of the cycle, the time-dependent anode voltages for the two modes are given by the solutions of Equations (52) and (53):

$$V_1 = E_o \left(1 - e^{-\lambda_1 t}\right) + V_{10}\, e^{-\lambda_1 t} \tag{54}$$

and

$$V_1' = E_o' \left(1 - e^{-\lambda_1' t'}\right) + V_{10}'\, e^{-\lambda_1' t'} \quad , \tag{55}$$

where $\lambda_1 = 1/R_oC_o$ and $\lambda_1' = 1/R_o'C_o$, recalling that it has been assumed that $R_o \ll R_1$ and $R_o' \ll R_1$.

For cyclic operation of the cell with charging and discharging times T and T', the maximum and minimum anode voltages are given by

$$V_{10}' = E_o \left(1 - e^{-\lambda_1 T}\right) + V_{10}\, e^{-\lambda_1 T} \tag{56}$$

and

$$V_{10} = E_o' \left(1 - e^{-\lambda_1' T'}\right) + V_{10}'\, e^{-\lambda_1' T'} \quad . \tag{57}$$

Equations (56) and (57) illustrate the flexibility of operation that is possible with the cell. For example, if operation within a particular anode voltage range is desired, these conditions can be achieved, within limits of course, by proper selection of source strength, grid bias, and charging and discharging times. For the assumptions made concerning the output impedance, operation of the cell is independent of its load, although this is not necessarily always true. It would probably be advantageous with respect to power-conversion efficiency to relax the condition that the load capacitance is small compared with the internal capacitance of the cell. The advantage could be gained only at the expense of either a smaller time constant or a larger source strength to maintain a given time constant.

Piezoelectric-Circuit Characteristics

The piezoelectric circuit portion of the converter conceptual design reduces the primary or cell anode voltage to a lower level through what is, in effect, a high-input-impedance transformer. One possible arrangement of transformer is shown in Figure 49. The anode voltage applied across the primary piezoelectric transducers produces a strain which is in turn applied to the secondary transducers, thereby inducing

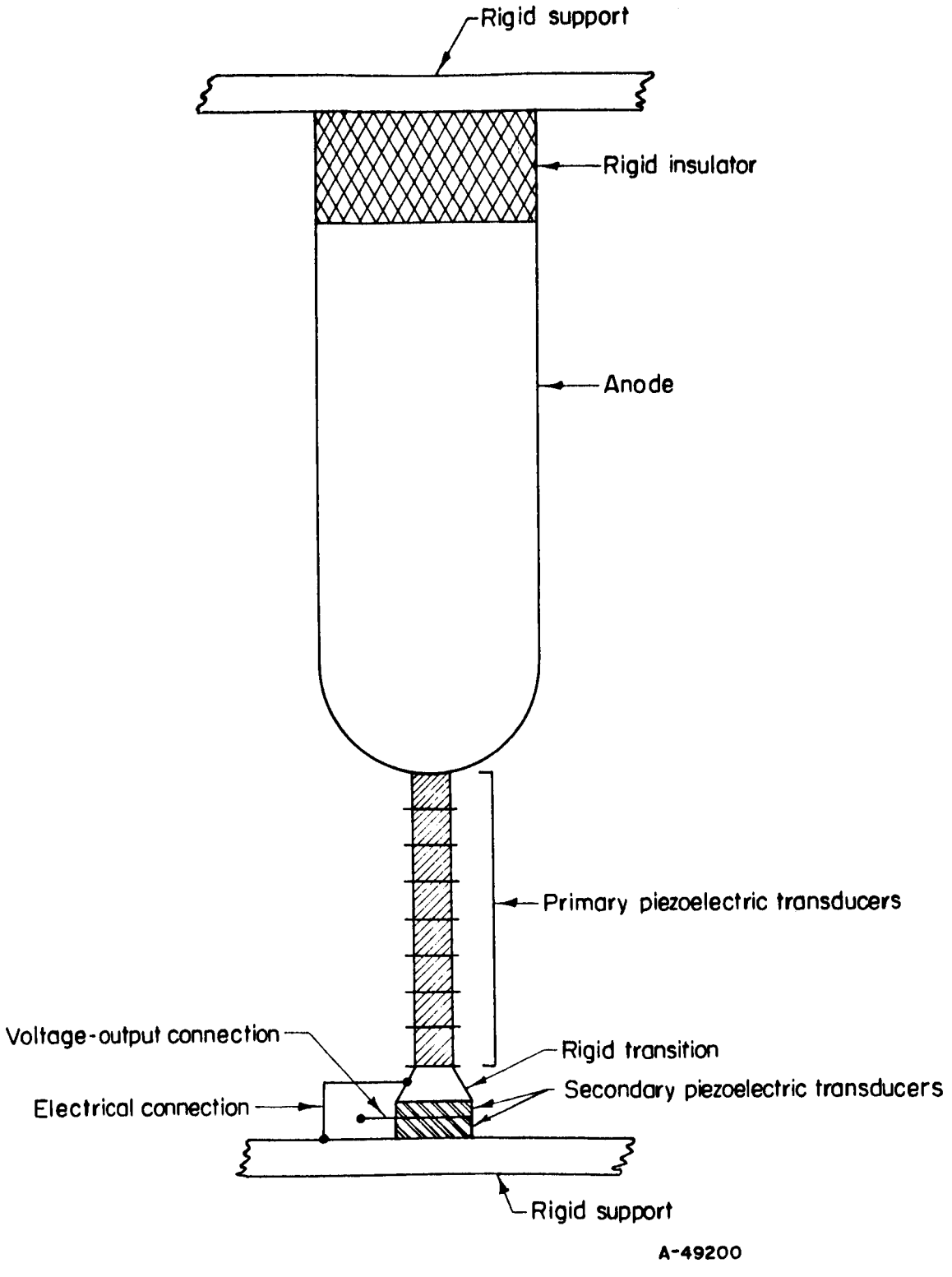

FIGURE 49. ARRANGEMENT OF PIEZOELECTRIC TRANSDUCER

a voltage across the secondary. The selection of the piezoelectric materials is such that the primary material produces a small strain per unit electric field and the secondary produces a small electric field per unit strain. This arrangement produces the desired voltage reduction. It is important, of course, that the material in the primary also have a high resistivity to maintain the high-resistance load that is necessary for efficient operation of the cell. Quartz has properties that are well suited to the conditions of cell and transformer operation and has been incorporated as the material in the primary of the conceptual design. There are several materials which could be used as the secondary transducer. The conceptual design incorporates a material having a high dielectric constant since it is desirable that the secondary transducer have a high capacitance.

An important limitation of the piezoelectric transformer itself should be mentioned. Since the primary transducers appear to the voltage source as a capacitor, it is necessary that the source provide both charging and discharging capability to obtain a continuing output from the secondary; otherwise, no output would be obtained after the initial charge buildup. The alpha cell, unlike most power sources, can be operated as both a positive and negative voltage source through grid bias control. Thus, it has, in this respect, a unique compatibility with the piezoelectric transformer in that it provides for the required cyclic operation without the use of an external discharging circuit.

The equivalent circuit of the complete system is shown in Figure 50. This circuit has been simplified to the extent that the dynamic mechanical parameters of the piezoelectric elements have been ignored. The circuit shown is a satisfactory representation of the transducers provided that the frequency of operation is well below the resonant frequency of the transducers. It is quite likely that there are significant advantages in operating the transducers in their resonant mode. The analysis of such operation, however, is beyond the scope of the studies conducted under this program.

Referring to Figure 50, the secondary transducer is represented by a voltage source that is proportional to the cell anode voltage and a series capacitance. The load is assumed to be resistive for simplicity. The voltage proportionality constant, k, is the primary-to-secondary piezoelectric-constant ratio.

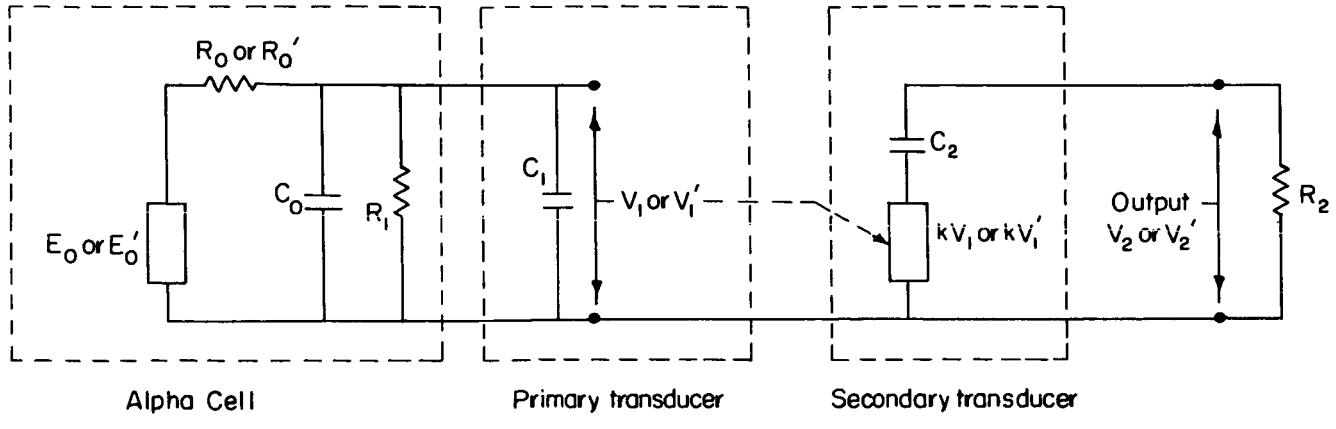

FIGURE 50. EQUIVALENT CIRCUIT OF ALPHA CELL AND POWER CONVERTER

Operation of the secondary circuit in the charging and discharging modes is described by the following equations, where the primed factors have the same meaning as before and the subscript 2 refers to secondary-circuit parameters:

$$\frac{dq_2}{dt} + \frac{1}{R_2 C_2} q_2 = kV_1 \tag{58}$$

and

$$\frac{dq_2'}{dt'} + \frac{1}{R_2 C_2} q_2' = kV_1' \quad . \tag{59}$$

Substituting Equations (54) and (55) for V_1 and V_2 yields the solutions

$$V_2 = k[(E_o - V_{10}) \frac{\lambda_1}{\lambda_2 - \lambda_1} (e^{-\lambda_1 t} - e^{-\lambda_2 t}] + V_{20} e^{-\lambda_2 t} \tag{60}$$

and

$$V_2' = k[(E_o' - V_{10}') \frac{\lambda_1'}{\lambda_2 - \lambda_1'} (e^{-\lambda_1' t'} - e^{-\lambda_2 t'})] + V_{20}' e^{-\lambda_2 t'} \quad , \tag{61}$$

where V_{20} and V_{20}' are the initial voltages for the charging and discharging modes, and $\lambda_2 = 1/R_2 C_2$.

As in the case of the primary circuit, Equations (60) and (61) suggest that there is considerable flexibility in the operation of the cell-converter system. The possible combinations of the parameters k, λ_1, λ_1', λ_2, T, and T' should provide an interesting array of output voltages and waveforms. Again, the analysis and optimization of a system of this complexity is beyond the scope of the present program.

Examples of System Operation

Several examples of system operation have been calculated under the simplifying condition that $\lambda_1 = \lambda_1' = \lambda_2 = \lambda$. Under this condition the solutions to Equations (58) and (59) are

$$V_2 = [k(E_o - V_{10}) \lambda t + V_{20}] e^{-\lambda t} \tag{62}$$

$$V_2' = [k(E_o' - V_{10}') \lambda t' + V_{20}'] e^{-\lambda t'} \quad . \tag{63}$$

It should be noted that the condition of equal time constants has been used for the example presented here strictly to ease the burden of the calculations. The example selected for this presentation is the one of several calculated which yielded the highest power-conversion ratio for the range of variables used. No attempt has been made to use optimum conditions for this example, and there is every reason to believe that more efficient operation can be achieved even for the case of equal primary and secondary time constants.

The assumed parameters for this example are

$V_{10} = 1.25 \times 10^6$ volt

$T = 1.00 \times 10^{-2}$ sec.

The factors associated with the piezoelectric transducers are

$$k = 1.21 \times 10^{-2} \text{ volt/volt}$$

$$C_2 = 1.00 \times 10^{-6} \text{ farad,}$$

and the alpha-cell constants are

$$E_o = 2.50 \times 10^{6} \text{ volts}$$

$$E_o' = -1.00 \times 10^{2} \text{ volts}$$

$$C_o = 6.20 \times 10^{-11} \text{ farad.}$$

Using these values and Equations (54), (55), (62), and (63), the time-dependent voltages were calculated. These are shown in Figure 51. The primary voltage varies from 1.25×10^6 to 2.04×10^6 volts and the secondary from -5.16×10^3 to $+3.66 \times 10^3$ volts. The rms output voltage is 2.78×10^3 volts.

The cell charging current is shown in Figure 52. It is interesting to note that for the conditions used here the power dissipated during the discharging part of the cycle is greater than that during the charging part. This suggests that a nonalternating output might be achieved by operating with a different time constant, i.e., grid bias, during discharge.

The power output for this case is 773 watts and the electrical-power-conversion efficiency is 9.48 per cent. The conversion efficiency used here is the ratio of output power, $V_{2\,rms}^2/R_2$, to source power, $i_{1\,rms}^2 R_o$, where i_1 is the cell current given by Equations (52) and (53).

Conclusions

This preliminary evaluation of the piezoelectric voltage-conversion system indicates that the system shows promise of being a practical means of converting the megavolt output of the alpha cell to usable power in the 10- and 100-kilovolt range. The scope of this program has permitted only a limited evaluation of the concept, but the indications are that it offers considerable flexibility in attainable output and that it is certainly worthy of further consideration.

Other Conversion Schemes Considered

Power Conversion by Particle-Ballistic Methods

In general, particle-ballistic methods of power conversion do not appear to be promising. The problems encountered with this approach are illustrated by the examples given below.

One of the concepts considered, which approaches the ideal converter from the standpoint of not changing the operating voltage, is shown in Figure 53. The scheme here is to replace the grid wires with radial fins and to replace the solid anode with a

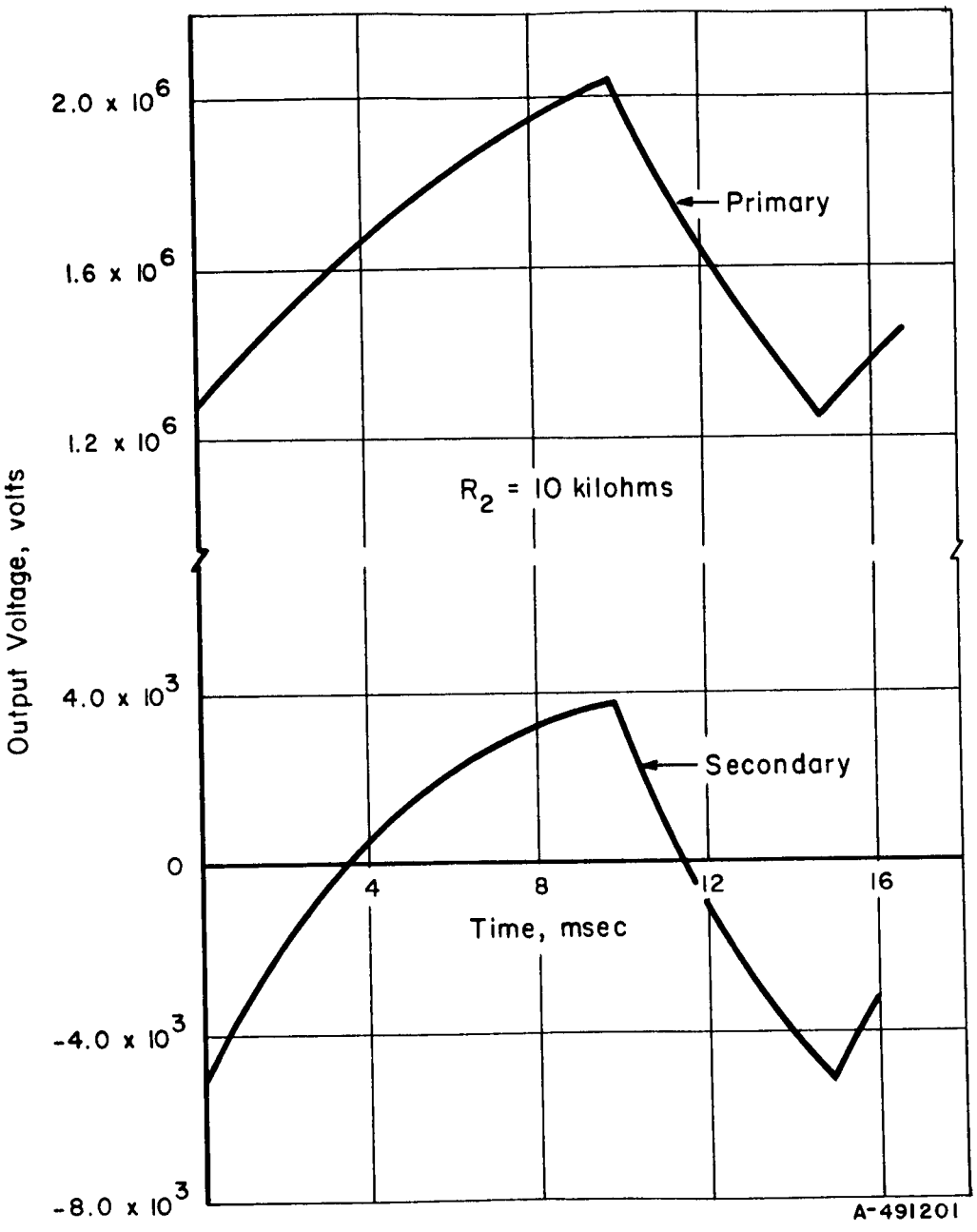

FIGURE 51. PIEZOELECTRIC-TRANSFORMER VOLTAGES

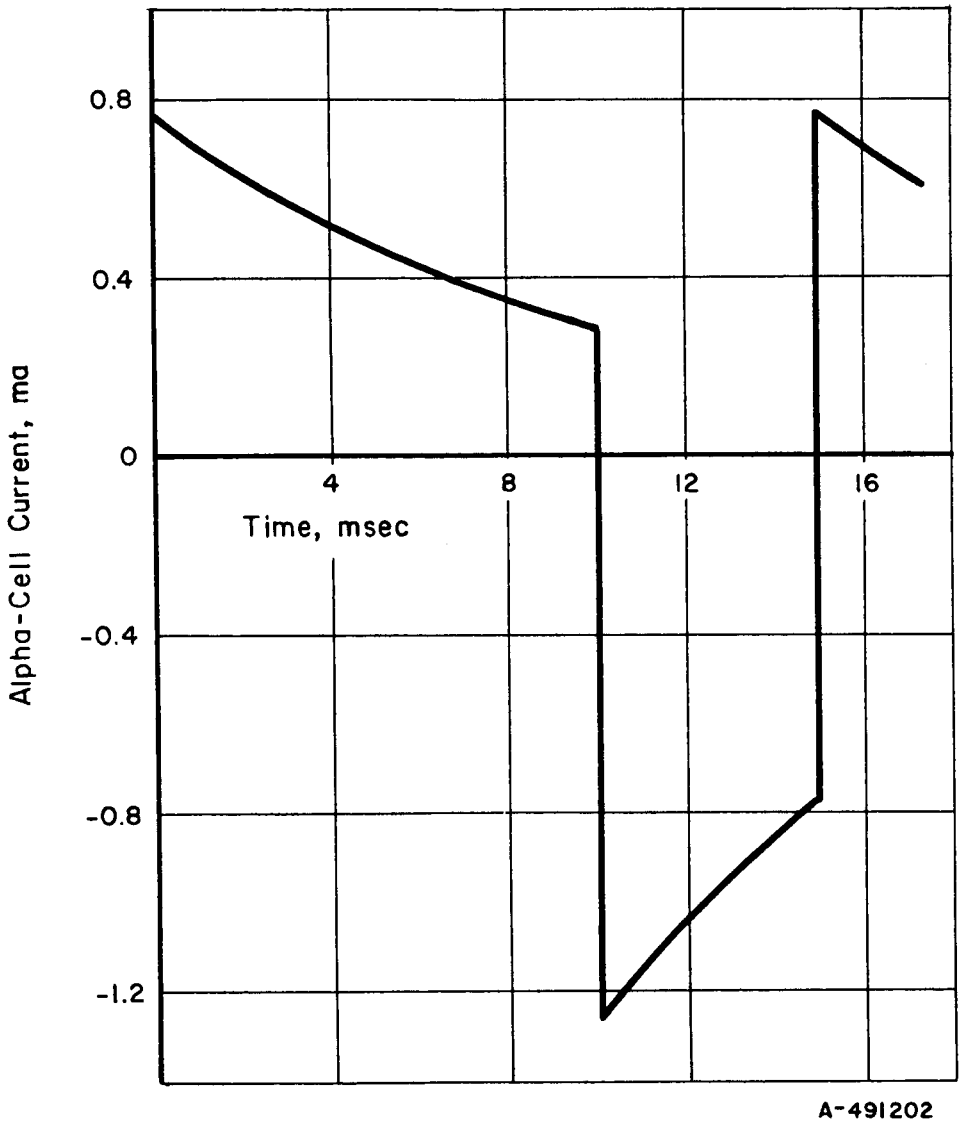

FIGURE 52. ALPHA-CELL CHARGING CURRENT

segmented electrode. An alternating output would be produced by focusing the alpha particles alternately on two sets of anode segments. In the figure, the "A" segments would be connected electrically and isolated from the "B" segments, which would likewise be electrically connected. The alpha particles would be focused alternately on the two sets of anode segments by applying different voltages alternately to adjacent grid fins. The applied grid voltage would always be negative, however, to suppress secondary-electron emission at the cathode. Although this scheme appears to meet the requirements of an acceptable converter, an investigation of the particle ballistics shows that because of the high deflection voltage required it is not feasible to assemble a cell with necessary fin spacing to prevent electrical breakdown between adjacent fins. An alternative means of producing the desired particle deflection is with a magnetic field. The required field strength is reasonable, but because of the relatively large volume through which the field must be applied, this scheme is not considered a practicable one at this time.

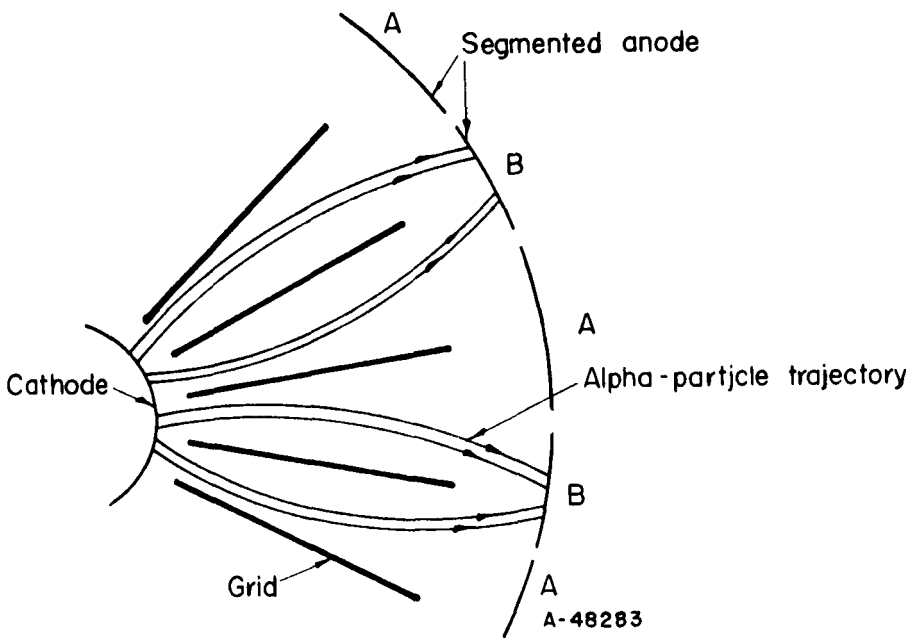

FIGURE 53. BUNCHING OF ALPHA PARTICLES BY MEANS OF A FINNED GRID

Another alpha-particle ballistic method considered to produce an alternating output applies the klystron concept to a beam of particles directed out of the cell. It appears that beam focusing can be accomplished by using the anode for electrostatic focusing. However, this method is not being given further attention because of the relatively large drift space required (tens of meters).

The possibility of producing an alternating output by causing the cell to oscillate by means of a feedback circuit has also been investigated. While this scheme is possible, it has the disadvantage that the average power output is considerably less than the maximum capability of the cell because of the low operating efficiency at low output voltage.

Power Conversion by External Circuitry

A second method in addition to the piezoelectric transformer has been considered for converting the cell output to a lower voltage by means of an external circuit. This method involves the series charging and parallel discharging of a bank of capacitors. One possible arrangement is shown in Figure 54. In this circuit, the triggering of a high-voltage gap is followed by the breakdown of low-voltage gaps, thus causing the entire capacitor bank to discharge in parallel through the load. For a bank of N capacitors, the output voltage is 1/N times the cell output voltage, and the total charge available at the load is N times that of each capacitor. In practice, the low-voltage gaps would be such that complete discharging would not occur, so cell operating voltage could be maintained in the region of high efficiency. The problems which require further consideration are the high-voltage gap, which must withstand the full cell output voltage, and the physical size of and power losses in the inductors. A similar scheme, employing resistive rather than inductive elements, has been suggested but has been given only secondary consideration because of the complicated switching required to produce the parallel and series configuration.

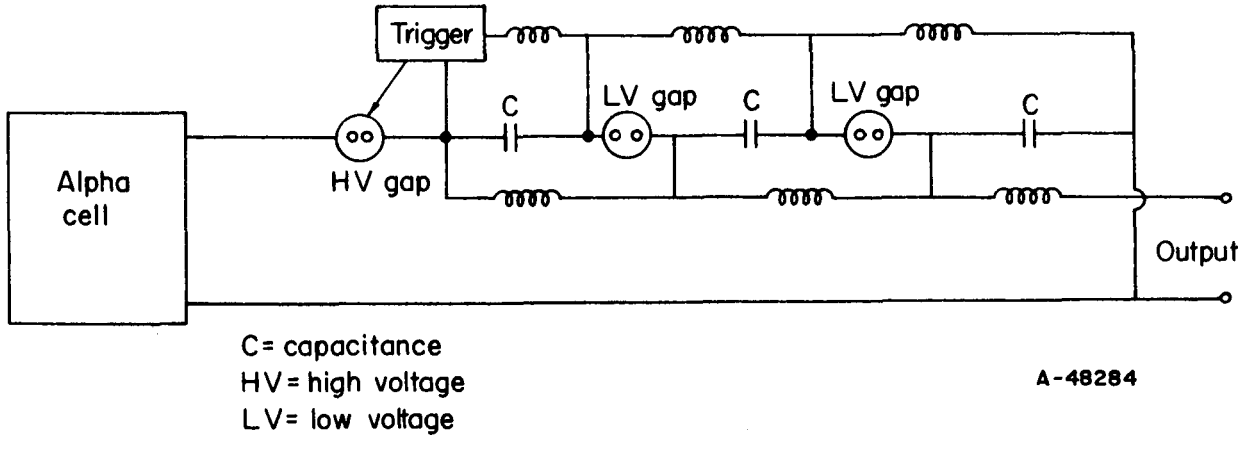

FIGURE 54. SERIES CHARGE-PARALLEL DISCHARGE CONVERTER

SUMMARY OF WORK PERFORMED DURING PROGRAM

The work performed on Contract No. NAS3-2797 during the 8-month study is briefly summarized below:

(A) Experimental Studies

(1) Constructed, installed and put into operation the apparatus for alpha-cell experiments

(2) Performed preliminary measurements and calibration prior to installing alpha emitter

(3) Performed measurements on alpha cell with anode grounded to obtain basis parameters for analysis

(4) Performed primary voltage-buildup experiments

(5) Determined current-voltage behavior of alpha cell to maximum voltage obtained

(6) Determined effect of grid voltage on anode voltage (amplification factor)

(7) Determined sensitivity of cell currents and voltage to cell pressure

(8) Observed transient response of cell currents and voltage to grid-voltage variation

(9) Determined effect of anode-geometry change on cell parameters

(10) Observed microdischarging phenomenon and stability of cell voltage.

(B) Analytical Studies

(1) Performed analysis in support of experiment design and construction

(2) Analyzed experimental data on current-voltage behavior to evaluate critical parameters that enter into theoretical prediction of cell efficiency and performance

(3) Analyzed the effects of changes made in the new cell design and geometry on cell performance

(4) Analyzed grid control on anode voltage

(5) Analyzed effect of "fall-back" alpha particles on cell currents and efficiencies

(6) Evaluated degradation of alpha-particle energy spectrum with emitter-coating thickness and with emitter-fuel thickness

(7) Investigated power-conversion techniques for the alpha-cell generator and produced a conceptual design of a conversion system.

Although much valuable information was gained from the study, because of the microdischarging problem the program fell short of its objective to extend cell voltage to a range where efficient operation is possible.

CONCLUSIONS AND RECOMMENDED DEVELOPMENT PROGRAM FOR THE ALPHA CELL

From the results of the experimental studies to date, it is concluded that the alpha cell performs as predicted in the low-voltage range and that the physics of operation are reasonably well understood. Further, one must conclude, based upon the results of both the NASA-sponsored experiment and the earlier Battelle-sponsored experiment, that microdischarging presents a rather fundamental limitation to experiments on voltage buildup with the alpha cell. Additional experiments on cell parameters at the high-vacuum region of operation (less than 10^{-4} to 10^{-5} torr) would appear to be pointless until the microdischarging problem is solved or circumvented.

Much work can and should be done to determine, and hopefully to eliminate, the causes of microdischarging. It would appear overly optimistic to presume that with a relatively small-scale program the fundamental problem of microdischarging can be solved. However, one might hope to relieve the problem and perhaps circumvent it at present by several courses of action:

(1) Pursue the effect of electrode surface cleanliness on microdischarging. Although reasonable precautions and procedures were taken to ensure clean surfaces in the past experiments, by no means were they elaborate. In this regard, a change from an oil-pumped vacuum system may be desirable.

(2) Provide means for conditioning the anode at high voltage from an external power supply with relatively high current capability. A standard technique in accelerator work, such conditioning could possibly permit short term studies at higher voltage.

(3) Use the anomalous pressure effect to study the alpha cell device in the high-voltage range and base conclusions on its performance at high vacuum on these studies.

Further experiments along these lines, even if not highly successful, can add to the stockpile of data on grid and cell design parameters (μ, η_g, x, etc.) and on the microdischarging problem which is common with all high-voltage, low-current devices.

It is therefore recommended that a follow-on program be established to continue experiments on the alpha cell, following the above three courses of action, with the same objective of obtaining higher voltage buildup in order to more clearly determine the capabilities of the alpha-cell generator.

REFERENCES

(1) H. G. J. Mosely and John Harling, "The Attainment of High Potentials by the Use of Radium", Proc. Roy. Soc., 88, 471-476 (1913).

(2) E. G. Linder and S. M. Christian, "The Use of Radioactive Material for the Generation of High Voltage", J. Appl. Phys., 23 (11), 1213-1216 (November, 1952).

(3) J. N. Anno, "Secondary Electron Production From Alpha Particles Emerging From Gold", J. Appl. Phys., 34 (12), 3495-3499 (December, 1963).

(4) Karl R. Spangenberg, Vacuum Tubes, First Edition, McGraw-Hill Book Company, Inc. (1948), p 128.

(5) Karl R. Spangenberg, op. cit., p 137.

(6) L. Granberg, J. Appl. Phys., 23, 518 (1952).

(7) J. R. Greening, "Contribution to the Theory of Ionization Chamber Measurements at Low Pressure", British Journal of Radiology, 27, 167 (March, 1954).

(8) Unpublished data by J. N. Anno, Battelle Memorial Institute.

(9) Alfred Schock, "A Direct Nuclear Electrogenerator", ASTIA (DDC), AD 216 712 (June 15, 1959).

(10) Harold L. Davis, "Radionuclide Power for Space - Part I", Nucleonics, 21, 61 (March, 1963).

(11) L. C. Northcliffe, "Passage of Heavy Ions Through Matter", Annual Rev. of Nucl. Sci., 13, 67 (1963).

(12) H. Geiger, Handbuch der Physik, Vol 24, edited by S. Flugge, Springer-Verlag, Berlin (1927), p 171.

(13) J. W. Kennedy, et al., "Some Experiments on Electrical Conduction in Vacuum", AECU-3989.

(14) L. H. Bettenhausen and W. J. Gallagher, "An Alpha-Particle Voltmeter", Nucleonics (June, 1964).

(15) Bethe, Rev. Mod. Phys., 22, 217 (1950).

(16) A. Maitland, J. Appl. Phys., 32 (November, 1961).

(17) L. I. Pivovar and V. I. Gordienko, "Prebreakdown Conduction Between Electrodes in Ultra-High and High Vacuum", translated from Zhurnal Tekhnicheskoi Fiziki, 32 (10), 1230-1236 (October, 1962).

(18) N. I. Ionov, "Mechanism for Prebreakdown Conductivity in Vacuum Interelectrode Gaps", translated from Zhurnal Tekhnicheskoi Fiziki, 30 (5), 561-567 (May, 1960).

(19) M. J. Kofoid, "Effect of Metal-Dielectric Junction on High-Voltage Breakdown Over Insulators in Vacuum", AIEE Transactions, 999-1004 (December, 1960).

(20) M. J. Kofoid, "Phenomena at the Metal-Dielectric Junctions of High-Voltage Insulators in Vacuum and Magnetic Field", AIEE Transactions, 991-999 (December, 1960).

(21) P. R. Gleichuaf, "Electric Breakdown Over Insulators in High Vacuum", J. Appl. Phys., 22 (5), 535-541 (1951).

(22) R. B. Britton, K. W. Arnold, and A. S. Denholm, "Ability of a Voltage-Graded Surface to Support a High Voltage in Vacuum and in a Pressurized Gas", Rev. Sci. Instr., 34, 185-187 (February, 1963).

(23) R. D. Evans, The Atomic Nucleus, McGraw-Hill Book Company, Inc., New York (1955), pp 633-636.

(24) E. J. Sternglass, "Theory of Secondary Electron Emission by High-Speed Ions", Phys. Rev., 108 (1), October, 1957.

(25) A. M. Plummer and J. N. Anno, "Battelle Studies on the Triode Concept of Direct Energy Conversion", a paper presented at the Summer Institute on Direct Conversion at the University of Illinois, July, 1963.

(26) J. S. Allen, Phys. Rev., 55, 336 (1939).

(27) B. Aarset, R. W. Cloud, and J. G. Trump, J. Appl. Phys., 25, 1365-66 (1954).

BIBLIOGRAPHY

(1) J. N. Anno, "A Direct-Energy-Conversion Device Using Alpha Particles", Nuclear News, 5 (12), 3-6 (December, 1962).

(2) A. M. Plummer and J. N. Anno, "Battelle Studies on the Triode Concept of Direct Energy Conversion", a paper presented at the Summer Institute on Direct Conversion at the University of Illinois, July, 1963.

(3) A. M. Plummer and J. N. Anno, "Conversion of Alpha Particle Kinetic Energy Into Electricity", ANL-6802, pp 170-180, AMU-ANL Conference on Direct Energy Conversion, November 4-5, 1963.

AMP/WJG/RGM/JNA:ims